IMPACT TEST SIMULATION WITH DIFFERENT IMPACT DIRECTION USING FEA FOR BUMPER CAR

This report is submitted in accordance with requirement of the Universiti Teknikal Malaysia Melaka (UTeM) for the Bachelor Degree of Mechanical Engineering (Structure and Material) (Hons.)

By

MUHAMMAD NABEL BIN ZAKARIA

FACULTY OF MECHANICAL ENGINEERING

2017

DECLARATION

I hereby, declared this report entitled “Impact Test Simulation with Different Impact Direction Using FEA for Bumper Car” is the results of my own research except as cited in references.

Signature : ……..

Author’s Name : MUHAMMAD NABEL BIN ZAKARIA

Date : ……..

APPROVAL

This report is submitted to the Faculty of Mechanical Engineering of Universiti Teknikal Malaysia Melaka (UTeM) as a partial fulfilment of the requirements for the degree of Bachelor of Mechanical Engineering (Structure and Material) (Hons.). The member of the supervisory is as follow:

.....

(DR. MOHD BASRI BIN ALI)

DEDICATION

To my beloved mother, Mashitah bt Mohd Yusop and my family who always there by my side during this whole Final Year Project duration.

ABSTRACT

Impact is the action of one object coming forcibly into contact with another. In term of vehicles, there are different point of impact on the car such as frontal, side and rear but the most severe crash happens from the frontal impact and then from side impact**.** Bumper is one of necessary part in passenger vehicle as it is the main tool to damp the energy from crashes**.** Therefore, this study was carried out to investigate how energy absorbed for the front bumper from different angle of impact**s** 0˚, 30˚, 45˚ using Finite Element Analysis (FEA). The velocity 80 km/hr is identified for the impactor and not to change through the analysis. For the material and design of the bumper it is decided to be a metal bumper as the beginning stage before studying the real material with the design of a GEN 2 front bumper. During the simulation, the meshing used is the tetrahedral type with the element size of 30 mm for all mesh in bumper and impactor. The results showed that the amount of energy absorption increase while the amount of the displacement decrease with the increase of impact angles.

ABSTRAK

Impak adalah perbuatan di mana satu badan menghentam satu badan lain secara paksaaan. Bagi kenderaan, ada beberapa titik impak di mana selalu terjadinya kemalangan seperti bahagian depan, bahagian sisi dan bahagian belakang tetapi impak yang paling teruk adalah pada depan dan sisi. Bumper adalah salah satu komponen penting pada kenderaan untuk menyerap impak daripada kemalangan. Oleh itu, kajian ini telah dijalankan untuk memahami bagaimana penyerapan tenaga pada bumper hadapan untuk sudut impak yang berbeza iaitu 0˚, 30˚, 45˚ menggunakan Finite Element Analysis (FEA). Kelajuan untuk impaktor telah ditetapkan pada 80 km/j dan tidak berubah sepanjang analisis. Bagi bahan dan rekabentuk untuk bumper pula telah ditentukan menggunakan bumper logam sebagai permulaan sebelum menggunakan bahan sebenar, bumper ini juga mengambil rekabentuk daripada bumper hadapan kereta GEN2. Keputusan akhir menunjukkan jumlah tenaga yang diserap bertambah manakala jumlah perubahan kedudukan berkurang apabila sudut impak bertambah.

ACKNOWLEDGEMENT

Foremost, I would like to express my greatest gratitude to Almighty God for giving me strength and courage to finally complete my bachelor degree project with the best I could. Indeed, without His Help and Well, nothing can be accomplished.

My deep and sincere gratitude goes to my most respected supervisor, Dr. Mohd Basri bin Ali, for his comprehensible instruction, stimulating encouragement and valuable suggestions in completing this project.

I also would like to take this opportunity to extend my sincere thanks to all person that helped me throughout this project. Besides, thanks to all my group members and whoever that helped me directly or indirectly for their support and contribution of idea while doing this project. The uphill struggle is hard and could not have been achieved without the inspiration and motivation from the people around me.

Not to forget, my special one, Puteri Eliani Fikri who had been there through the ups and downs of this whole project. Her continuous support, generous ideas and coherent guidance helped me tremendously to complete this project.

Lastly, I would like to acknowledge the endless love, passion and support of my beloved mother and siblings. Thank you for the unconditional support and encouragement in completing this project.

CONTENT

LIST OF TABLES

LIST OF FIGURES

LIST OF ABBEREVATIONS

NCAP	New Car Assessment Programme
FMVSS	Federal Motor Vehicle Safety Standards
FEA	Finite Element Analysis

LIST OF SYMBOLS

°	=	angle
s	=	seconds
J	=	Joules
mm	=	millimeter
N	=	Newton
E_A	=	energy absorption
F	=	force
U	=	displacement
%	=	percentage
km	=	kilometre
h	=	hour
m	=	mass
v	=	velocity
e	=	coefficient of restitution
δ_{max}	=	maximum deflection
K_{eq}	=	equivalent stiffness

CHAPTER 1

INTRODUCTION

1.1 Background

Impact is the action of one object coming forcibly into contact with another or can also be called collision or crash. In term of registered vehicles, passenger vehicles are 90% from the total number. In 2009, rough calculations showed that 9,640,000 vehicles were reported crashed and 95% from these crashes involved passenger vehicles (Davoodi et al., 2012). With every crash, there are different point of impact on the car such as frontal, side and rear. In addition, each of them has their own severity towards the passengers. However, the most severe crash happens from the frontal impact and then from side impact. Figure 1.1 shows the presentation of data from Volvo's accident data base (Cheon, Choi, & Lee, 1995; Donga, 2011).

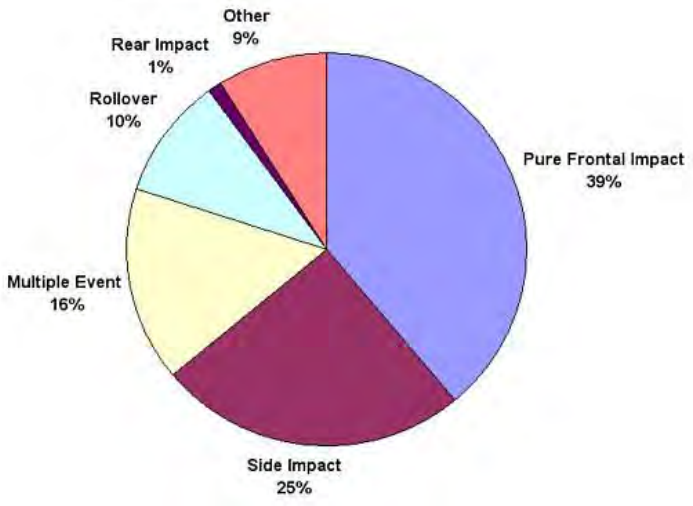

Figure 1.1: Volvo's distribution of serious-to-fatal crashes (Donga, 2011).

There are many tries to lessen the effect from the frontal impact crashes using air bags and energy absorption bumper.(Cheon et al., 1995). Bumper is one of necessary part in passenger vehicle as it is the main tool to damp the energy from crashes and also protect others of vehicle such as lamps, hood and cooling system especially the front bumper (Dange, Buktar, & Raykar, 2015; Davoodi et al., 2011). The bumper system consists three main parts: fascia, energy absorber, and bumper beam as shown in Figure 1.2 (Davoodi et al., 2011, 2012).

The Oblique Moving Deformable (MDB) Test as shown in Figure 1.3 below is expected to represent serious oblique real world crashes notable frontal engagement with significant intrusion and is intended to represent an oblique vehicle to vehicle crash with each vehicle advancing at 50-60 km/h or with one vehicle advancing at 100-120 km/h (Hollowell, Gabler, Stuckl, Summers, & Hackney, 1999).

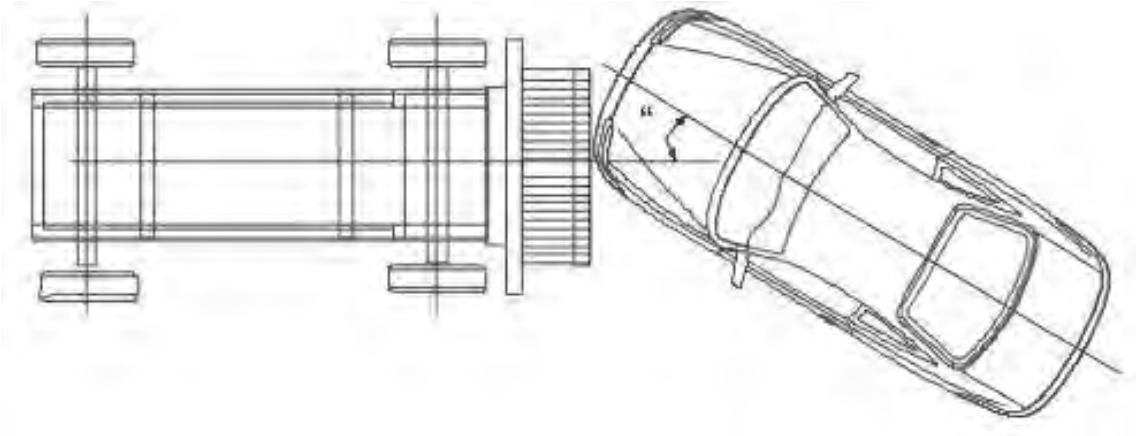

Figure 1.2: Oblique Moving Deformable (MDB) Test (Hollowell et al., 1999).

Studies also showed that critical penetration energy increase as the curvature increase, impact angle increase and interface increase (Yang, Cho, Im, Cha, & Kim, 2006) and oblique angle is a crucial factor not only on the penetration resistance of the target plate but also on its deformation/failure modes (Ni, Jin, & Lu, 2014).

1.2 Problem Statement

Studies shows that many crashes happened form the frontal impact and this lead to many injuries and vehicles damage (Cheon et al., 1995; Donga, 2011). During all these frontal crashes, the first part that receives impact is the front bumper (Davoodi et al., 2012).This shows that for the front bumper, the energy absorption is really important because it is a main tool to damp the energy from crashes.

An investigation about how energy absorbed for the front bumper from different angle of impact is important because most severe crashes involves frontal impact. Moreover, all the crashes that happened had different location or direction of impact and every location has different energy absorption. With the different impact angle, the deflect angle also varies as each part of where the impact hit has different surface built. However, doing experiment for impact test can use a lot of cost and this can be avoided by using Finite Element Analysis (FEA) software such as ABAQUS.

1.3 Objectives

Impact test simulation with different impact direction using FEA for bumper car.

1. To determine the energy absorbed with different angle of impact direction.
2. To correlate the energy absorbed with different impact direction.
3. To compare the results with previous studies.

1.4 Scope

This study focuses on studying the energy absorption for the front bumper at different impact angle of 0˚, 30˚, 45˚ using the Finite Element Analysis (FEA) with the specification of ABAQUS software. The velocity and force of impact are identified and not to change through the analysis. For the material and design of the bumper it is decided to be a metal bumper as the beginning stage before studying the real material with the design of a GEN 2 front bumper. During the analysis, the meshing used is the same optimum mesh that produce best result with acceptable time for each impact angle and the bumper model is modelled using the accurate scale of the manufactured bumper.

CHAPTER 2

LITERATURE REVIEW

2.1 Introduction

Bumper is one of necessary part in passenger vehicle as it is the main tool to damp the energy from crashes and also protect others of vehicle such as lamps, hood and cooling system especially the front bumper (Dange et al., 2015; Davoodi et al., 2011). In previous chapter, the studies about severity of type of crashes and bumper development history are brought up to show the importance of car bumper. However, in this chapter more studies will be referred to explain the details of car bumper system, crash test standard, impact mechanics and the effect of impact direction towards impact response. These are important things to be reviewed so that the energy absorption on front car bumper during frontal or even oblique impact.

2.2 Function of Bumper

Bumper is a protective layer that is designed to fit on the front and rear sides of the car to produce a shielding effect thus enabling certain range of safety from collision. (Moona, Yadav, Singh, & City, 2015). The common material that used to make bumpers are steel, aluminium, or plastic (Jamal, 2009; Moona et al., 2015).

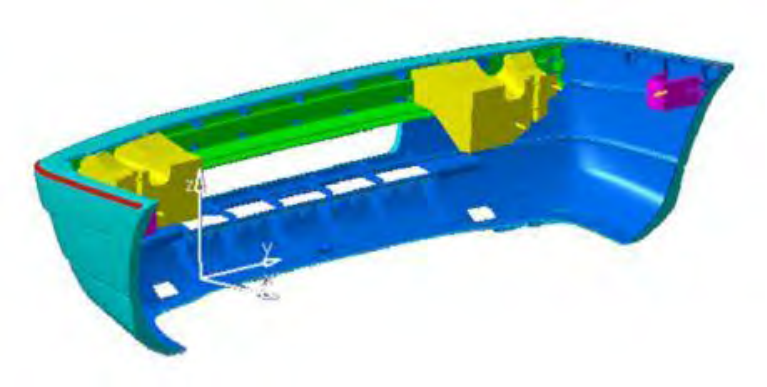

Figure 2.1: Bumper systems components (Davoodi et al., 2011)

Passive safety car system is the physical system that shield the passengers during collision such as front and rear car bumpers that can absorb impact energy (Calienciug, 2012). The main purpose of bumper is the absorption of impact energy to reduce the damage which can affect the car, passengers and even pedestrian. (Bohra & Pawar, 2014; Calienciug, 2012; Davoodi, Sapuan, & Yunus, 2008; Marzbanrad, Alijanpour, & Kiasat, 2009; Moona et al., 2015). Bumper reduces the damages of collision with other cars and objects due to their large deformation zones by deforming itself and absorb the force (kinetic energy) during a collision (Kleisner & Zemˇ, 2009)

However, bumper shows it most importance in absorption of impact energy during low speed collision and prevent serious damages (Belingardi, Beyene, & Koricho, 2013; Beyene, Koricho, Belingardi, & Martorana, 2014; Jamal, 2009). This is because, bumper can only absorb impact energy efficiently until 5 mile/h collision regulation and impact energy is not absorbed enough at higher speed collision (Cheon et al., 1995). In addition, bumper also intended to protect and shield the nearby component of car such the hood, trunk, grille, fuel tank, exhaust and this also includes the engine and rear part (Jamal, 2009; Moona et al., 2015)

2.3 Bumper Systems

The whole frontal bumper system consists the following main parts, a fascia, energy absorber and bumper beam (Davoodi et al., 2011; Kleisner & Zemˇ, 2009). There are important factors that an engineer or designer must put in thought when selecting a bumper system. The most crucial factor is the ability of the bumper system to absorb enough energy (Steel Market Development Institute, 2013). Figure 2.1 shows the diagram for types of bumper systems.

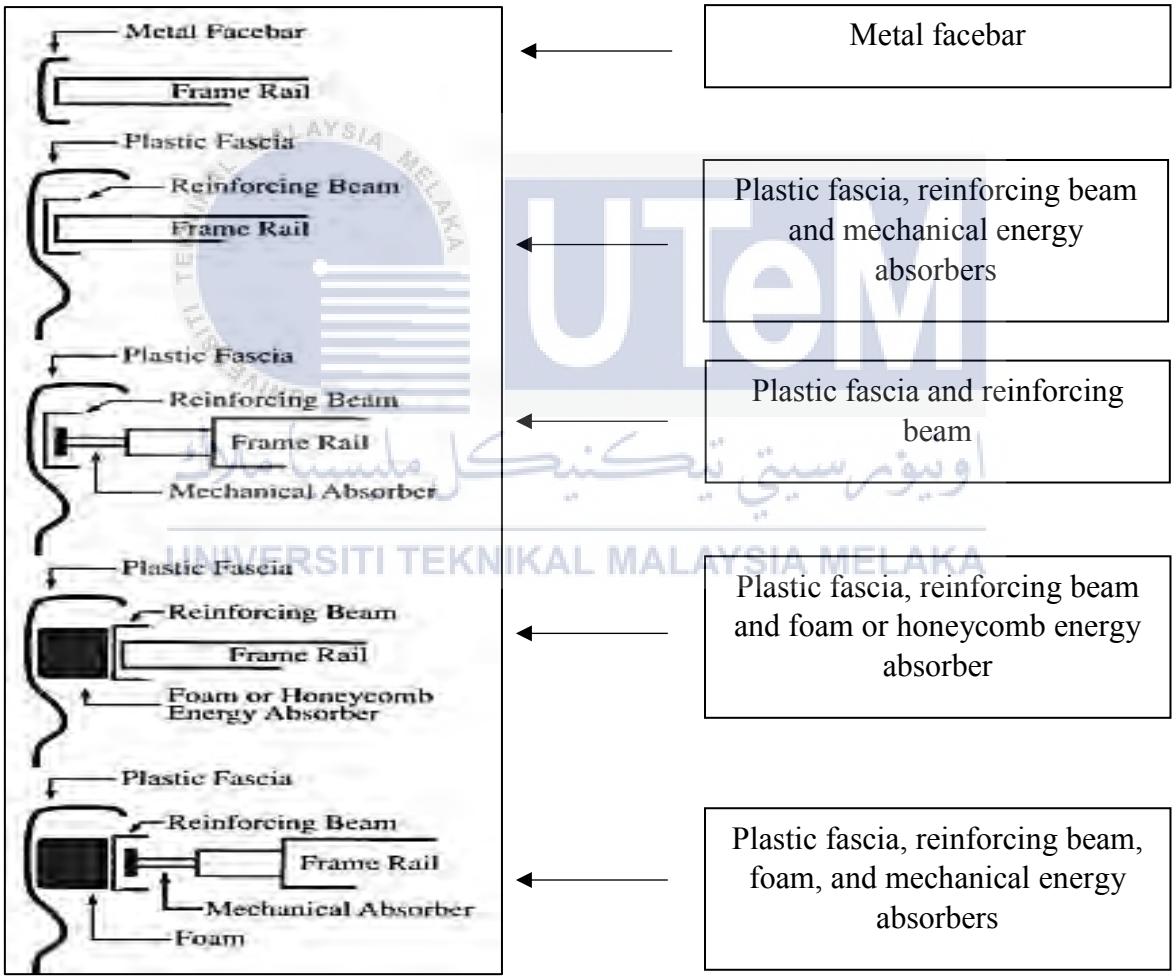

Figure 2.2: Diagram for types of bumper system (Steel Market Development Institute, 2013)

2.4 Components of Bumper System

There are many components in a bumper system with various functions such as cosmetic value, aerodynamical value, and energy absorbing capability high-speed or low-speed impact.

2.4.1 Fascia

A fascia cannot defend against impact energy so it is classed as a non-structural component (Davoodi et al., 2008). Used mainly for aesthetical values, this component must has low air resistance to give a good air flow all over the car (Davoodi et al., 2008; Steel Market Development Institute, 2013). There are many curves and edges to make fascia's shape and this can differentiate one car manufacturer from another. Moreover, fascia need to be lightweight and can be easily mass-produced. Practically, all fascia use material such as polypropylene, polyurethane or polycarbonate for its material (Steel Market Development Institute, 2013).

2.4.2 Energy absorber

The designing of energy absorber is to receive some of kinetic energy from a car accident (Davoodi et al., 2008; Steel Market Development Institute, 2013). In slow crash, the efficiency of the energy absorber is very high because the bumper springs will return to its initial position. There are few types of energy absorber such are foam, honeycomb, and mechanical devices. For foam and honeycomb, polypropylene, polyurethane, or low-density polyethylene are used as the material.

Meanwhile, for the mechanical energy absorber or crush can is metallic and occasionally look alike shock absorber. In terms of weight, the mechanical energy absorber is several times heavier than foam energy absorber but it can defend against a lot more impact

and mechanical energy absorber also has better energy absorption criteria (Steel Market Development Institute, 2013).

2.4.3 Facebar

The production of facebar usually uses the stamping process and has plastic or stainless-steel finishing. Steel facebar is commonly made from steels with a low to medium yield strength. Higher yield strength steels are being ventured to reduce the dimension and mass of facebar. After stamping, steel facebar are chrome plated or painted for visual values and anti-corrosion reasons (Steel Market Development Institute, 2013)

2.4.4 Reinforcing beam or bumper beam

Bumper beam is an main structural component that supports to reduce the kinetic energy from a high speed crash and to contribute bending resistance in a low speed crash (Davoodi et al., 2008; Steel Market Development Institute, 2013). For very high-strength steel, roll forming and hot stamping are main method used on to produce steel bumper beam. Roll formed beam is easier to be found rather than hot stamped one but beam produced from hot stamping has the lowest average mass from all steel bumper systems (Steel Market Development Institute, 2013).

2.5 Frontal Crash Test Standard

Rigid barrier test is used widely in FMVSS No.208 and NCAP (Hershman & Hershman, n.d.). In the rigid barrier test, both FMVSS No.208 and NCAP have the objective to measure the crashworthiness of passenger vehicle (Hollowell et al., 1999; National Highway Traffic Safety Administration (NHTSA), NHTSA, & National Highway Traffic Safety Administration (NHTSA), 2012). A rebound velocity varies for every vehicles but

commonly has a maximum value if 10% of the impact velocity for a total speed of up to 53 km/h (Hollowell et al., 1999).

2.5.1 New Car Assessment Programme (NCAP)

Standard facility for frontal NCAP Rigid Barrier Impact Test as shown in Figure 2.2 below, the requirements are the barrier must have a minimum standard of 6 feet height, 6 feet thick and 12 feet width with a weight of around 100, 000 pounds that are made from reinforced concrete structure. The velocity of the car must reaches and retains a range from 55.5 km/h to 57.1 km/h (National Highway Traffic Safety Administration (NHTSA) et al., 2012).

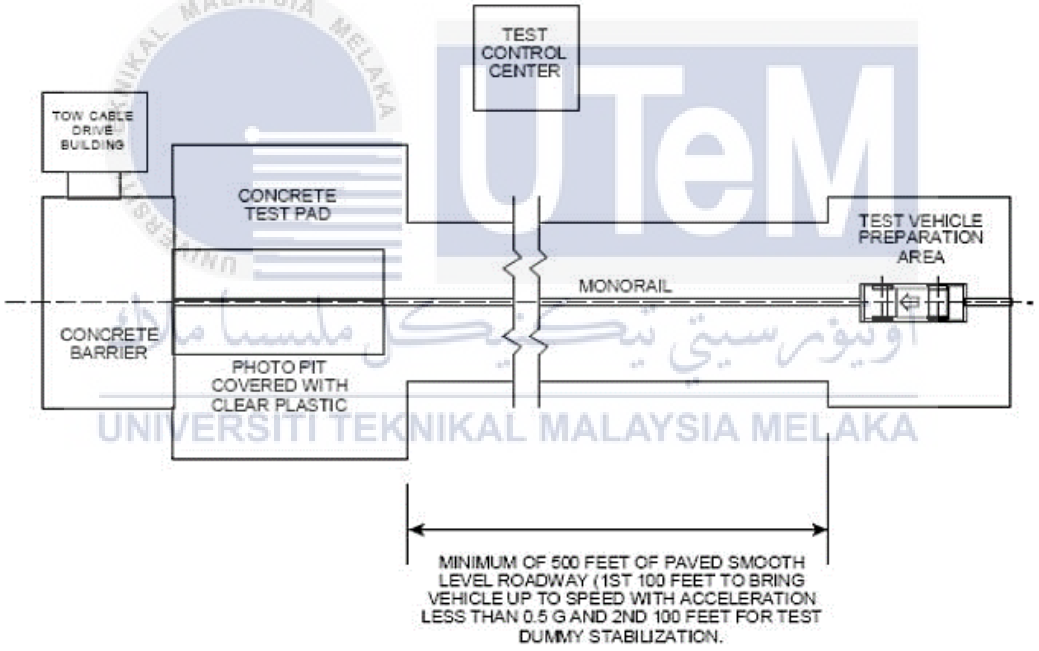

Figure 2.3: Standard facility for NCAP Rigid Barrier Test (National Highway Traffic Safety Administration (NHTSA) et al., 2012)

2.5.2 Federal Motor Vehicle Safety Standards (FMVSS) No. 208

FMVSS is a. federal regulations specifying design, construction, performance, and durability requirements for motor vehicles and regulated automobile safety-related components, systems, and design features in United States.

2.5.2.1 The Full Frontal Fixed Rigid Barrier Test

The Full Frontal Fixed Barrier Crash test (or Rigid Barrier test) as shown in Figure 2.3 below simulates when a car is crashing to another car frontally with the same speed. It is a total test which assesses the safety or both the energy-absorbing vehicle design and the occupant restraint system. The vehicle is required to have the speed of 48 km/h before impact. The kinetic energy of the crash (½ MV^2) is dissipated by crush of vehicle and rebound velocity (Hollowell et al., 1999).

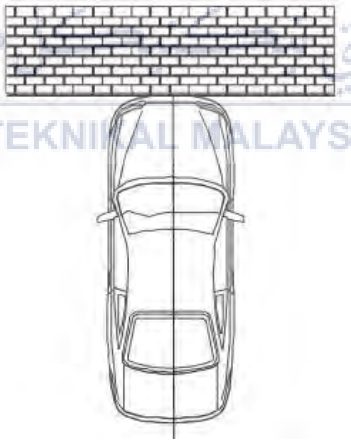

Figure 2.4: Full Frontal Fixed Rigid Barrier Test (Hollowell et al., 1999)

2.5.2.2 The Oblique Frontal Fixed Rigid Barrier Test

The Oblique Frontal Fixed Rigid Barrier Test as shown in Figure 2.4 below is designed so that the vehicle will be impacted to the rigid barrier with little frontal

engagement and the impact will become more oblique with velocity up to 53 km/h. It is a total test which assesses the safety added by both the energy-absorbing vehicle structure and the occupant restraint system. The kinetic energy of the crash (½ MV^2) is dissipated by crush of vehicle, continuing final velocity, and vehicle rotation (Hollowell et al., 1999).

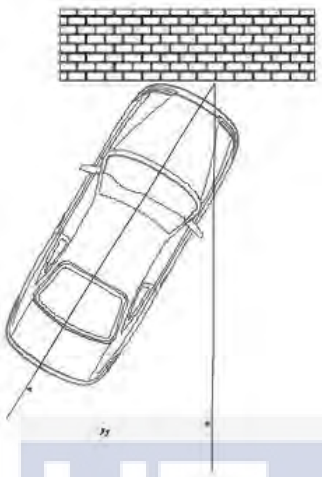

Figure 2.5: Oblique Frontal Fixed Rigid Barrier Test (Hollowell et al., 1999)

2.6 Impact Mechanics

The impactor is considered as stern body and the front bumper is made of composite and metallic materials, the load of the impact dispersed unevenly along the joining area over the joining region of the bumper beam. When the bumper is exposed to impact loading, it always commences a consistent deformation δ_{max}. In the elastic impact, energy conservation principle is considered. Kinetic energy is conserved before the impact and again converted to elastic energy. Kinetic energy of automobile and the impactor during its maximum deflection can be showed as follows (Roopesh & Rao, 2015):

$$\frac{1}{2} m_1 v_1^2 = \frac{1}{2} K_{eq} \delta_{max}^2 + \frac{1}{2} m_1 v_0^2 + \frac{1}{2} m_2 v_0^2 \quad (1)$$

Where v_1 is the speed of impactor before the impact and v_0 is the final speed at maximum deflection point of the vehicle and the impactor, m_1 is the impactor mass and m_2 is the vehicle mass and K_{eq} is the equivalent stiffness of the vehicle bumper beam which can be attained from the relationship of reaction forces and displacement from a study of beam. Another crucial concern in the case of momentum is that it can neither be created nor destroyed. Therefore, the momentum before the impact is as same as after impact. Principle of momentum conservation at the moment of its maximum deflection before and after the impact can also be showed as follows (Roopesh & Rao, 2015):

$$m_1 v_1 = (m_1 + v_1) v_0 \tag{2}$$

From the above equations (1) and (2), maximum deflection δ_{max} can be obtained as follows (Marzbanrad et al., 2009):

$$\delta_{max}^2 = \left(\frac{1}{K_{eq}}\right)\left(\frac{m_1 m_2}{m_1 + m_2} v_1^2\right) \tag{3}$$

After disengagement point, energy and momentum conservation equations can be showed as follows (Marzbanrad et al., 2009):

$$\frac{1}{2} m_A v_A^2 = \frac{1}{2} m_A v_{A2}^2 + \frac{1}{2} m_B v_{B2}^2 \tag{4}$$

$$m_A v_A = m_A v_{A2} + m_B v_{B2} \tag{5}$$

Where V_{A2} and V_{B2} are the final velocities of the impactor and vehicle, respectively in disengagement point. In the elasto-plastic impact, the concept of linear momentum conservation satisfies, since impact forces are equal and opposite (Dange et al., 2015).

$$m_A v_A + m_B v_B = m_A v_{A2} + m_B v_{B2} \tag{6}$$

In this case, the velocities after impact may be calculated with the coefficient of restitution (e). The coefficient of restitution (COR) is the ratio of speed of separation to speed of approach in a collision (Dange et al., 2015).

$$e = (v_{B2} - v_{A2}) - (v_A - v_B) \quad (7)$$

An object with a COR equals to 1 collides elastically, while an object with a COR of 0 will collide in elastically making the object it crashed remain with it. The coefficient of restitution is a scale which shows how much kinetic energy, resides after a collision of two objects. Referring to the ratio, if the coefficient is nearing 1, almost no kinetic energy is lost and if the coefficient is nearing 0 there is a lot of kinetic energy lost in other energy forms (Dange et al., 2015).

2.7 Oblique Impact

In an oblique impact, the normal direction, n is decided at the moment of impact along the line that connect the centres of the two body and the tangential direction, t along the tangential line between the two body surfaces as shown in Figure 2.5 below (Peraire & Widnall, 2009)

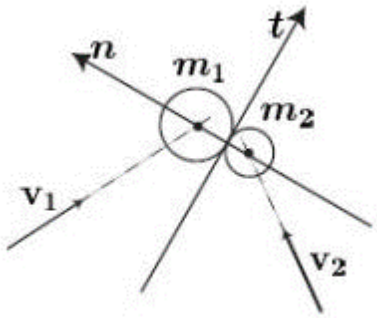

Figure 2.6: Normal and tangential line of oblique impact (Peraire & Widnall, 2009).

The equation of momentum conservation written in both tangent and normal direction and since the force of contact is predicted along the normal direction, the equation for tangential direction. As for in this study, the mass could be cancel out as only the impactor is mobbing and not the bumper. The formulas involved is written as:

$$m_1(v_1)_t = m_1(v_1')_t \quad => \quad (v_1')_t = (v_1)_t \tag{8}$$

$$m_2(v_2)_t = m_2(v_2')_t \quad => \quad (v_2')_t = (v_2)_t \tag{9}$$

$$m_1(v_1)_n + m_2(v_2)_n = m_1(v_1')_n + m_2(v_2')_n \tag{10}$$

$$e = -\frac{(v_1')_n - (v_2')_n}{(v_1)_n - (v_2)_n} \tag{11}$$

$$e = -\frac{(v_2')_n}{(v_2)_n} \tag{12}$$

For 1D normal direction, the collision problem is solved using equation (10) which determines the $(v_1')_n$ and $(v_2')_n$ (Peraire & Widnall, 2009).

A relationship was made after experimenting the effect of different attack angle on the energy distribution and the damage area of glass fibre-reinforced composites. The

observation during the experiment suggest that the energy distribution by the target decreased and increased with the attack angle (Siva Kumar & Balakrishna Bhat, 1998).

Studying the effect of oblique impact and curvature on the penetration nature of composite laminate shells shows that the critical penetration energy increase as the curvature increase, impact angle increase and interface increase (Yang et al., 2006)

By investigating the effect of high velocity impacts on carbon/epoxy tape quasi-isotropic laminates, results present that the damage done by the oblique impact is less than the normal impact at speed under the ballistic limit. However, the nature is vice versa when the speed is above the ballistic limit (Pernas-Sánchez, Artero-Guerrero, Varas, & López-Puente, 2014)

The aluminium plate thickness and the obliquity angle have a considerable effect on the residual velocities and on the absorbed energy by the plate during impact and perforation event. The numerical results have been compared with experimental and analytical results with good interaction (Fadhil, 2012).

Results suggest that the oblique angle is a crucial factor not only on the penetration resistance of the target plate but also on its deformation/failure modes. The ballistic limit speed of the hybrid cored sandwich increases with increasing oblique angle and the critical oblique angle at which the penetration process is changed from perforation to embedment is about 45˚ (Ni et al., 2014).

CHAPTER 3

METHODOLOGY

3.1 Introduction

In this chapter, the focus is on how this study will be conducted and the steps involved during this study. A flowchart is used to make the process flow more presentable and to achieve the objectives, all step must be done as precise or better to produce the best results. First, determining the bumper design is a crucial step in this project and second to determine the parameter such as the impactor velocity and bumper material. Then the next phase where the project is mainly involving computer software such as CATIA and ABAQUS for modelling and simulation. This phase also includes adding the material properties, step and interaction, boundary condition and type and size of mesh. Lastly, the results obtained will be compared with other related studies to further understanding for this study.

3.2 Flowchart

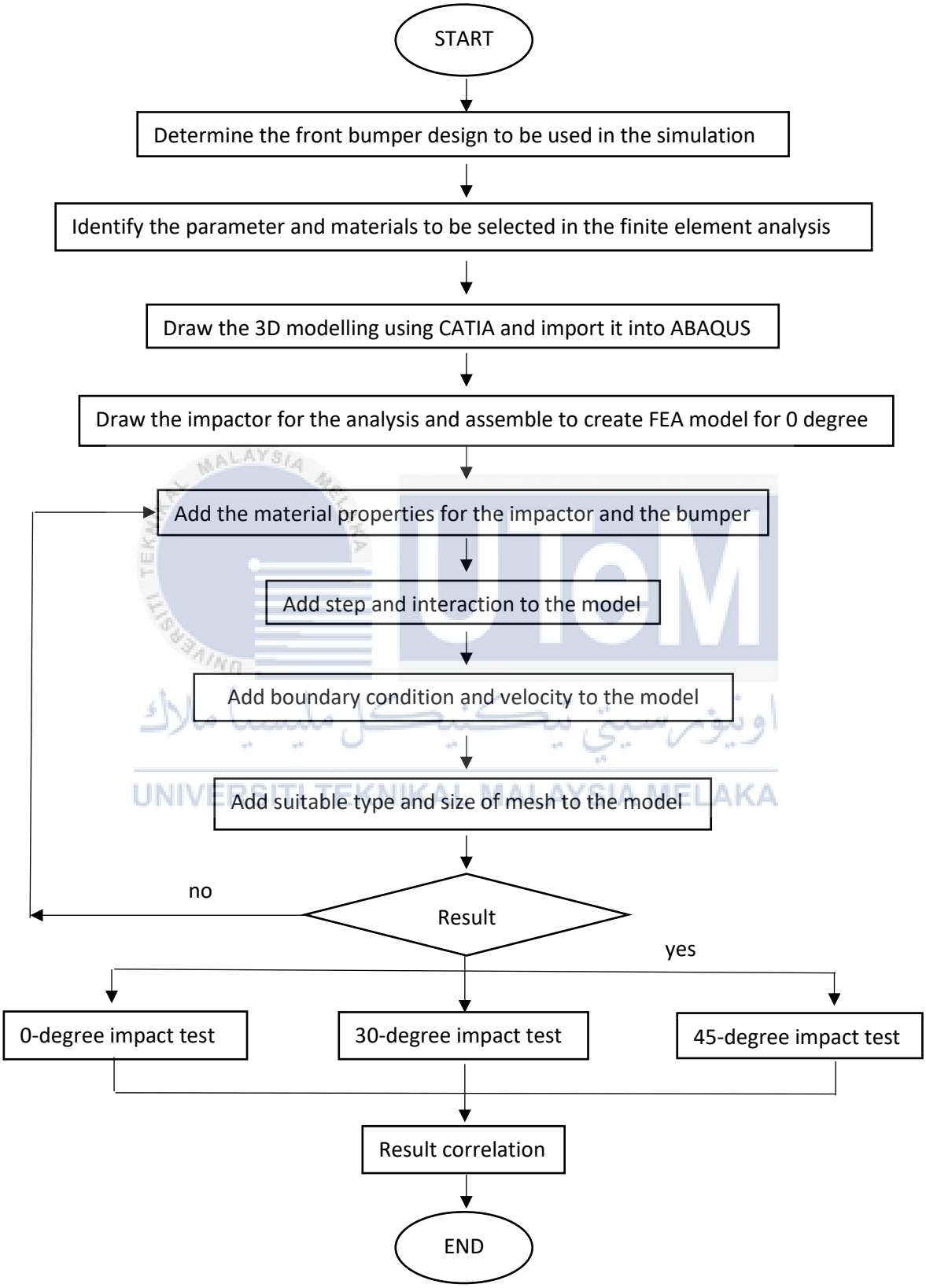

Figure 3.1: Project Flow Chart

3.3 Determining the Front Bumper Design

The design of front bumper was taken from a GEN2 standard front bumper. The accessibility to get the bumper and how the bumper has common features such as cavities for head lamps and low lamps, honey comb area for the air flow into the engine compartment and deformable are the main reasons as why the design was chosen.

3.4 Identifying the Parameters

There are parameters that are needed to be identify before furthering the study that are needed to be obtained from research such as velocity for the impactor that 80 km/hr and material for bumper and impactor which is steel.

3.4.1 Material selection

For the bumper's material, aluminium was firstly selected because it is a common material and it is easy to get its characteristics to be used in the ABAQUS. In addition, aluminium is still suitable to be manufactured as bumper compared to other common materials because of its lightweight. Furthermore, aluminium was used as a preparation material before using the real material such as polypropylene, a composite material that is frequently used for its weight and strength. As for the impactor, steel was chosen as the material.

3.4.2 Velocity of impactor

In this study, the velocity chosen for the impactor is the same for all the angle 0˚, 30˚, 45˚ that is 80 km/h or 22222.2 mm/s. This was decided between the velocities mention

in FMVSS No.208 for vehicle crash with each vehicle advancing at 50-60 km/h or with one vehicle advancing at 100-120 km/h (Hollowell et al., 1999).

3.5 3D Modelling

In this study, there are two ways of 3D modelling that had been used that are CATIA and ABAQUS though CATIA is more suitable for complex modelling.

3.5.1 Bumper

For the bumper, the drawing started from within the CATIA as this is more suitable in drawing and modelling complex 3D model. During this process, all the details from the real GEN2 bumper was added such as the dimensions, curves, and edges. By completing the modelling for half of the bumper, it was mirrored to produce a full completed bumper. Only after the modelling, the bumper model was imported to ABAQUS as shown n Figure 3.2 below.

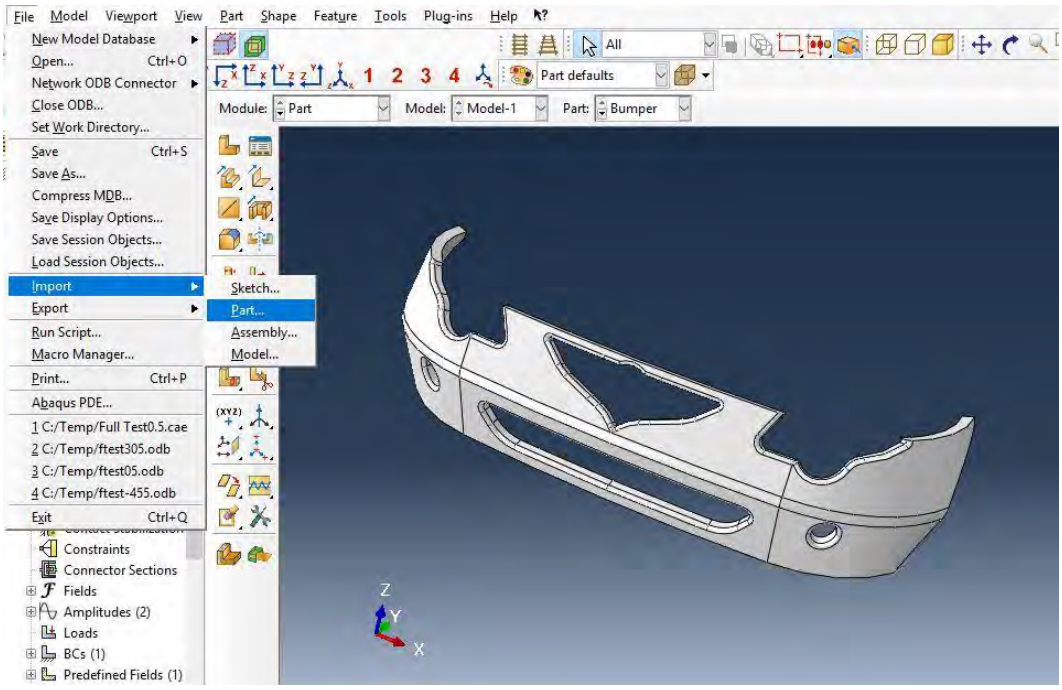

Figure 3.2: Imported front car bumper in ABAQUS.

3.5.2 Impactor

The impactor was drawn after the bumper model was imported into ABAQUS and this impactor is used for all the impact angle analysis. Under the part module, the create part button was chosen and the settings used as shown in Figure 3.3 below. Then the impactor with was drawn with a front radius of 25 mm because in a standard testing the impactor has a front radius between 20 mm to 30 mm before the value of 150 mm was entered for thickness extrusion.

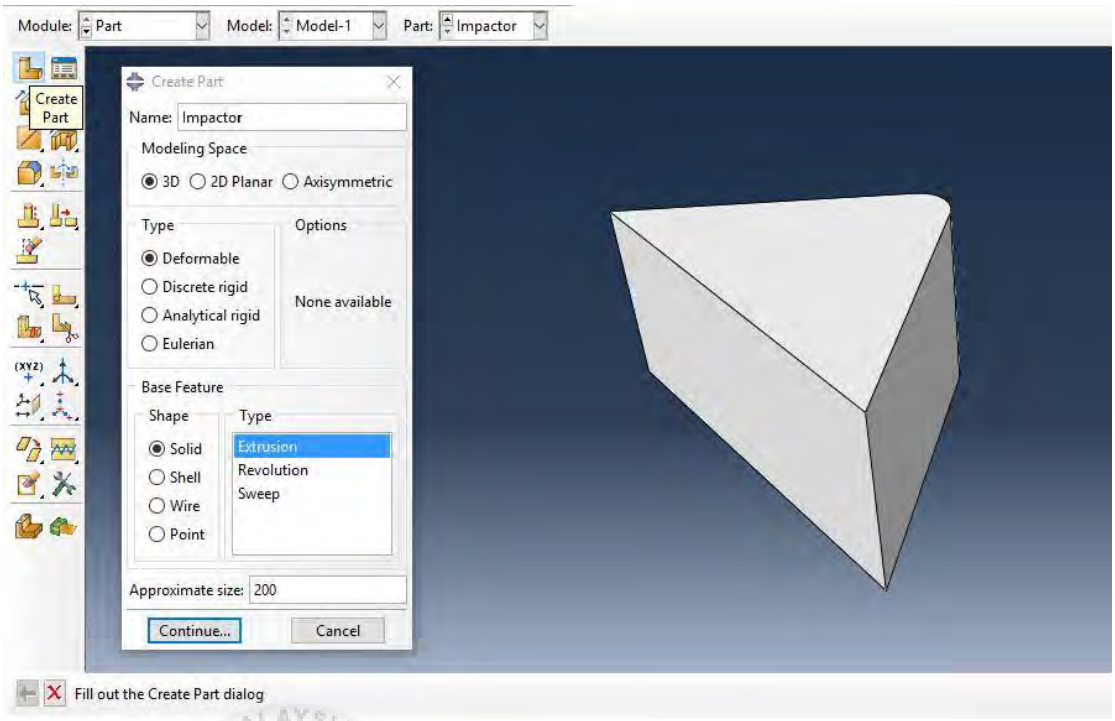

Figure 3.3: Settings to create part for impactor.

3.6 ABAQUS Sequences

The steps used in ABAQUS are further discussed in the next points

3.6.1 Assembly

The bumper and impactor were assembled, they were to face each other with the impactor need to in position of 0˚ or perpendicular towards the centre line of the bumper. This is the point where when the result of analysis is acceptable the angle is increased to 30˚ and then 45˚. The assembly module was used, the create instance button was chosen and then both impactor and bumper were picked to insert them as shown in Figure 3.4 below.

After both were inserted, the impactor's front peak was adjusted to be at the centre of bumper for distance of 5 mm from the bumper surface using translate instance button. Another button called rotate instance was used to change the angle of bumper to 30˚ and then 45˚, before the bumper was repositioned back to the 5 mm distance from the bumper surface.

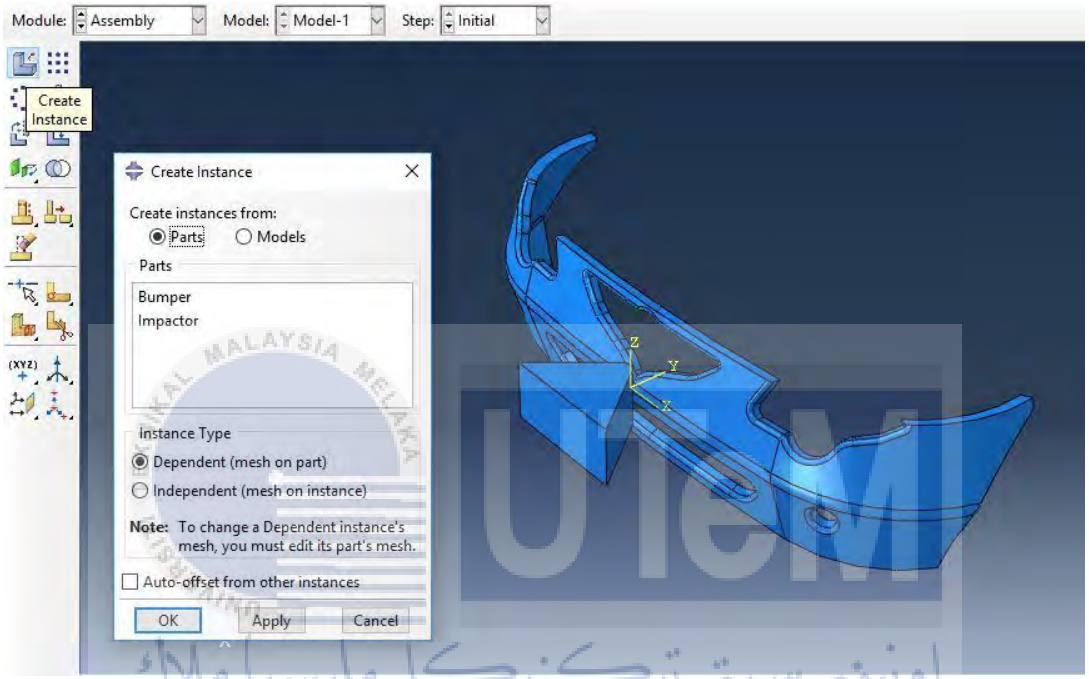

Figure 3.4: Creating assembly from impactor and bumper.

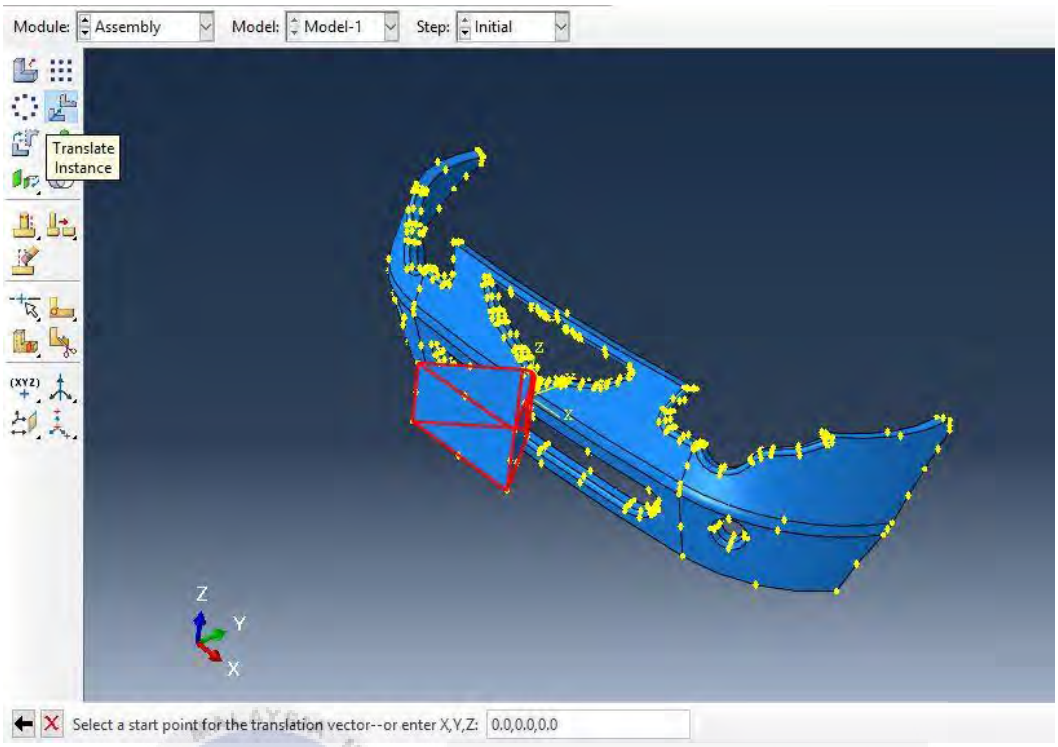

Figure 3.5: Points (yellow) used for instance (red) translation.

3.6.2 Material properties

The properties were inserted for materials of steel and aluminium as shown in Table 3.1 below for mass density, Young's modulus, and Poisson ratio. All the units used are in SI millimetre (mm). Under the property module, the create material button was chosen and it was named aluminium, after that the density and elastic material behaviours were chosen and the data was inserted as in the Table 3.1 as shown in Figure 3.6 below. The steps were repeated for material properties of steel.

Table 3.1: Material properties for aluminium and steel (Cambridge University Engineering Department, 2003).

Material	Mass density (kg/mm^3)	Young's modulus (MPa)	Poisson ratio
Aluminium	2.6E-6	70000	0.33
Steel	7.9E-6	200000	0.30

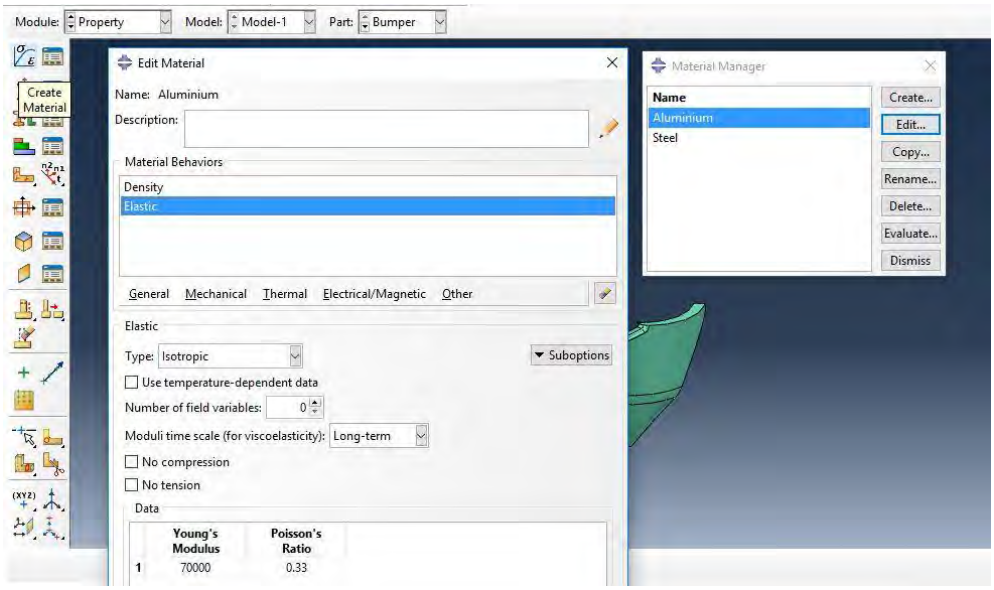

Figure 3.6: Inserting the material properties for aluminium and steel.

The material was applied towards the bumper and impactor, a section must be created first before assigning the material. As shown in Figure 3.7, the create section button was chosen and then it was named as the material that will be assigned to it, the same settings in figure were used and then the material was assigned. In Figure 3.8, both the impactor and bumper change its colour to green after it was correctly assigned to one of the material.

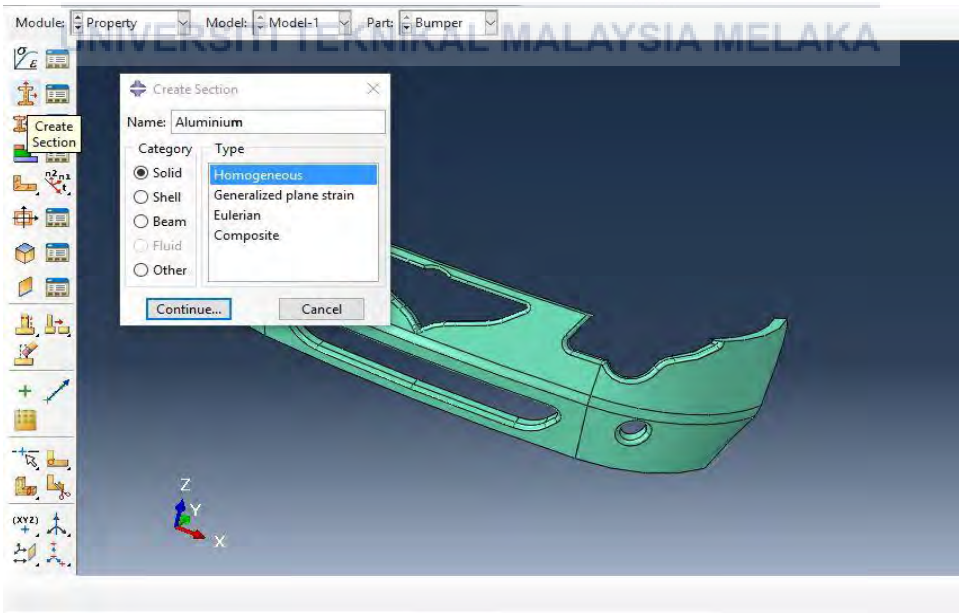

Figure 3.7: Creating section for each material.

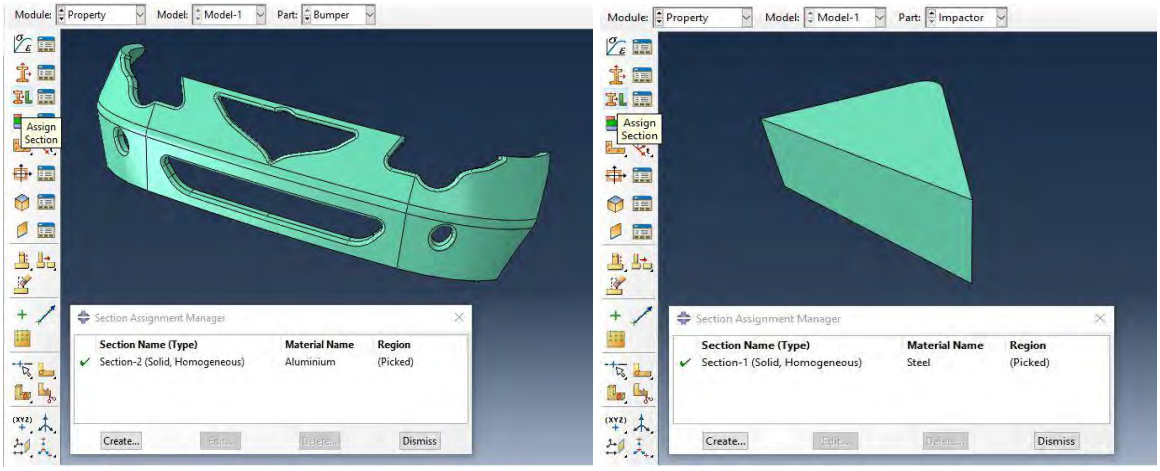

Figure 3.8: Green bumper and impactor indicate that the materials are correctly assigned.

3.6.3 Step

In this step module, the main things to be taken note is the type of step after the initial step. The create step button was chosen and it was named Step-1 and the settings as shown in Figure 3.9 below was used and continue to set the period appropriately. For this study, the period was set 0.0015 second because although the 0˚ simulation can proceed until 0.01 second, the other 30˚ and 45˚ simulation cannot proceed further than that or the simulation will abort. In this step, the Field output and History output were managed, however the default settings are already enough for this study results so nothing else was changed.

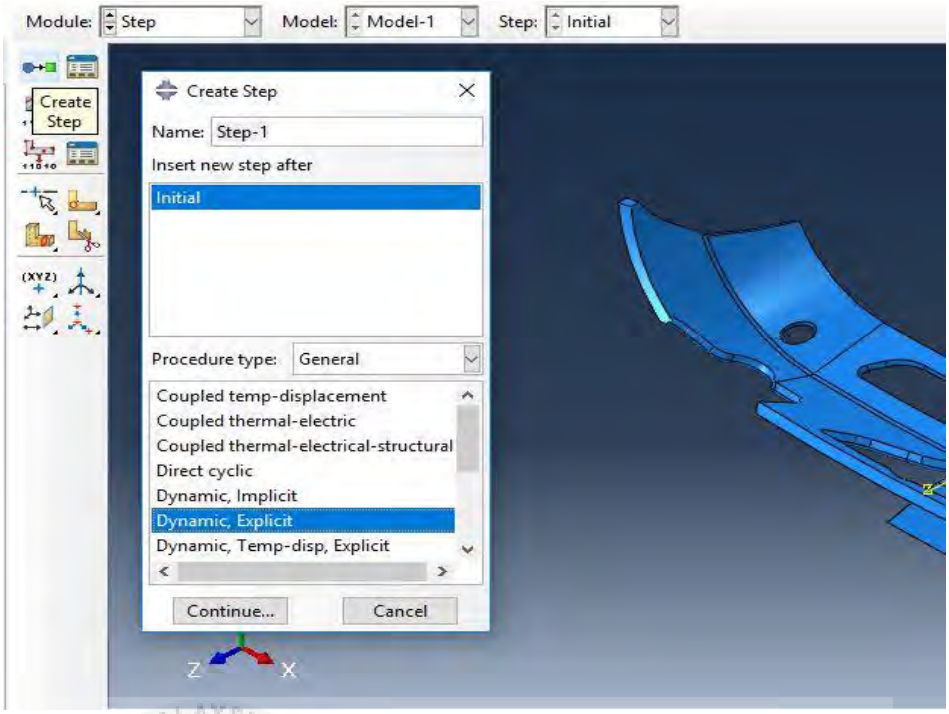

Figure 3.9: Settings for the Step-1.

3.6.4 Interaction

Interaction step module required the setting as shown below in Figure 3.10 this was done after choosing the create interaction button. Type and step chosen were made sure to the same as figure. Then the create the interaction property button was chosen and the setting was inputted as in Figure 3.11, the tangential and normal behaviour were picked as the property but nothing else was changed.

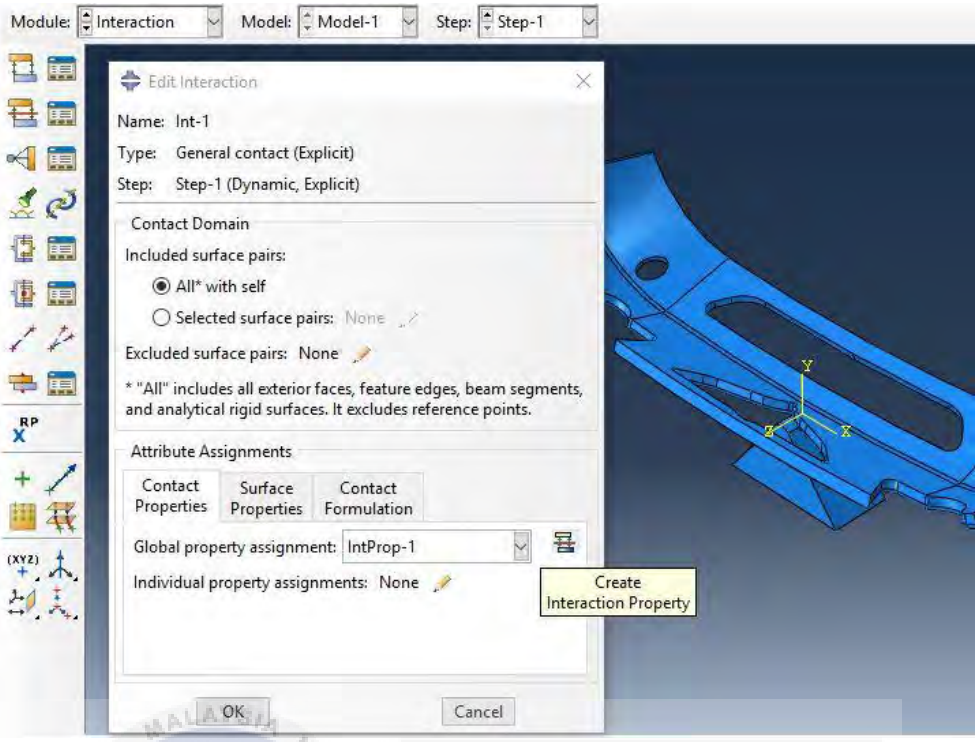

Figure 3.10: Settings for interaction.

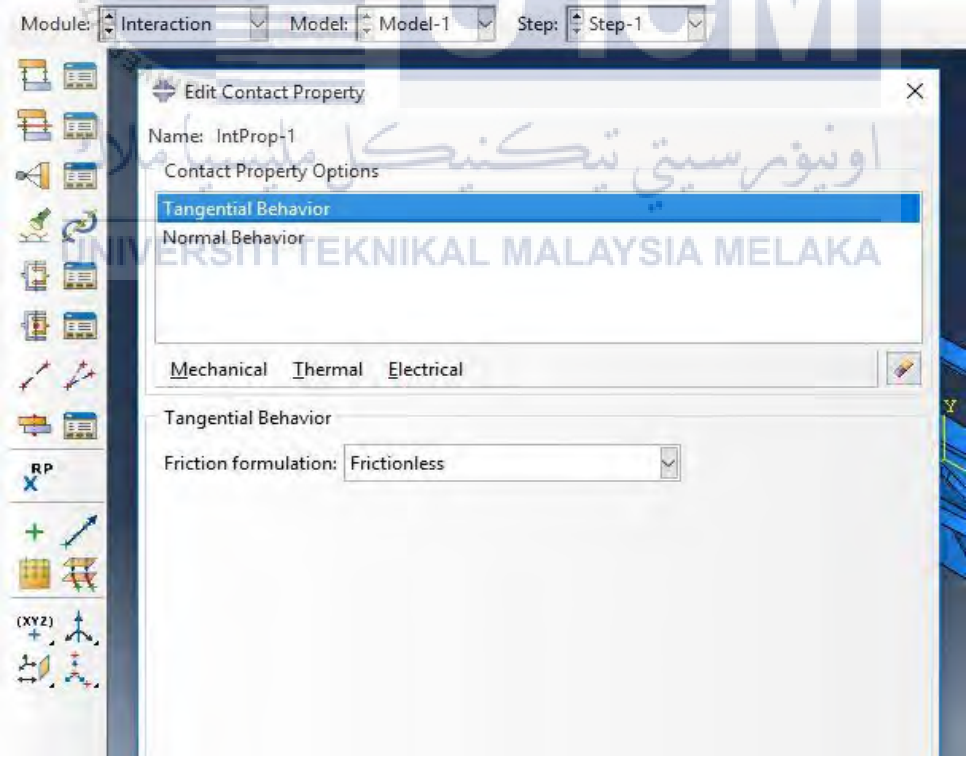

Figure 3.11: Settings for the interaction property.

3.6.5 Load

Boundary condition on the bumper was determined from the position of the pin on the original bumper and settings used was made sure are the same as the settings in the Figure 3.12 for its type, step and point chose for the pins. From Figure 3.13, the velocity inserted on V2 area was shown as positive because V2 represents velocity in y-axis direction with positive direction.

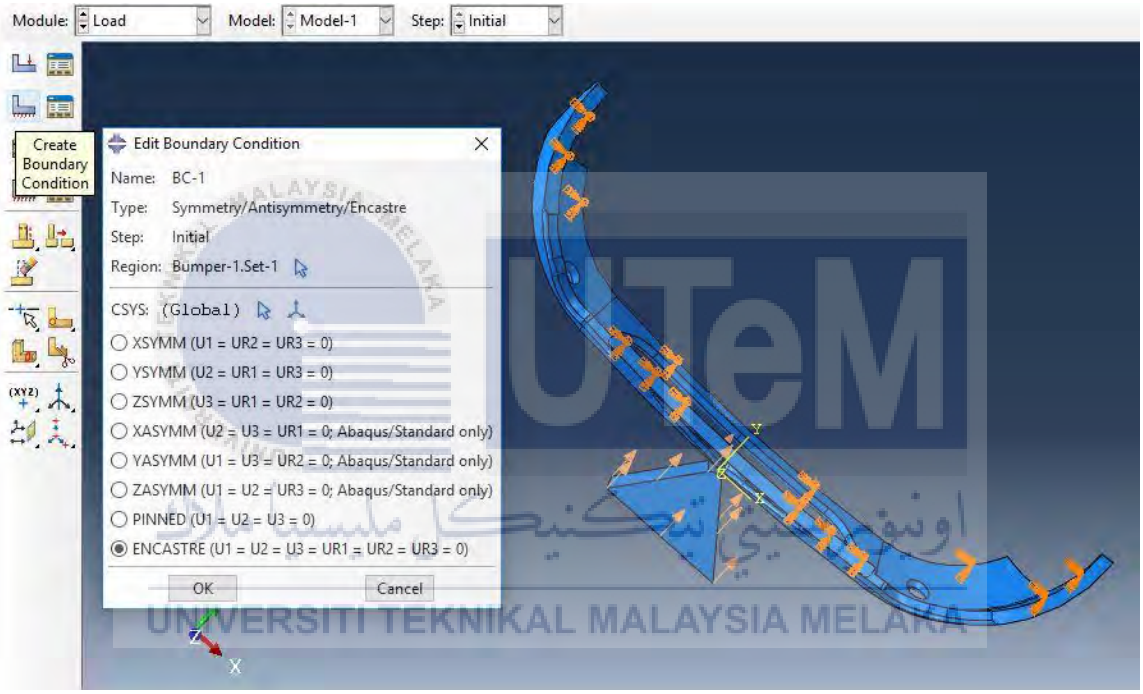

Figure 3.12: Settings for boundary condition on bumper.

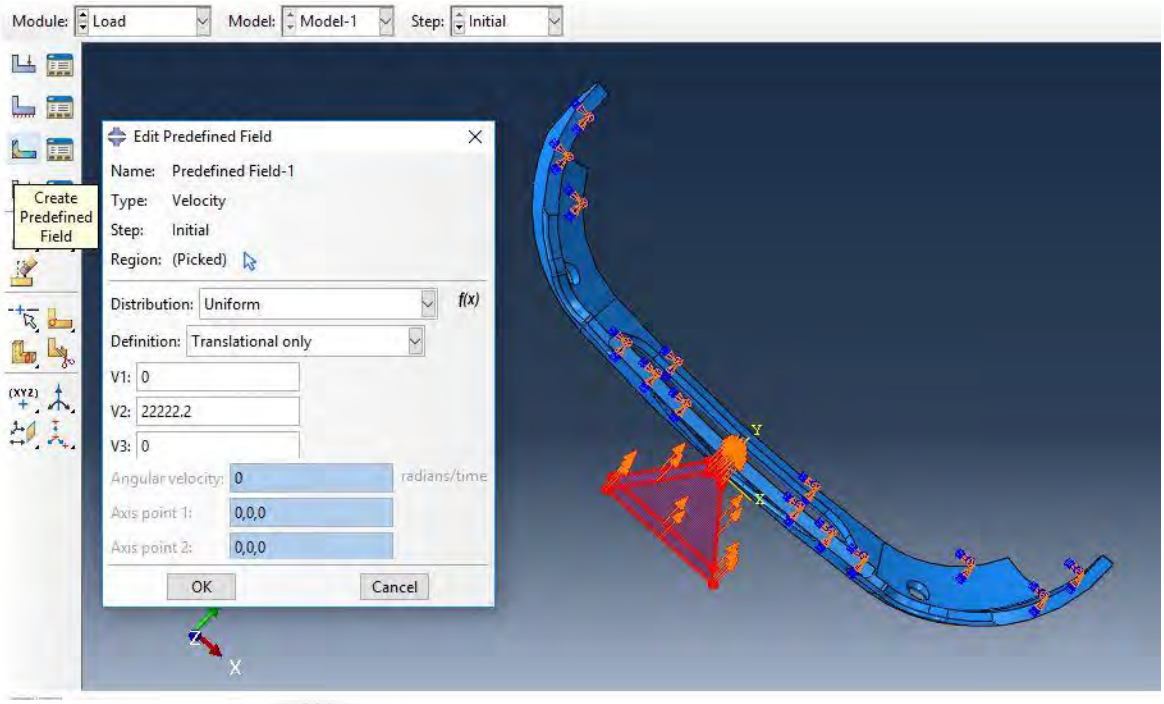

Figure 3.13: Inserting the velocity for impactor.

3.6.6 Meshing

The mesh model of bumper was constructed using tetrahedral element because of its irregularity (Chang & Yang, 2009). The model of the impactor was created with hexahedral element because it has more uniform shape. All the mesh used the 30 mm sizing, after choosing the type of mesh, the mesh part button was chosen to perform the meshing. This can be seen in Figure 3.14 and Figure 3.15 below. After the meshing was done, the impactor had produced a total number element of 340 while the bumper had produced a total number element of 9596.

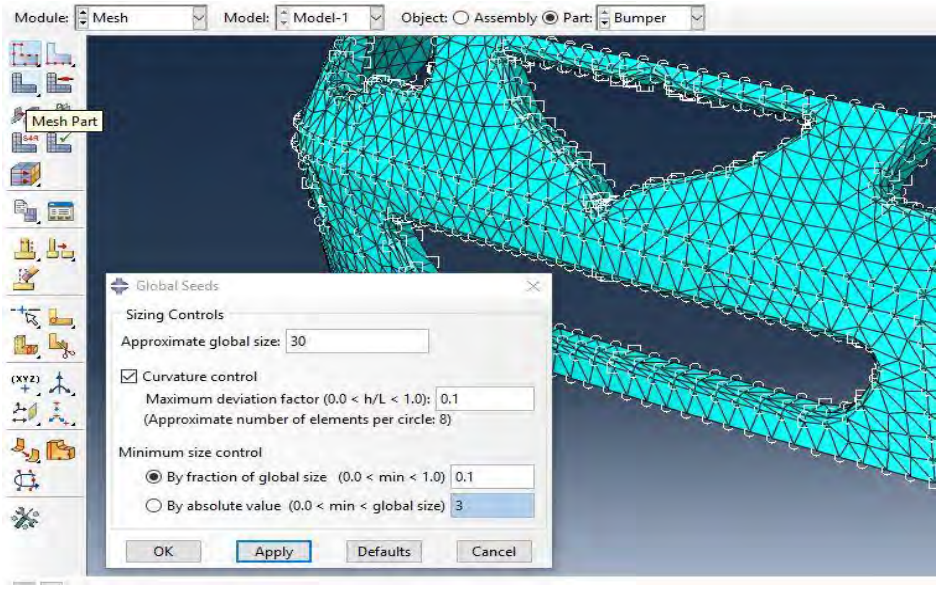

Figure 3.14: Tetrahedral meshing for bumper.

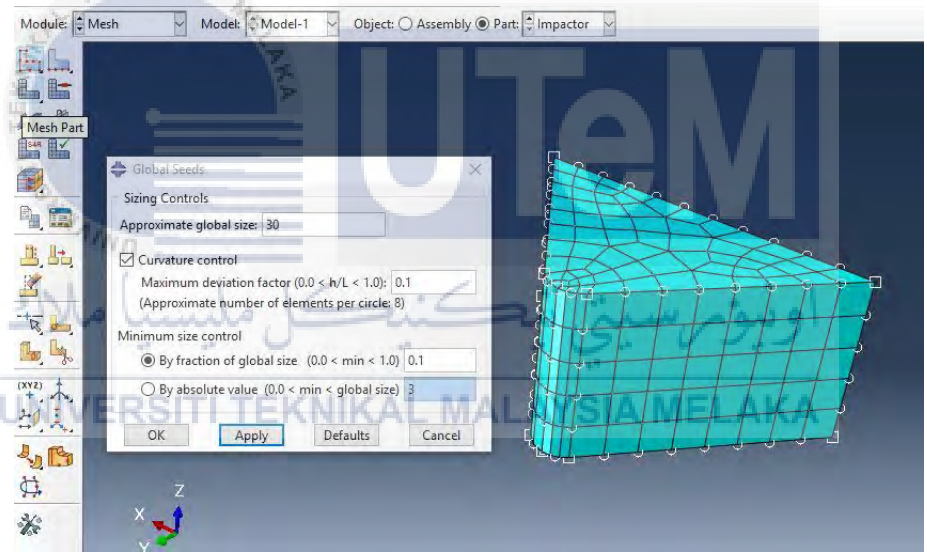

Figure 3.15: Hexahedral meshing for impactor.

3.6.7 Job

In the job module, a new job was created and other setting was not change and the job was submitted for simulation as shown in Figure 3.16. After that ABAQUS was let to run until the results came out. If there is any problem, troubleshoot it in needed model by referring the error report from ABAQUS.

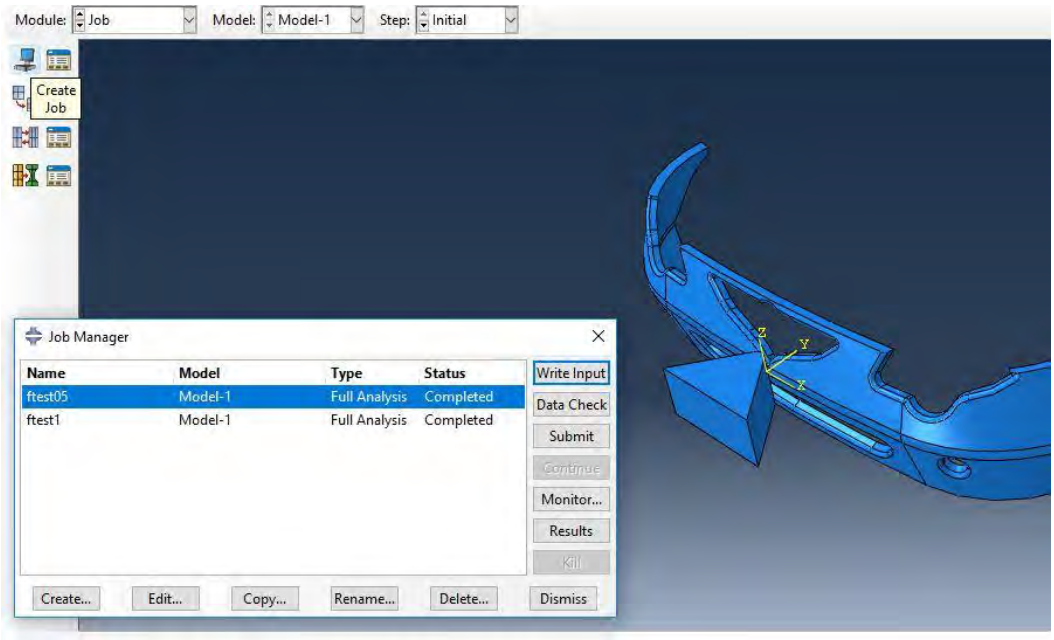

Figure 3.16: Submitting data on job module.

3.7 Result

The first analysis done is for the 0˚ because with no angle of impact the analysis should be simpler and this will make any troubleshooting for parameters, meshing or boundary condition easier. When this 0˚ analysis produced a good data, then the impact angle was changed to 30˚ and 45˚. The simulation was run all over until all the needed data are obtained.

Chapter 4

RESULT, ANALYSIS, AND DISCUSSION

4.1 Introduction

The simulation of deformation in a front car bumper has been studied. The brief methodology of the study is a front car bumper has been chosen to be impacted by an impactor with constant velocity for 3 different 0˚, 30˚ and 45˚ impact angle. The energy absorption is obtained from the force-displacement graph for each impact angle.

4.2 Deformation in Simulation for 0˚ Impact

The simulation of 0˚ impact is prepared according to the previous flowchart in Chapter 3 and the results after the simulation can be seen in Figure 4.1 below.

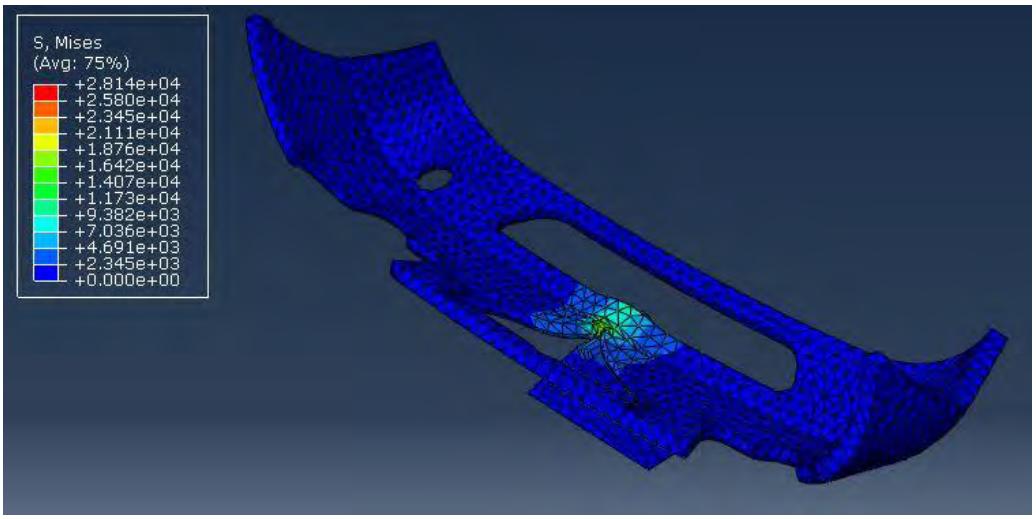

Figure 4.1: Von Mises stress for 0˚ impact.

However, for this study, the data needed is the force and displacement on the bumper to show the energy absorption of bumper as shown in Figure 4.2 and Figure 4.3 below. The reaction force obtained is from the two top pins at the centre, this is because the impactor strike at the centre of bumper, however there is no reaction from the bottom because the space between the impact area and bottom pins. In addition, the reaction force is taken from the highest value available. For the displacement on the bumper, the result shows that the most displaced area located directly in front of the tip of the impactor and the value is taken at this point.

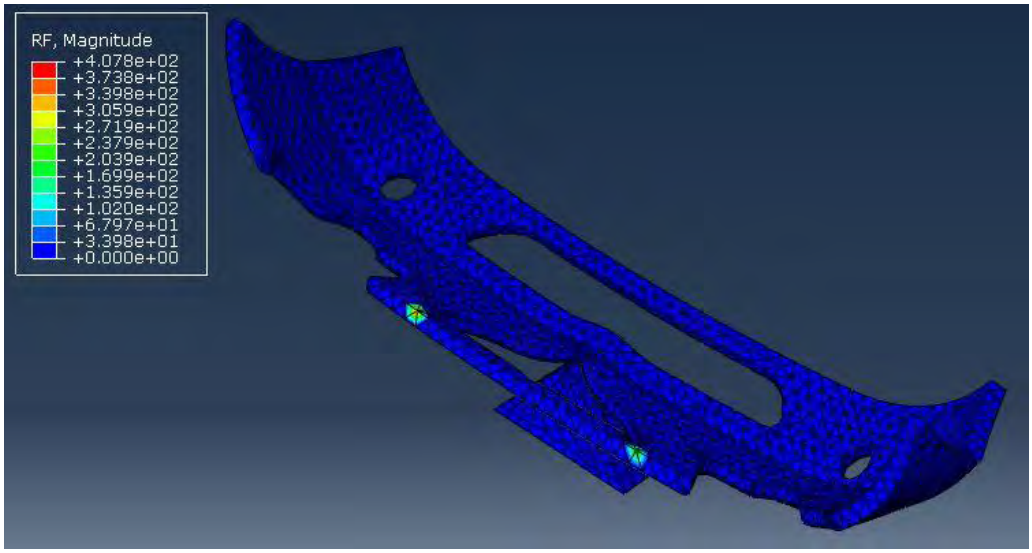

Figure 4.2: Reaction force on the top pins.

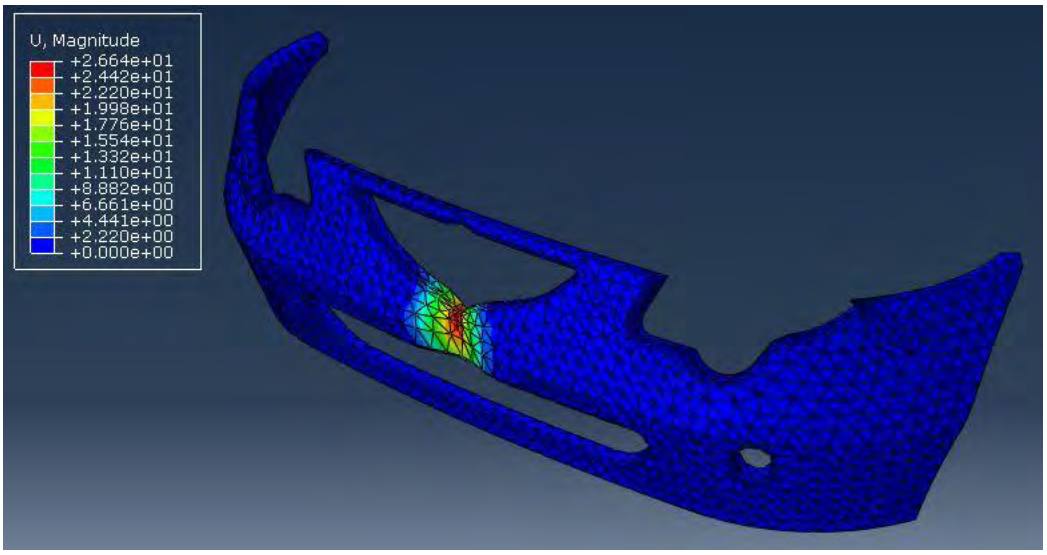

Figure 4.3: Displacement on the bumper.

It is needed to obtain the average value from the area inside the red zone (highest displacement) therefore 4 nodes are chosen for their displacement values as can be seen in Figure 4.4 below. From the Figure 4.5, the graph shows that all the four force-displacement graph line have the same trend.

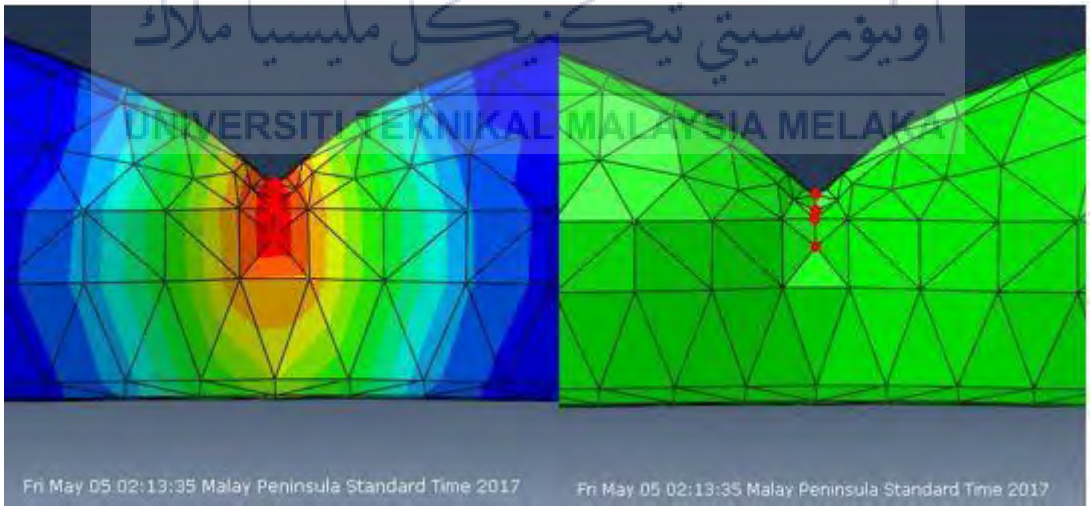

Figure 4.4: Four nodes taken for 0˚ impact.

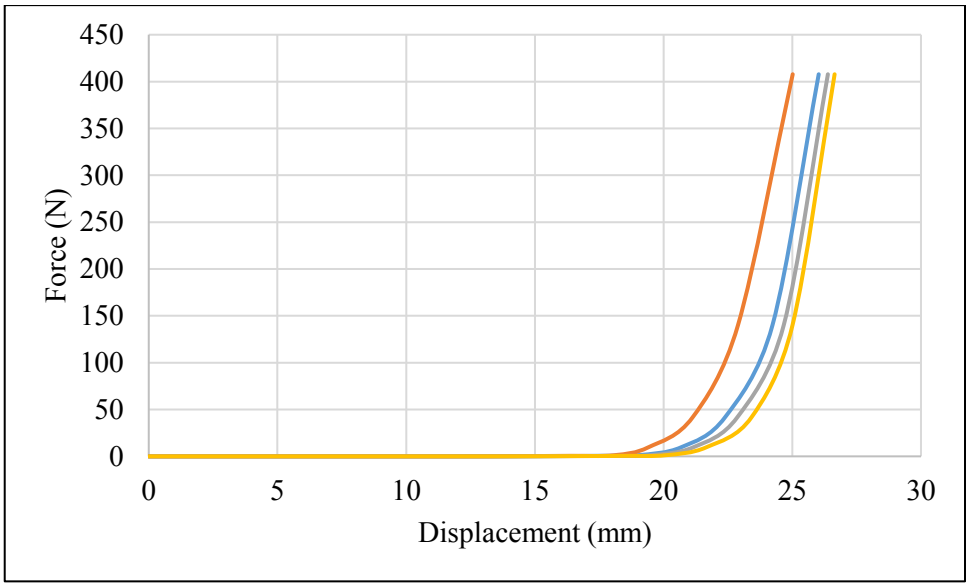

Figure 4.5: Graph of force-displacement at four nodes for 0˚ impact.

The data for average reaction force and displacement are shown in Table 4.1 and the graph of average force-displacement can be seen in Figure 4.6 below. From the Table 4.1 we can see that highest displacement is 26.0182 mm and highest reaction force is 407.805 N but there is still increasing force during the whole process. However, in the graph in Figure 4.6 there is no notable force increases in the early displacement until it reaches the 19 mm because of the previous values are too small.

Table 4.1: Average displacement and force values in 0˚ impact.

Displacement (mm)	0.2018	1.3879	17.6279	19.1626	26.0182
Force (N)	0	5.14E-17	0.560333	1.2244	407.805

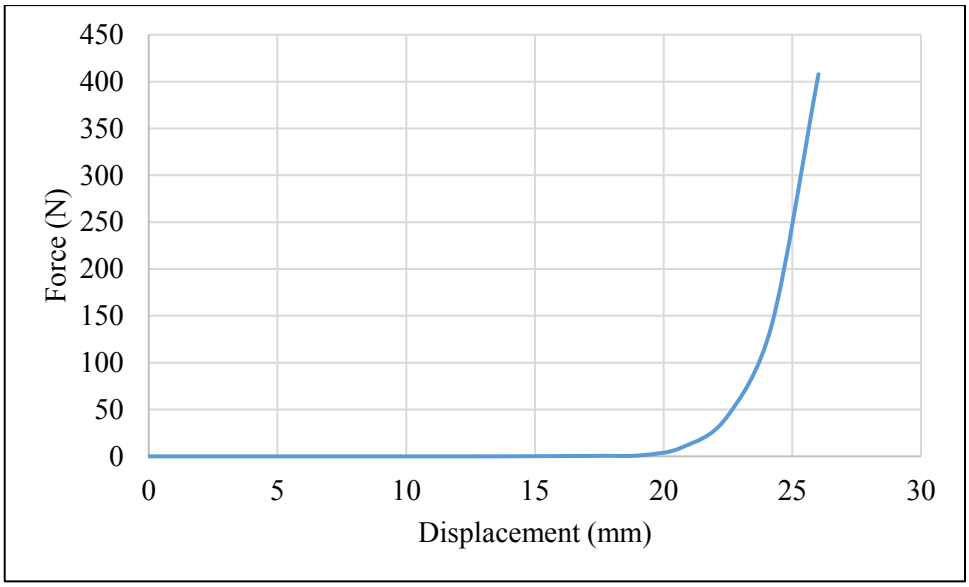

Figure 4.6: Graph of average force-displacement for 0˚ impact.

The simulation also gives the data for the internal energy and kinetic energy at the last simulation time for the whole model. When the kinetic energy decrease, the internal energy should increase because of the energy balance and for the 0˚ impact the highest value for internal energy is 2.21E+^{08} J and for the kinetic energy 9.31E+^{09} J both for the duration of 0.0015 second as shown in the Figure 4.7 and Figure 4.8 below.

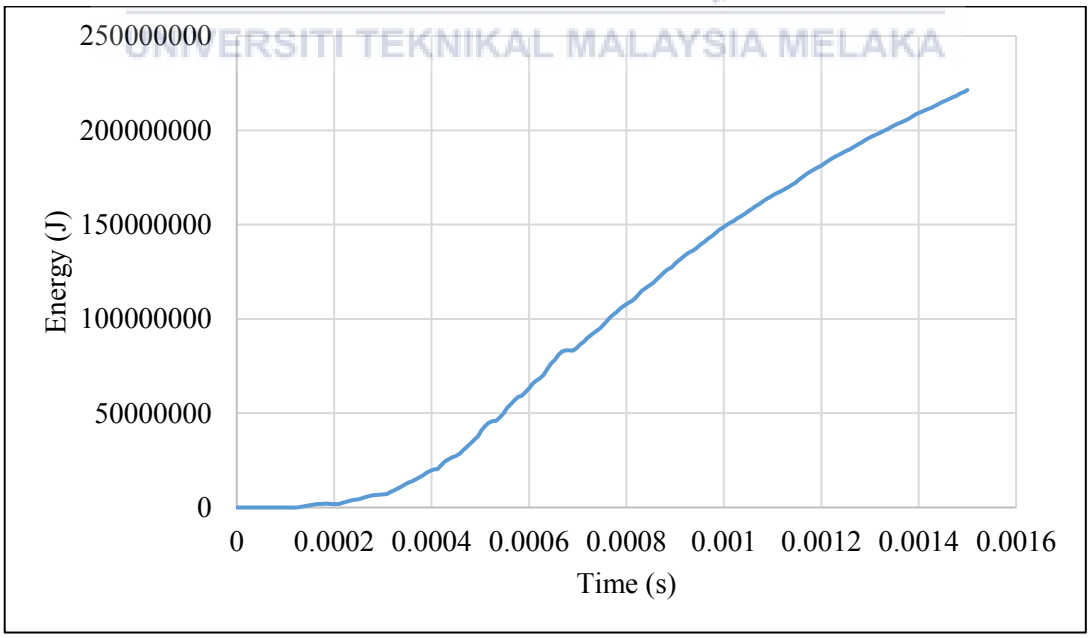

Figure 4.7: Internal energy graph for 0˚ impact.

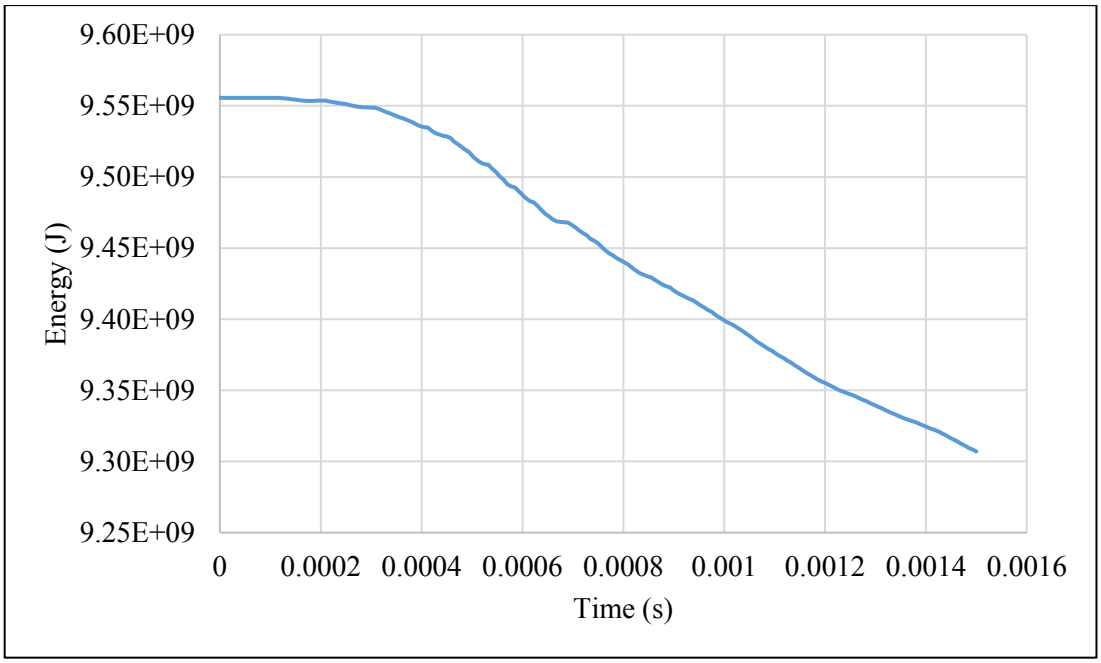

Figure 4.8: Kinetic energy graph for 0˚ impact.

4.3 Deformation in Simulation for 30˚ Impact

In the simulation of 30˚ impact, the result obtained is shown in the Figure 4.9 below.

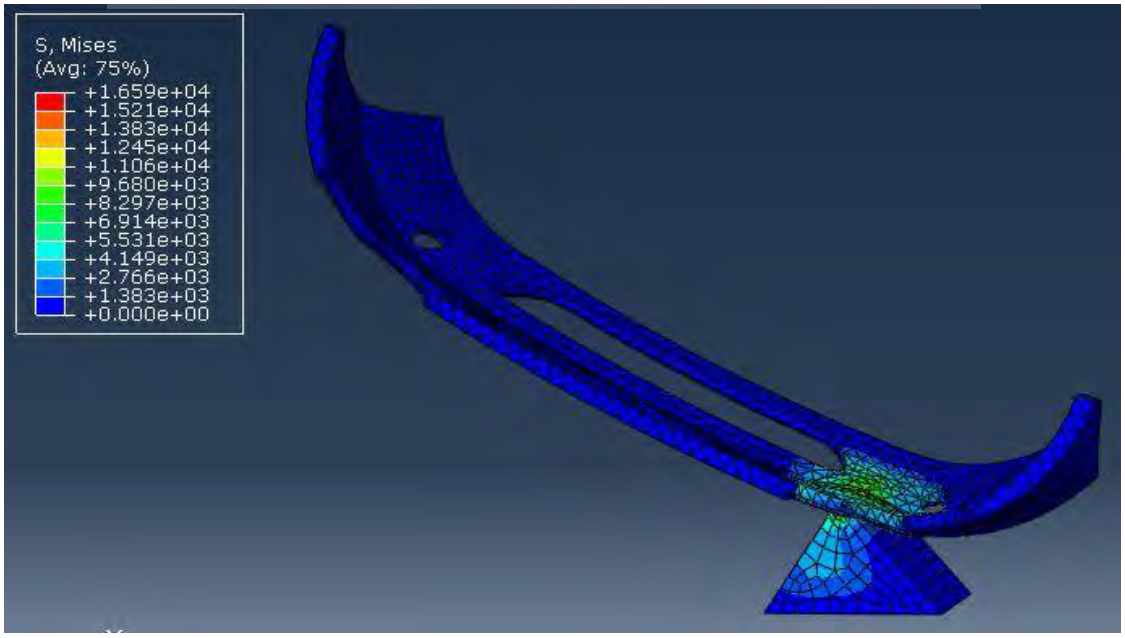

Figure 4.9: Von Mises stress for 30˚ impact.

For this 30˚ impact, the reaction force obtained is from the two top pins on the right side above the impactor. This is because the impactor strikes near that area, however there is no reaction from the bottom pin because the impactor is closer to the top pin. The reaction force and the displacement on the bumper is obtained from the point of the highest value. The reaction force area and displacement area is shown in Figure 4.10 and Figure 4.11 below.

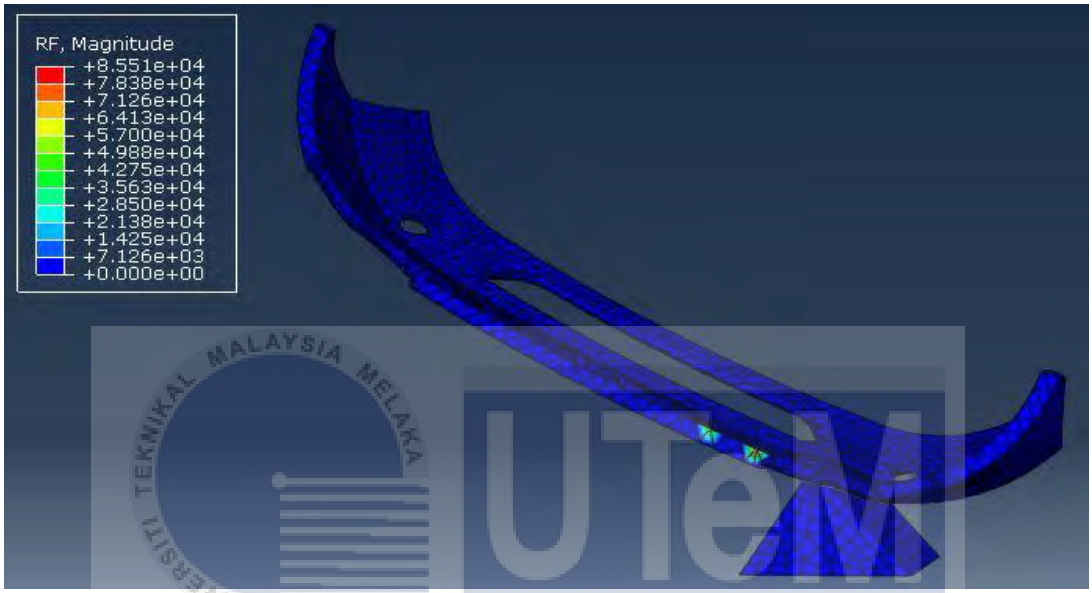

Figure 4.10: Reaction force on the top right-side pins.

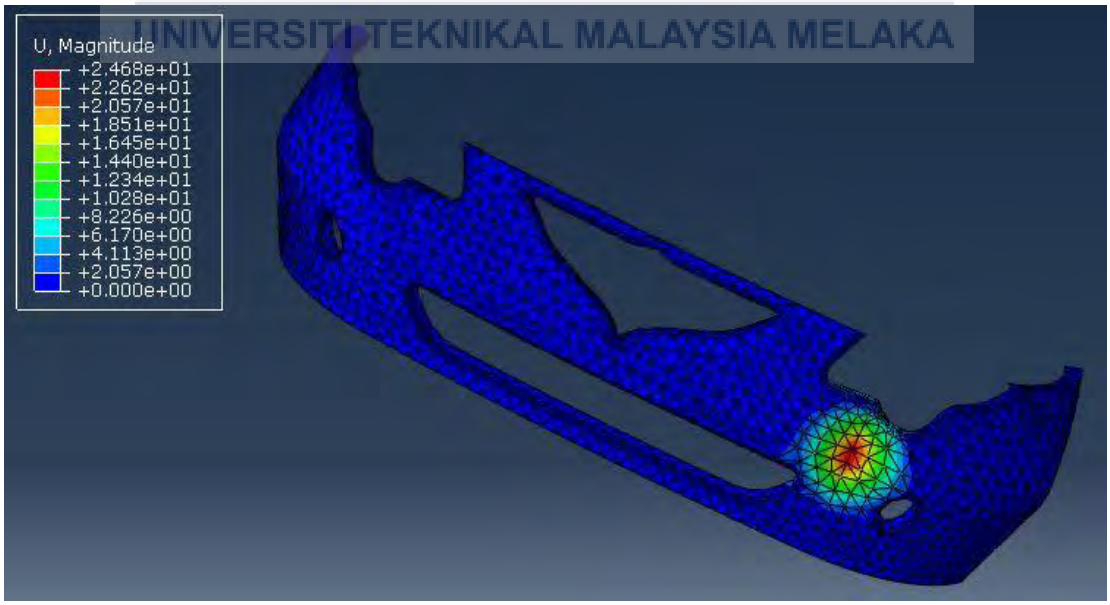

Figure 4.11: Displacement on the bumper.

It is needed to obtain the average value from the area inside the red zone (highest displacement) therefore 4 nodes are chosen for their displacement values as can be seen in Figure 4.12 below. From the Figure 4.13, the graph shows that all the four force-displacement graph line have the same trend with the nodes that are not in the red zone showed less displacement. In this simulation two nodes taken are in the red zone and the other two in orange zone.

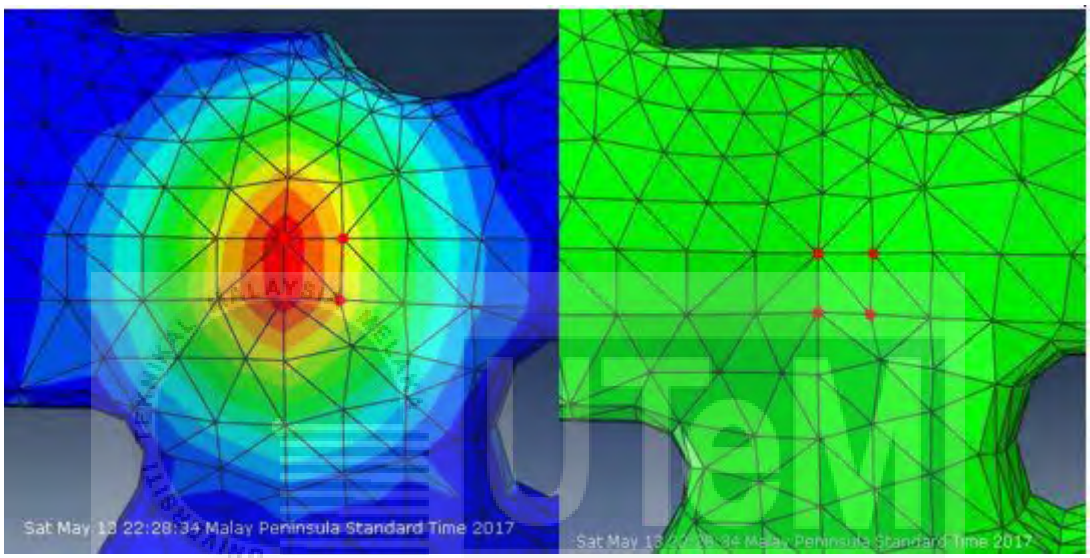

Figure 4.12: Four nodes taken for 30˚ impact.

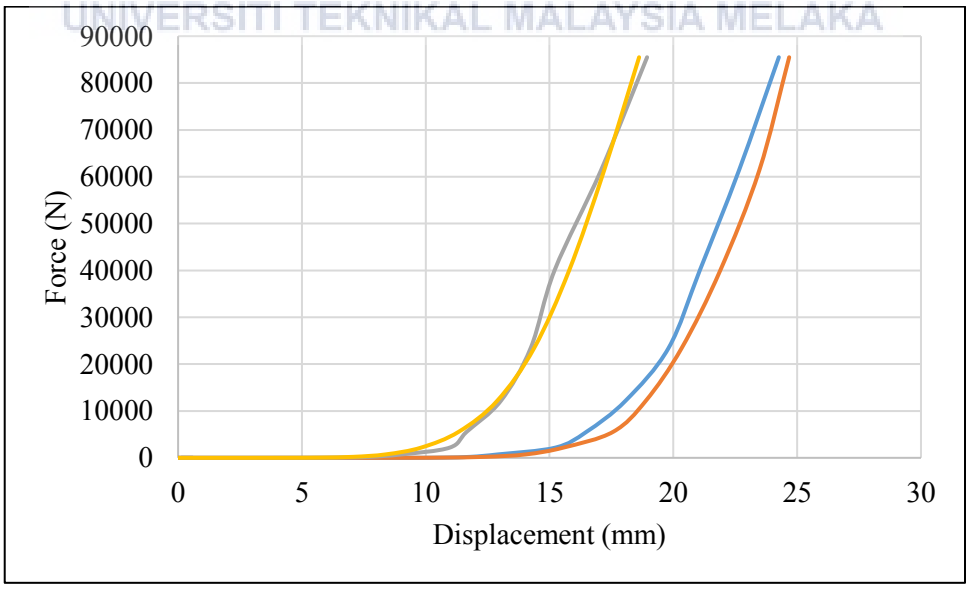

Figure 4.13: Graph of force-displacement at four nodes for 30˚ impact.

The data for average reaction force and displacement are shown in Table 4.2 and the graph of average force-displacement can be seen in Figure 4.14 below. From the Table 4.2 we can see that highest displacement is 24.6241 mm and highest reaction force is 85506.4 N but there is still increasing force during the whole process. However, in the graph in Figure 4.14 there is no notable force increase in the early displacement until it reaches the 10 mm because of the previous values are too small.

Table 4.2: Average displacement and force values in 30˚ impact

Displacement (mm)	0.2335	0.4280	5.7067	9.7745	21.6241
Force (N)	0	9.30E-13	1.40668	214.77	85506.4

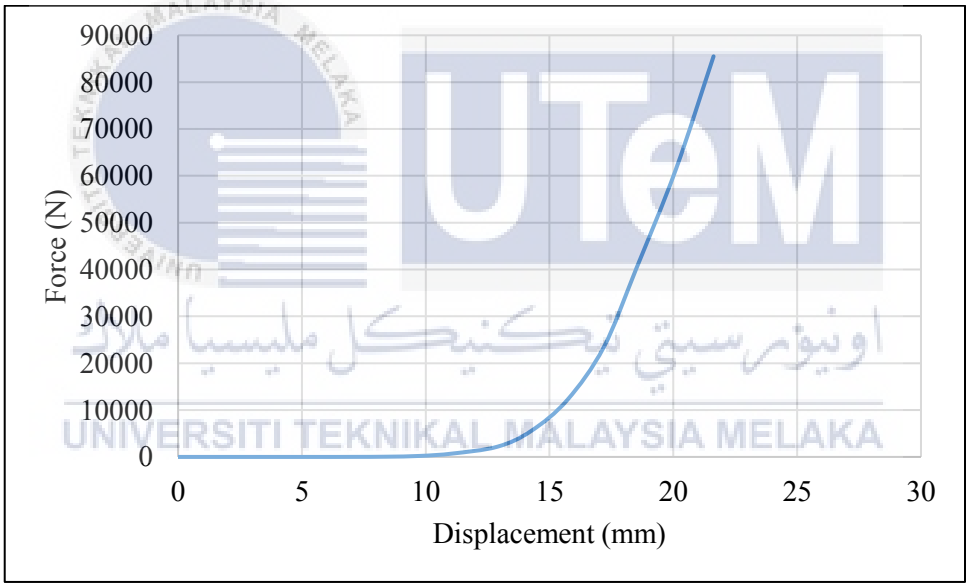

Figure 4.14: Graph of average force-displacement for 30˚ impact.

.

In this 30˚ impact simulation, the graph also shows that the internal energy increase when kinetic energy decrease. The highest value for internal energy is 3.29E+^{08} J and for the kinetic energy 9.22E+^{09} J both for the duration of 0.0015 second as shown in the Figure 4.15 and Figure 4.16 below.

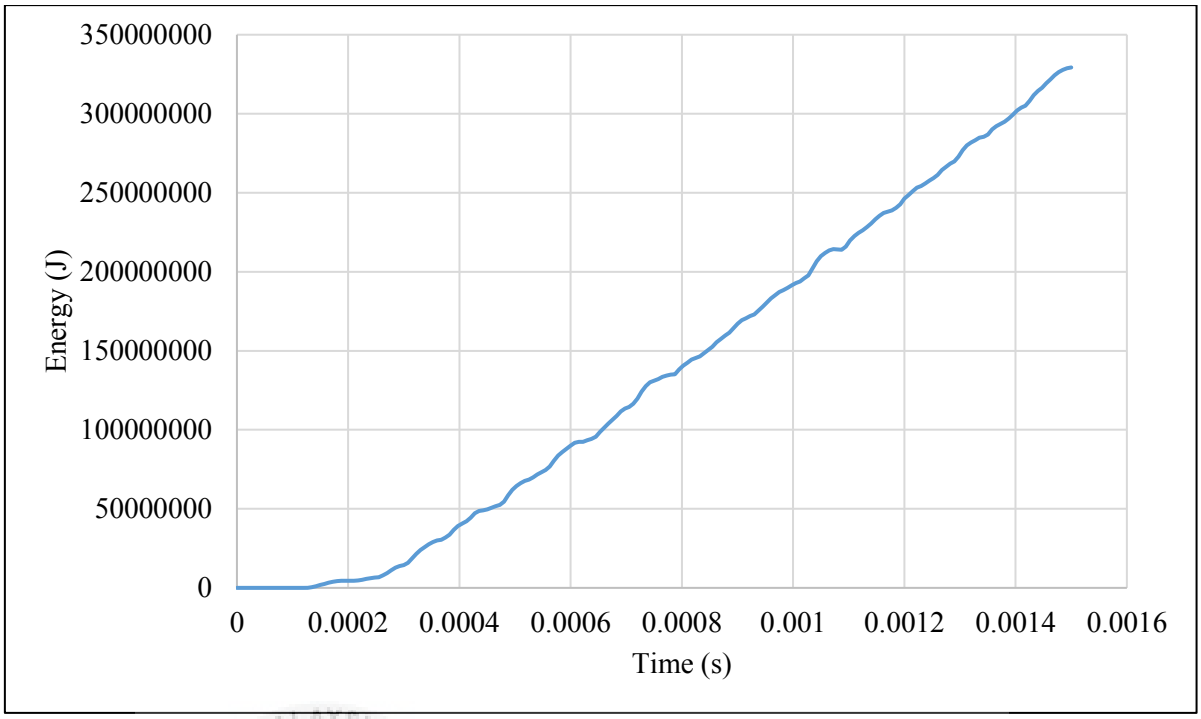

Figure 4.15: Internal energy graph for 30˚ impact.

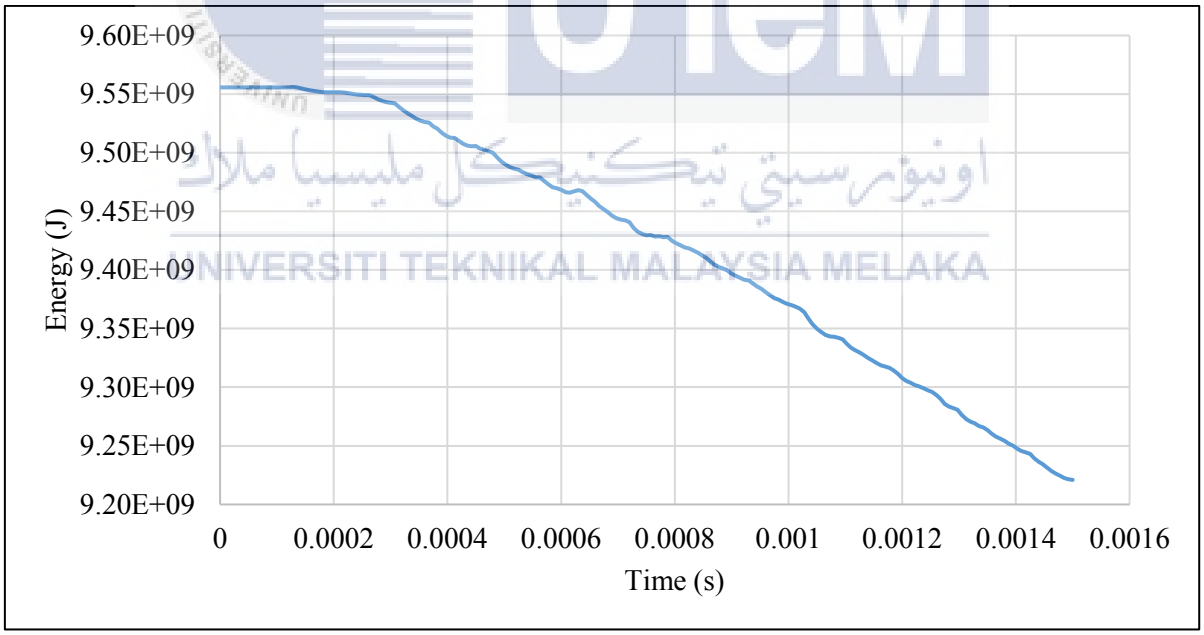

Figure 4.16: Kinetic energy graph for 30˚ impact.

4.4 Deformation in Simulation for 45° Impact

In the simulation of 45° impact, the result obtained is shown in the Figure 4.17 below.

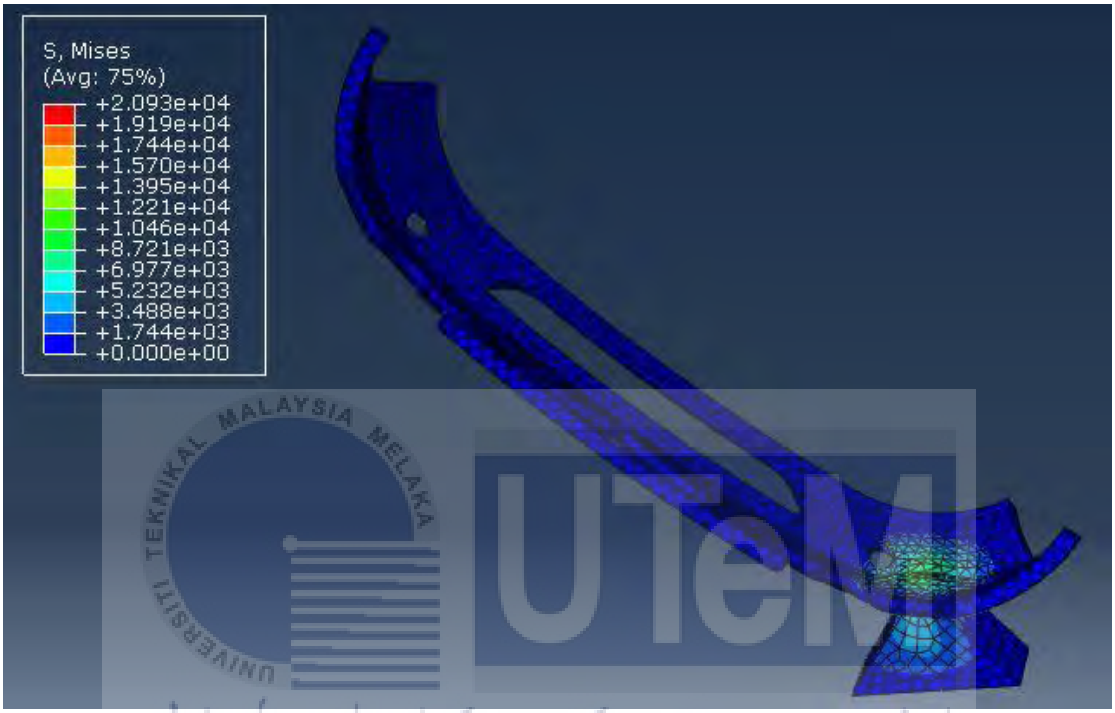

Figure 4.17: Von Mises stress for 45° impact.

For this 45° impact, the reaction force obtained is from the bottom pin on the right side below the impactor. This is because the impactor strikes an area under the head lamp, therefore there is no pin on the top and only a single pin on the bottom. The reaction force and the displacement on the bumper is obtained from the point of the highest value. The reaction force area and displacement area is shown in Figure 4.18 and Figure 4.19 below.

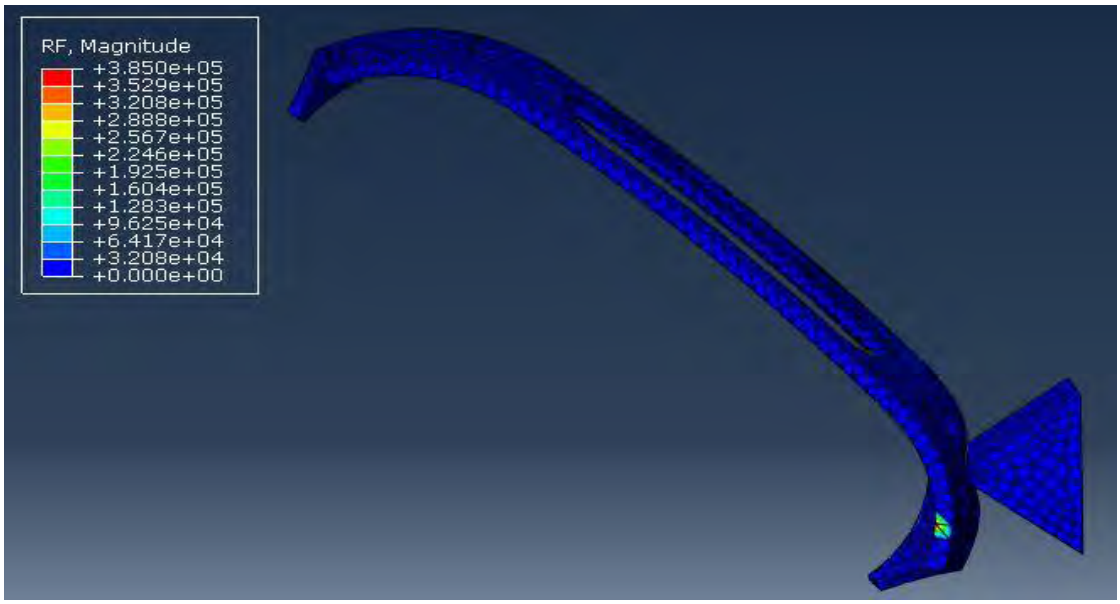

Figure 4.18: Reaction force on the bottom right-side pin.

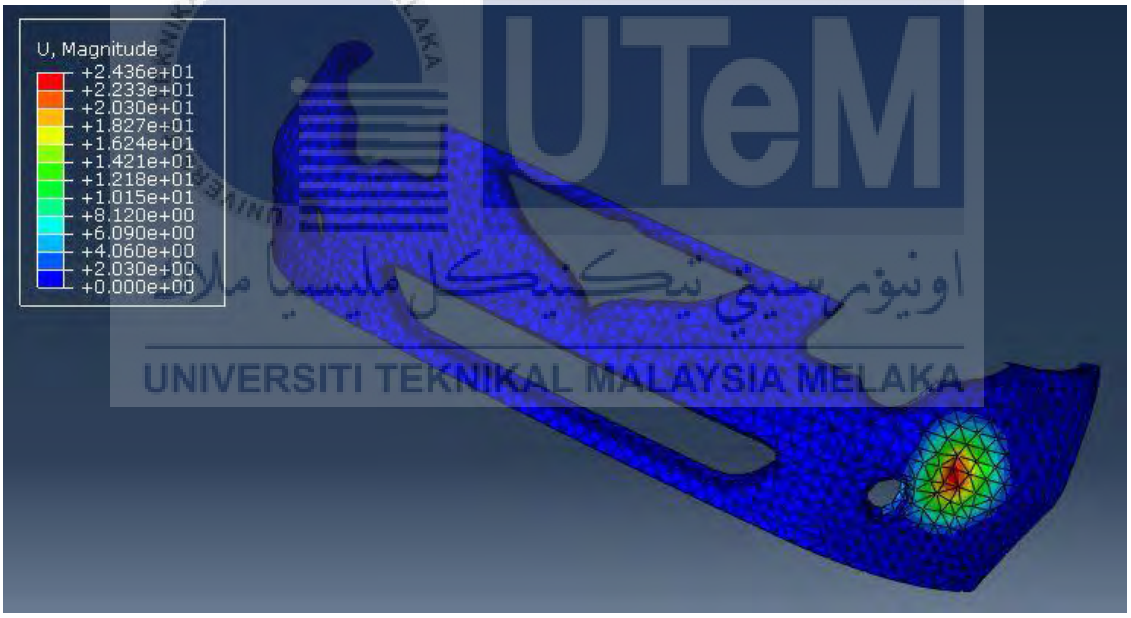

Figure 4.19: Displacement on the bumper.

It is needed to obtain the average value from the area inside the red zone (highest displacement) therefore 4 nodes are chosen for their displacement values as can be seen in Figure 4.20 below. From the Figure 4.21, the graph shows that all the four force-displacement graph line have the same trend with the nodes that are not in the red zone showed less displacement. There are two nodes in red zone but only one is at centre of red zone and the other is at the edge thus the displacement value is less from at the centre.

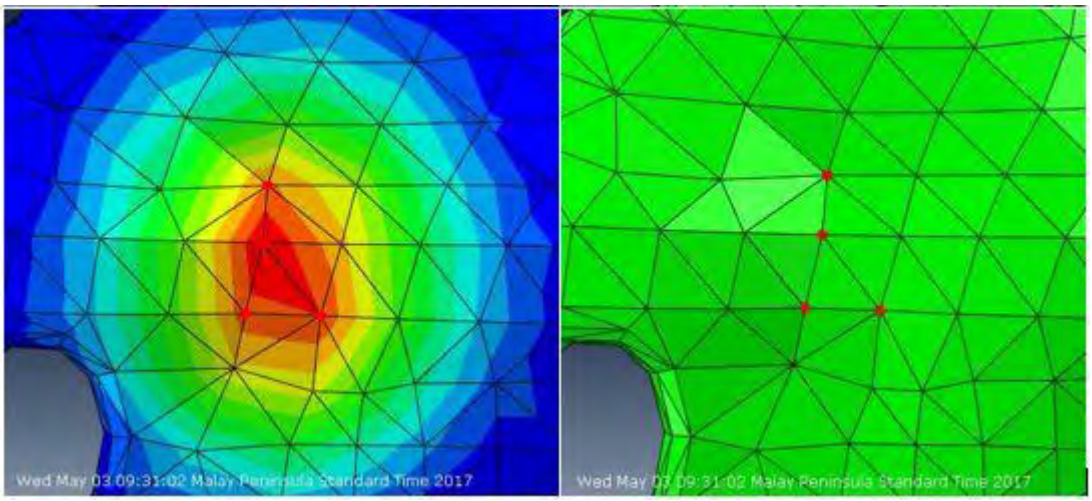

Figure 4.20: Four nodes taken for 45˚ impact.

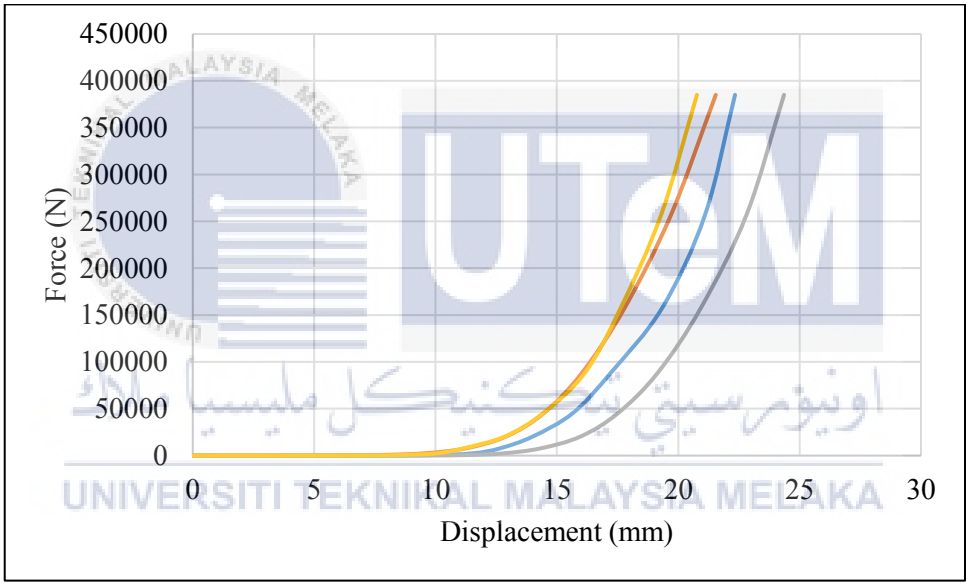

Figure 4.21: Graph of force-displacement at four nodes for 45˚ impact.

The data for average reaction force and displacement are shown in Table 4.3 and the graph of average force-displacement can be seen in Figure 4.22 below. From the Table 4.3 we can see that highest displacement is 24.25425 mm and highest reaction force is 385019 N but the force always increases depending on time. However, in the graph in Figure 4.22, the force can be only seen to increase when the displacement reaches the 11 mm because of the previous values are too small.

Table 4.3: Average displacement and force values in 45˚ impact.

Displacement (mm)	0.03378	4.77258	10.98869	15.53183	22.25425
Force (N)	2.00E-18	2.72282	2448.47	45588.1	385019

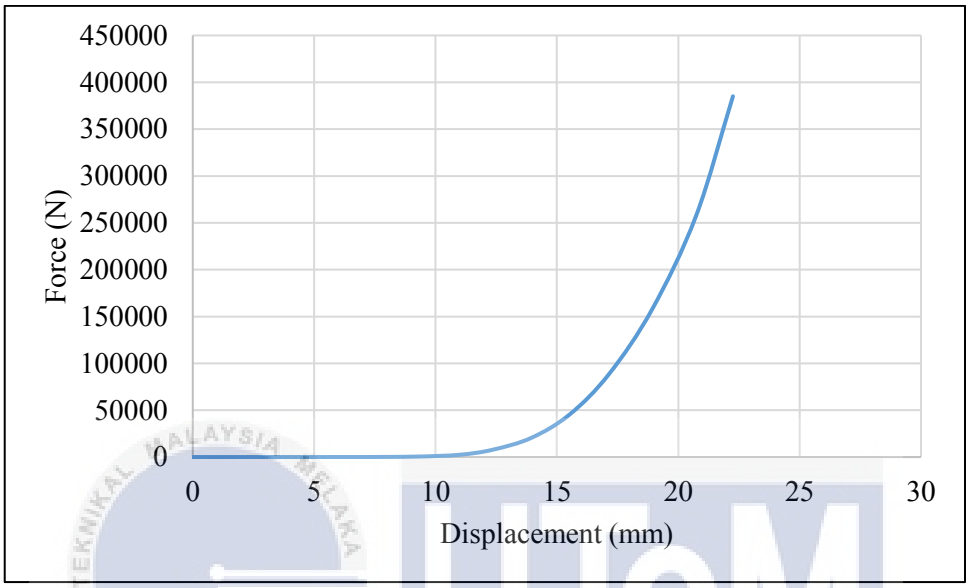

Figure 4.22: Graph of average force-displacement for 45˚ impact.

In this 45˚ impact simulation, the graph also shows the same relationship between the internal energy and kinetic energy where when one decreases another increase. The highest value for internal energy is 4.03E+^{08} J and for the kinetic energy 9.13E+^{09} J both for the duration of 0.0015 second as shown in the Figure 4.23 and Figure 4.24 below.

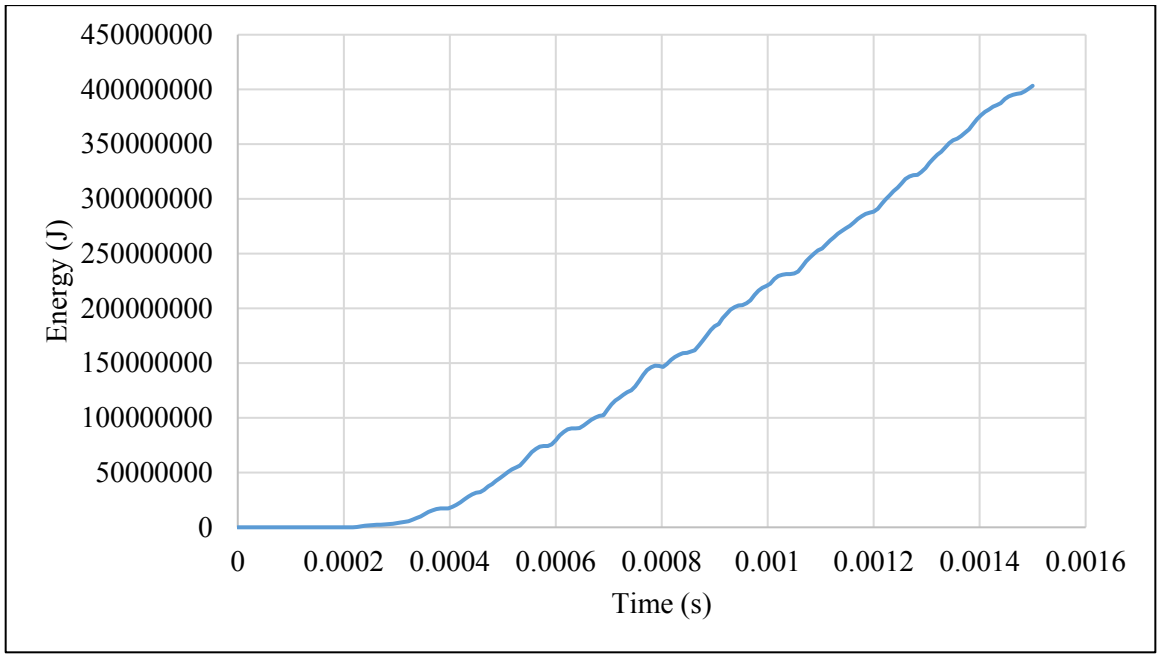

Figure 4.23: Internal energy graph for 45˚ impact.

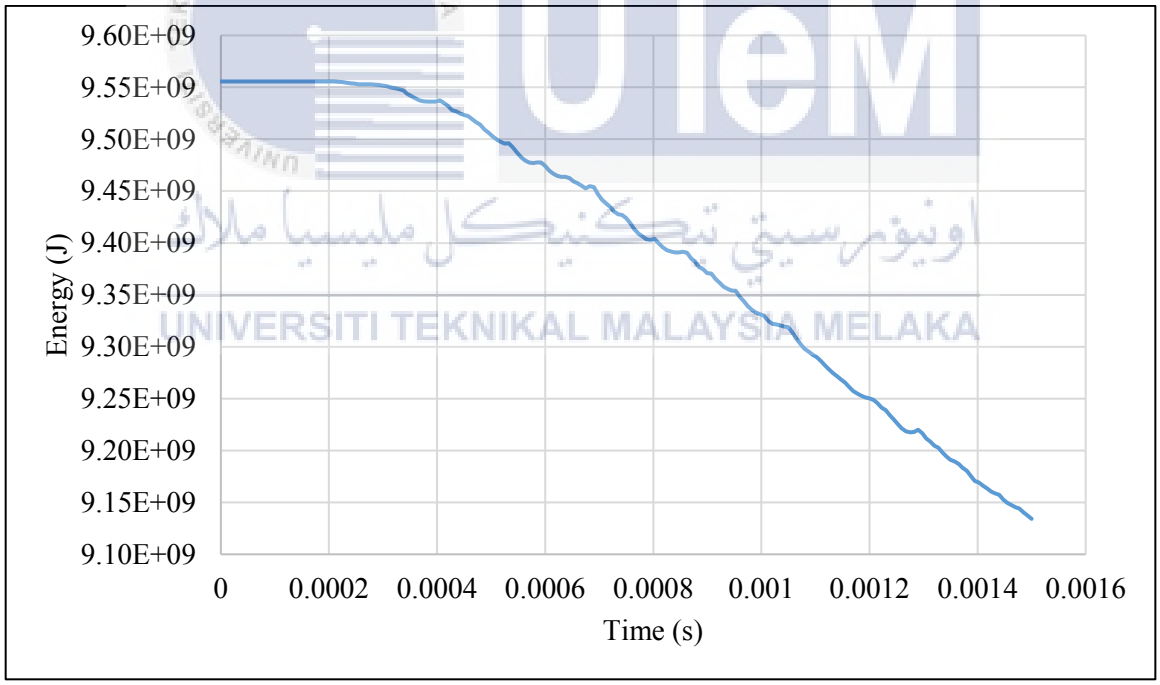

Figure 4.24: Kinetic energy graph for 45˚ impact.

4.5 Impact Angles of 30˚, 45˚, -30˚, and -45˚.

Main angles that are being simulated in this study is 0˚, 30˚, and 45˚, for the 0˚ the impact simulation is considered consistent as the impactor strike at the centre of the bumper. However, for the 30˚ and 45˚ impact angles that involves changing the orientation of the bumper and only one side of the bumper it is worrisome that the results can be inconsistent. Therefore, to provide a way to validate the results in 30˚ and 45˚ impact angles simulation were also done for 30˚ and 45˚ impact angles where the bumper is rotated counter-clockwise thus giving the value -30˚ and -45˚.

4.5.1 Deformation in simulation for -30˚ Impact.

In the simulation of -30˚ impact, the result obtained is shown in the Figure 4.25 below.

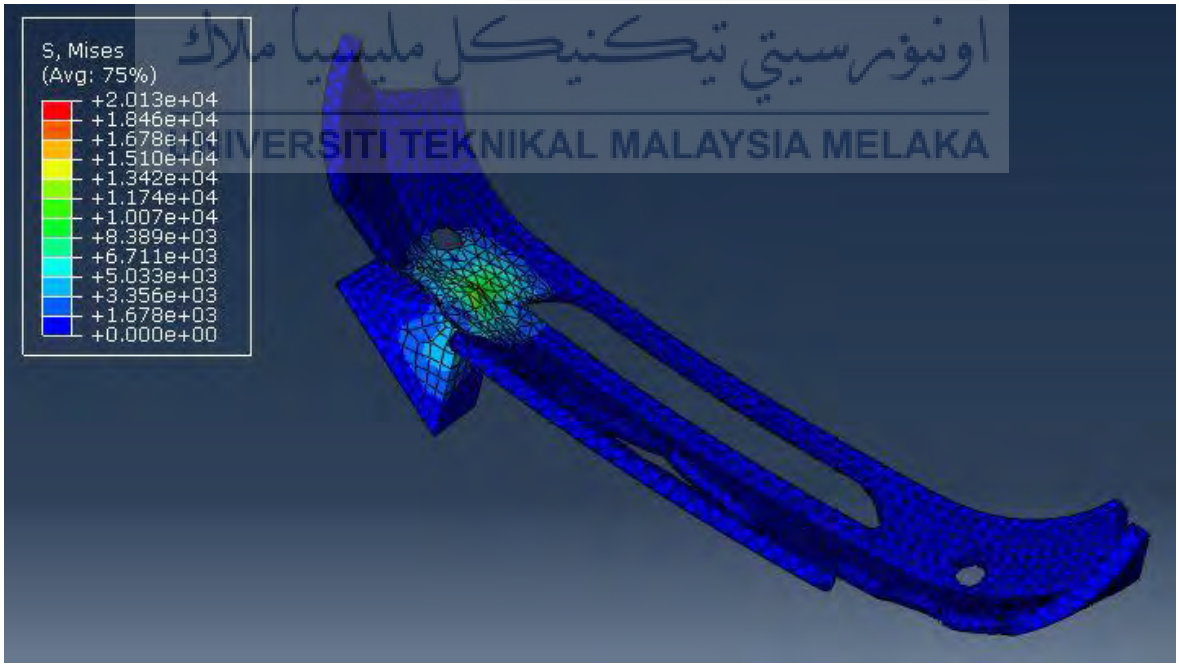

Figure 4.25: Von Mises stress for -30˚ impact.

For this -30˚ impact, the reaction force obtained is from the top pins on the left side above the impactor and both reacted pins are on top because the impactor is closer to the top area. The reaction force and the displacement on the bumper is obtained from the point of the highest value. The reaction force area and displacement area as shown in Figure 4.26 and Figure 4.27 below.

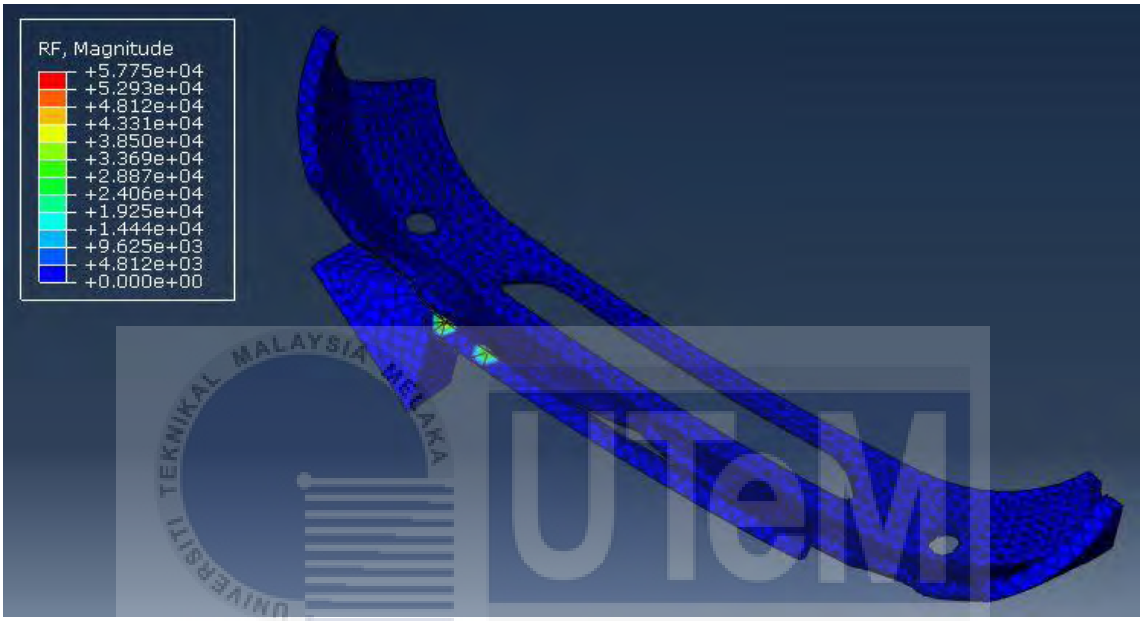

Figure 4.26: Reaction force on the top left-side pins.

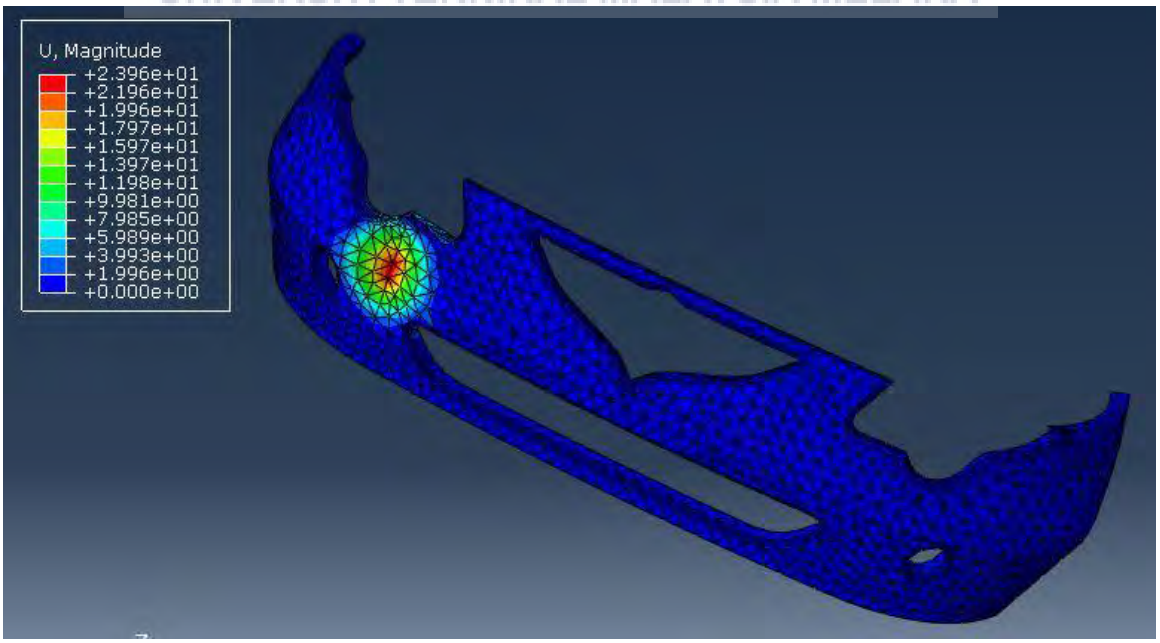

Figure 4.27: Displacement on the bumper.

It is needed to obtain the average value from the area inside the red zone (highest displacement) therefore 4 nodes are chosen for their displacement values as can be seen in Figure 4.28 below. From the Figure 4.29, the graph shows that all the four force-displacement graph line have the same trend with the nodes that are not in the red zone showed less displacement. In this simulation two nodes taken are in the red zone and the other two in yellow zone.

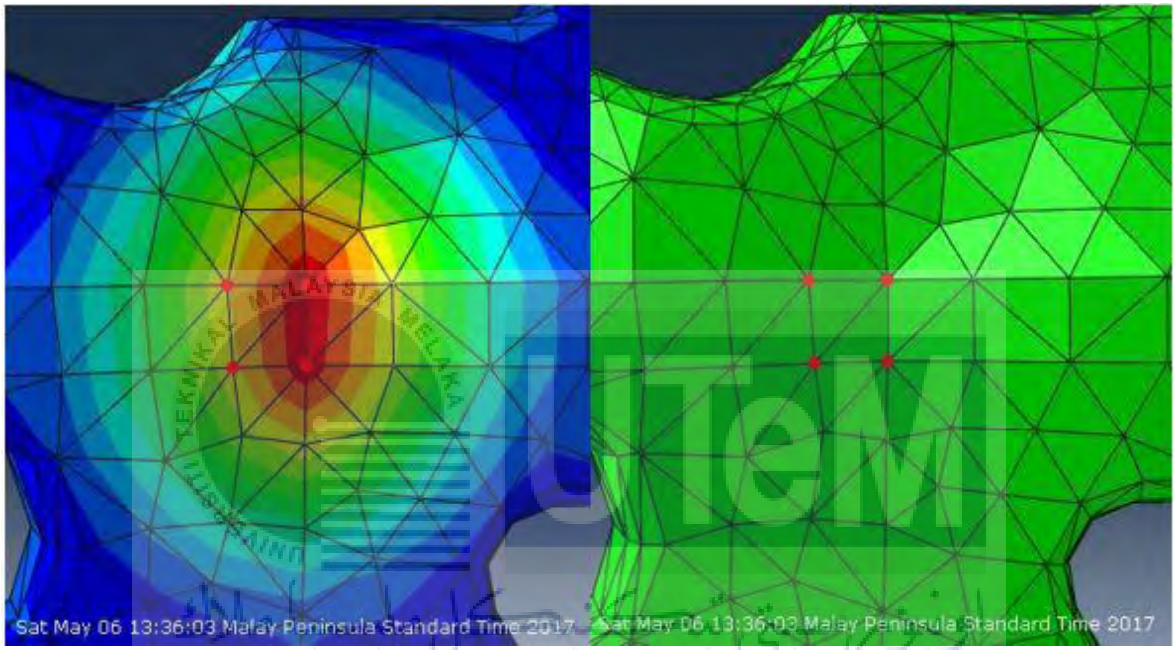

Figure 4.28: Four nodes taken for -30˚ impact.

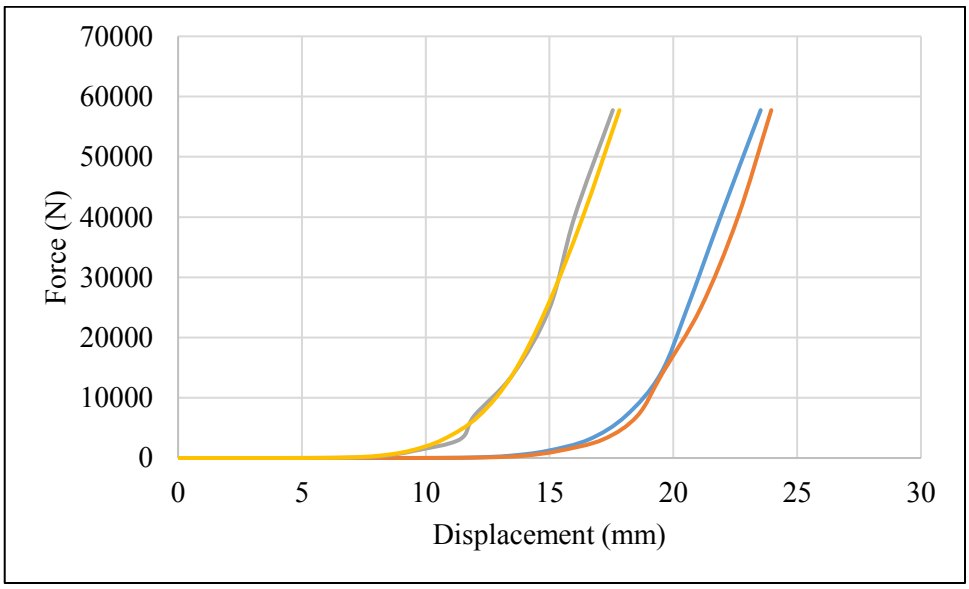

Figure 4.29: Graph of force-displacement at four nodes for -30˚ impact.

The data for average reaction force and displacement are shown in Table 4.4 and the graph of average force-displacement can be seen in Figure 4.30 below. From the Table 4.4 we can see that highest displacement is 20.7154 mm and highest reaction force is 57747.2 N but the force always increases depending on time. However, in the graph in Figure 4.30, the force can be only seen to increase when the displacement reaches the 10 mm because of the previous values is too small.

Table 4.4: Average displacement and force values in -30˚ impact.

Displacement (mm)	0.0879	0.4206	5.7451	10.9800	20.7154
Force (N)	0	6.41E-14	0.403981	381.295	57747.2

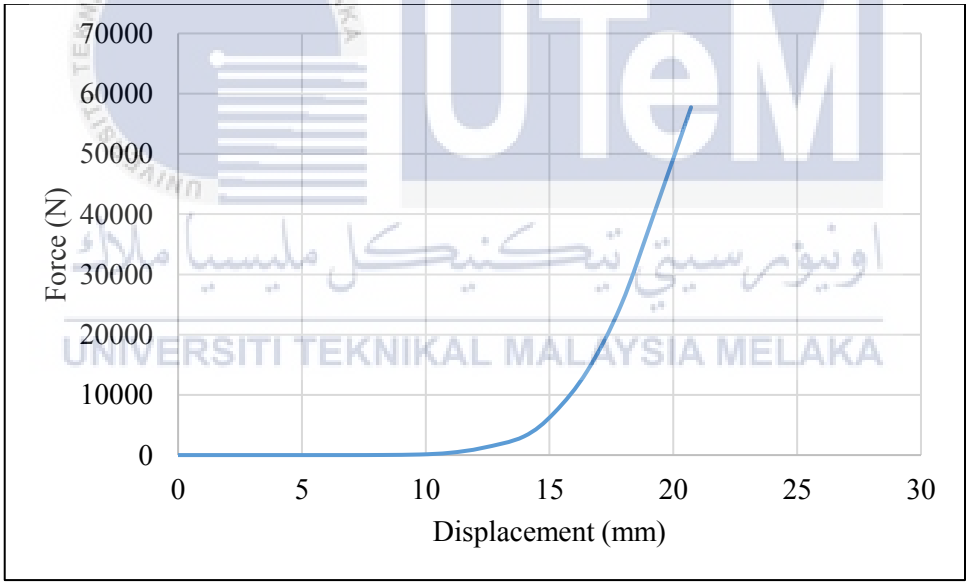

Figure 4.30: Graph of average force-displacement for -30˚ impact.

In this -30˚ impact simulation, the graph also shows the same relationship between the internal energy and kinetic energy where when one decreases another increase. The highest value for internal energy is 3.16E+^{08} J and for the kinetic energy 9.23E+^{09} J both for the duration of 0.0015 second as shown in the Figure 4.31 and Figure 4.32 below.

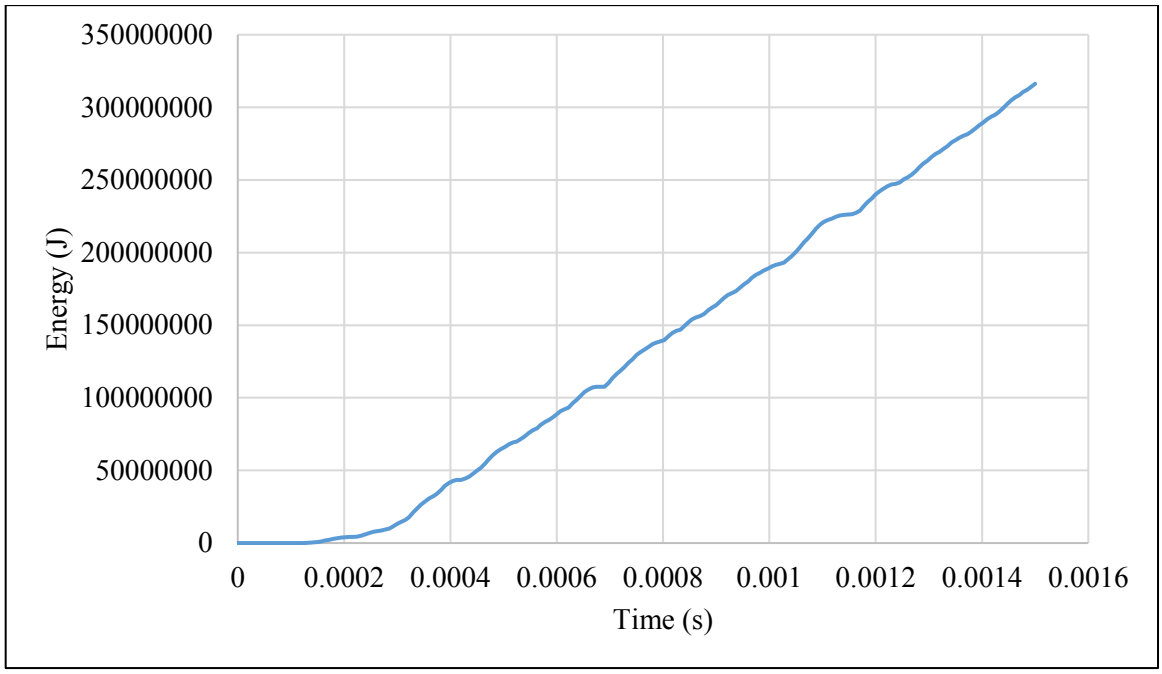

Figure 4.31: Internal energy graph for -30˚ impact.

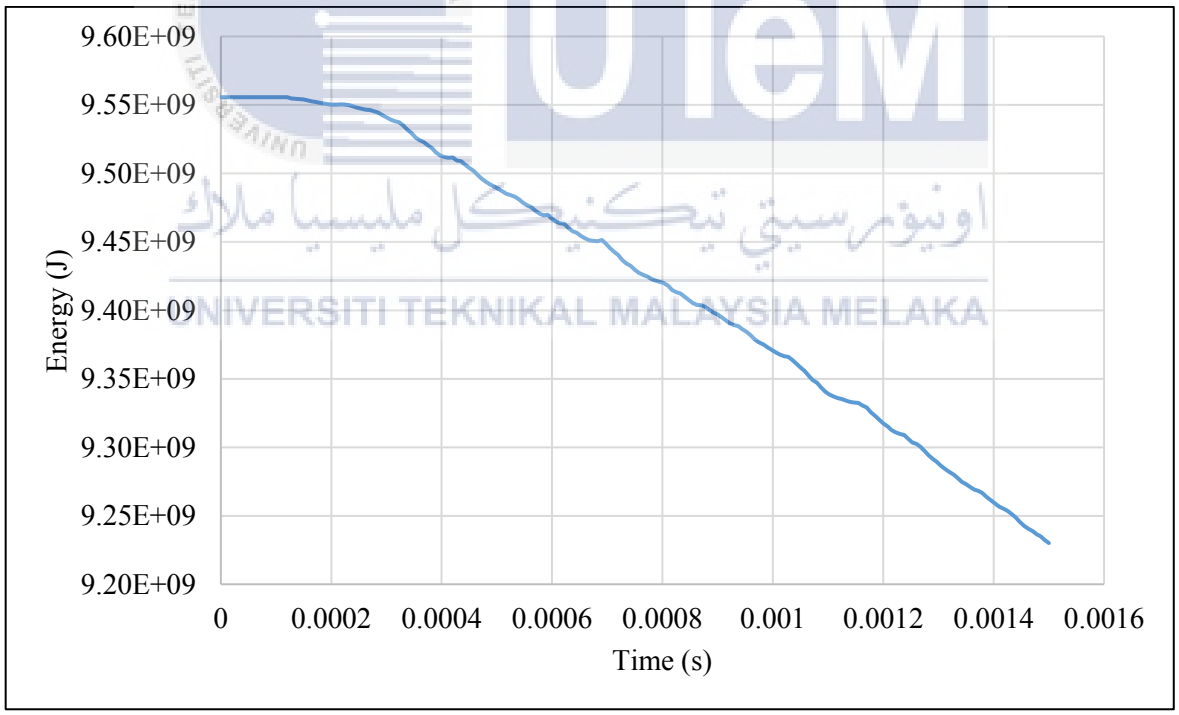

Figure 4.32: Kinetic energy graph for -30˚ impact.

4.5.2 Deformation in simulation for -45˚ Impact.

In the simulation of -45˚ impact, the result obtained is shown in the Figure 4.33 below.

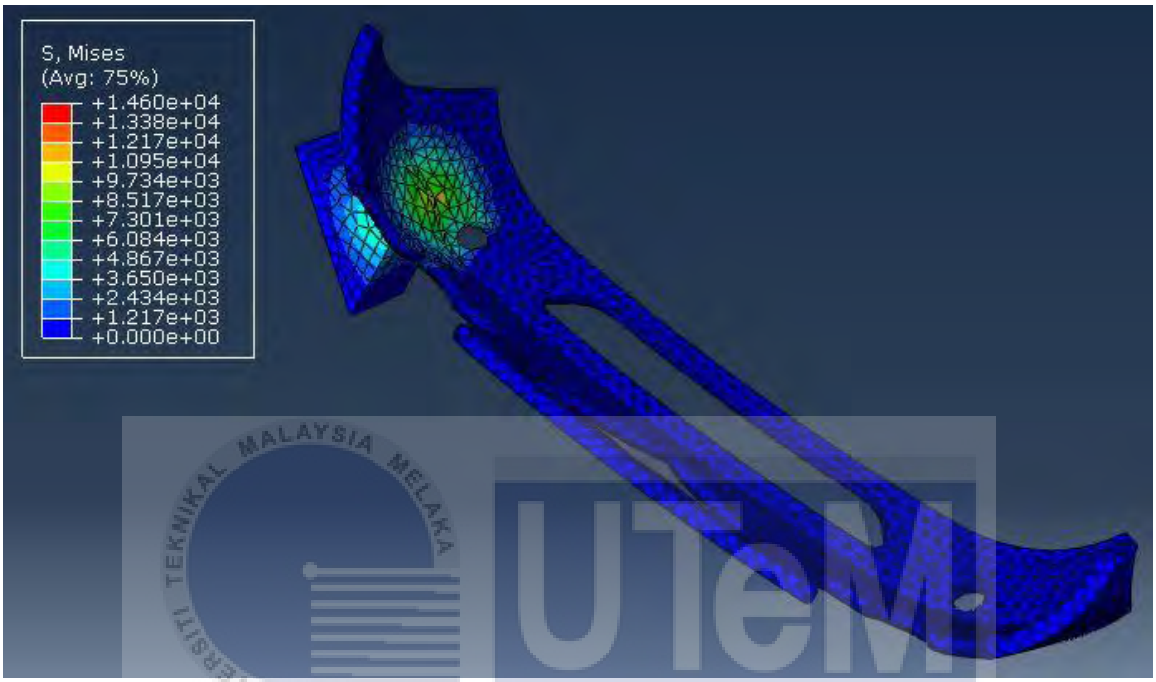

Figure 4.33: Von Mises stress for -45˚ impact.

For this -45˚ impact, the reaction force obtained is from the bottom pin on the left side below the impactor because the impactor strikes an area under the head lamp, therefore there is no pin on the top and only a single pin on the bottom. The reaction force and the displacement on the bumper is obtained from the point of the highest value as shown in Figure 4.34 and Figure 4.35 below.

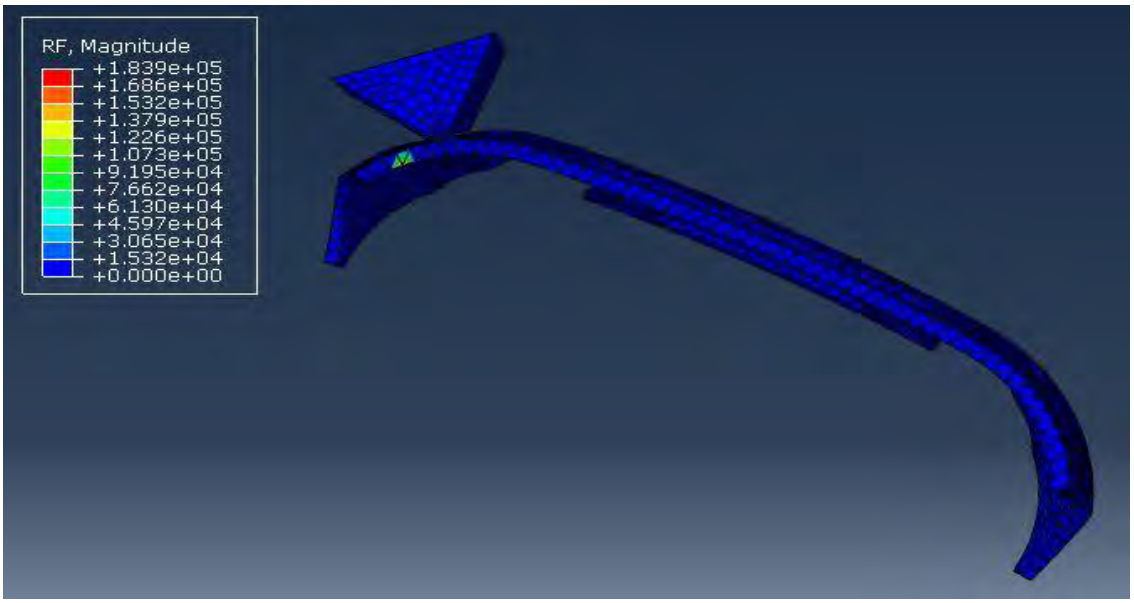

Figure 4.34: Reaction force on the bottom left-side pin.

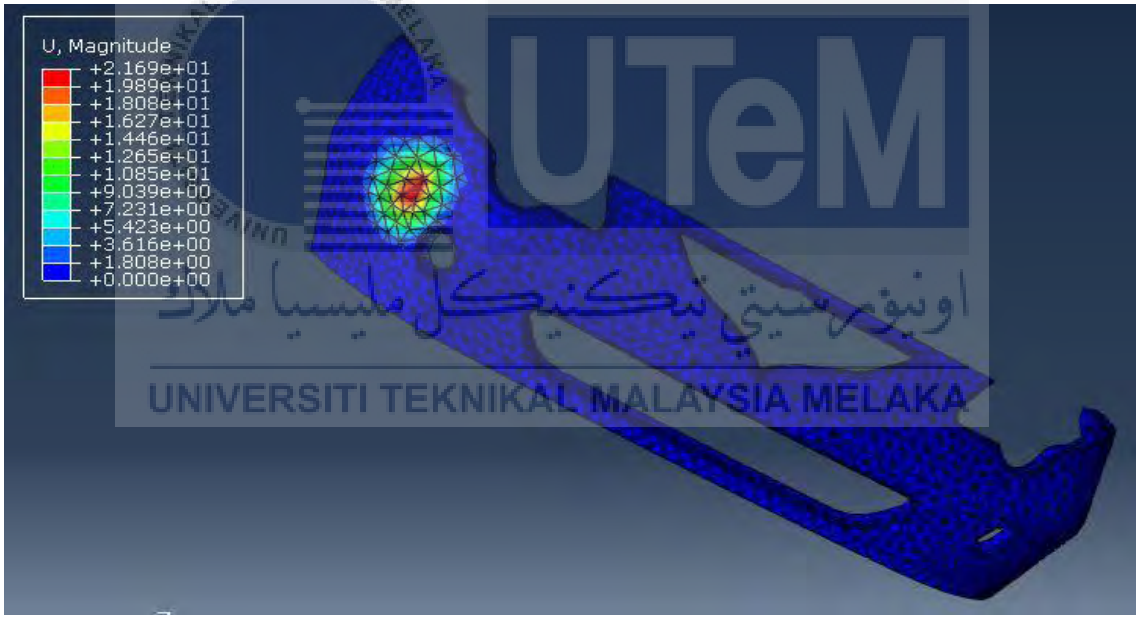

Figure 4.35: Displacement on the bumper.

It is needed to obtain the average value from the area inside the red zone (highest displacement) therefore 4 nodes are chosen for their displacement values as can be seen in Figure 4.36 below. From the Figure 4.37, the graph shows that all the four force-displacement graph line have the same trend with the nodes that are not in the red zone showed less displacement.

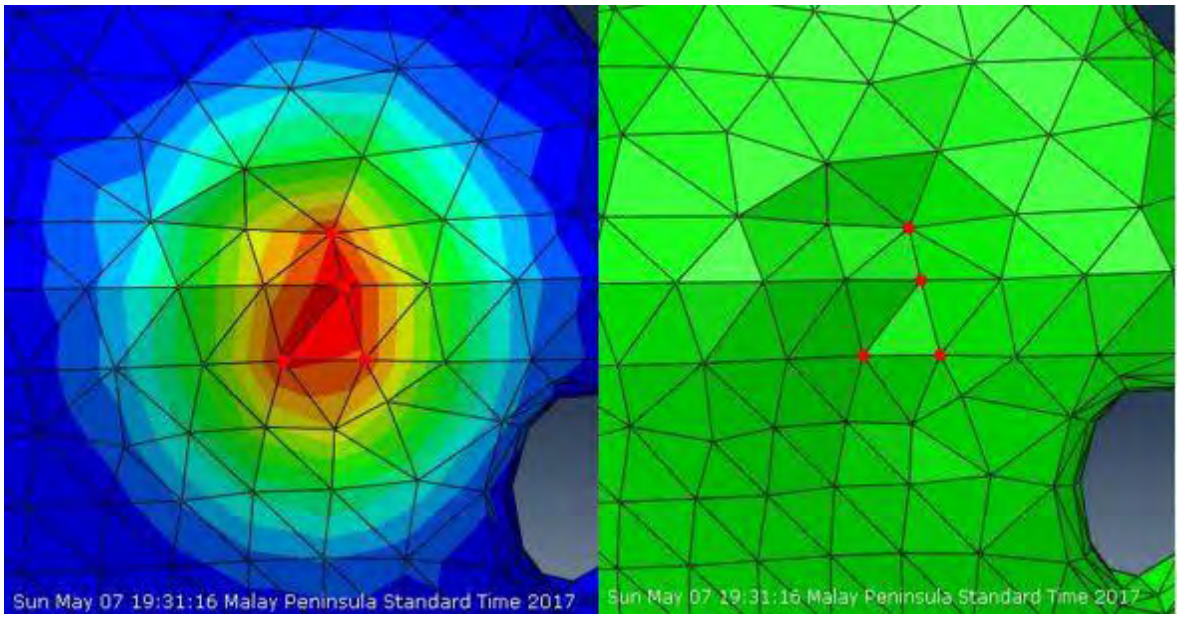

Figure 4.36: Four nodes taken for -45˚ impact.

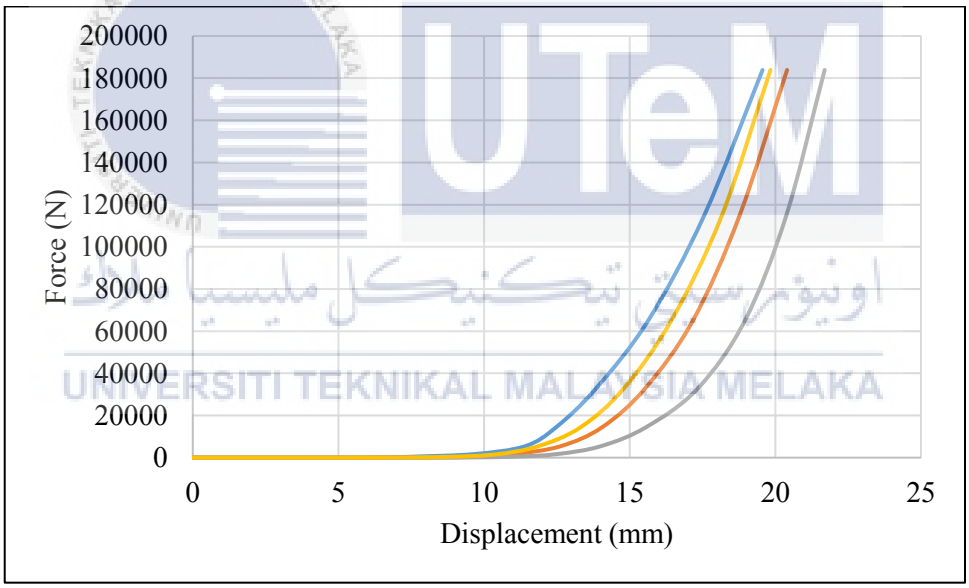

Figure 4.37: Graph of force-displacement at four nodes for -45˚ impact.

The data for average reaction force and displacement are shown in Table 4.5 and the graph of average force-displacement can be seen in Figure 4.38 below. From the Table 4.5 we can see that highest displacement is 20.3726 mm and highest reaction force is 183893 N but the force always increases depending on time. However, in the graph in Figure 4.38, the force can be only seen to increase when the displacement reaches the 10 mm because of the previous values is too small.

Table 4.5: Average displacement and force values in -45˚ impact.

Displacement (mm)	0.2460	5.2193	10.9374	15.3789	20.3726
Force (N)	3.07E-11	3.75666	1706.92	32852.6	183893

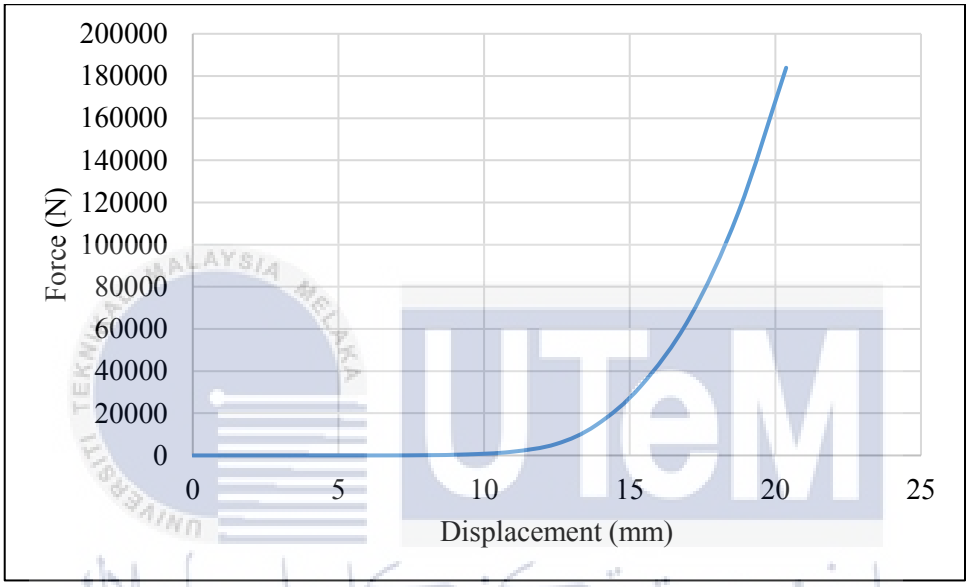

Figure 4.38: Graph of average force-displacement for -45˚ impact.

In this -45˚ impact simulation, the graph also shows the same relationship between the internal energy and kinetic energy where when one decreases another increase. The highest value for internal energy is 3.73E+^{08} J and for the kinetic energy 9.17E+^{09} J both for the duration of 0.0014 second as shown in the Figure 4.39 and Figure 4.40 below. The duration for simulation of -45˚ is less than the others by 0.0001 second because the simulation aborted every time it reaches 0.00143 mark and this is because one of the element in meshing deforms too fast during the simulation.

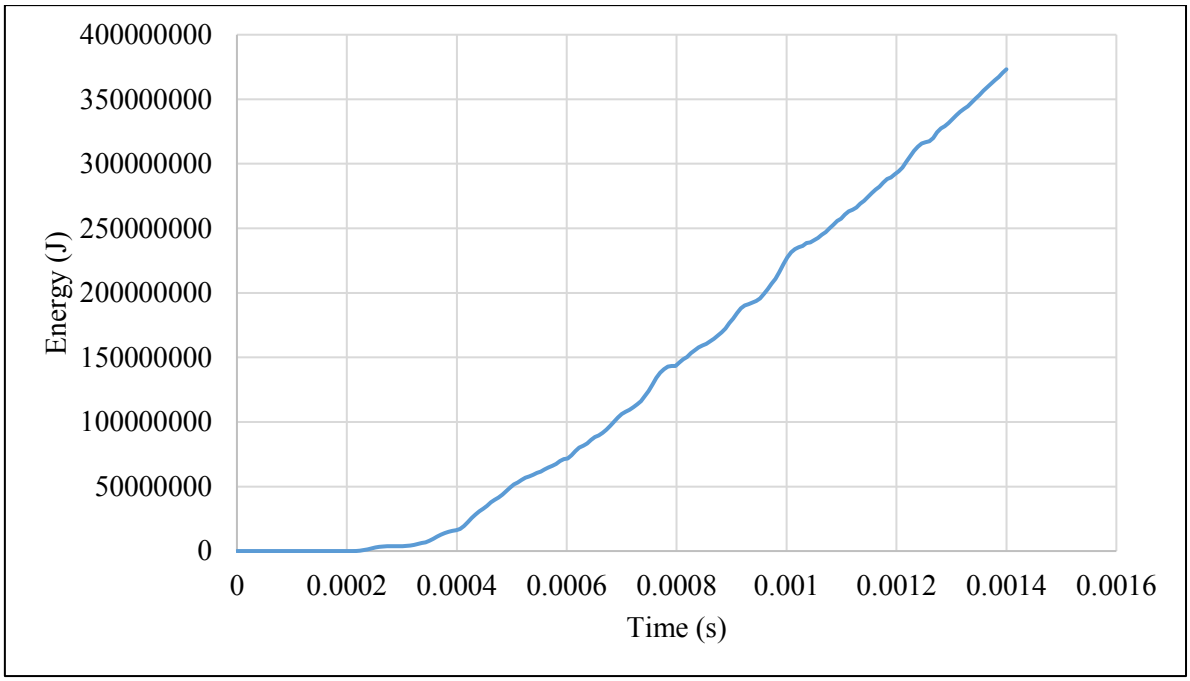

Figure 4.39: Internal energy graph for -45˚ impact.

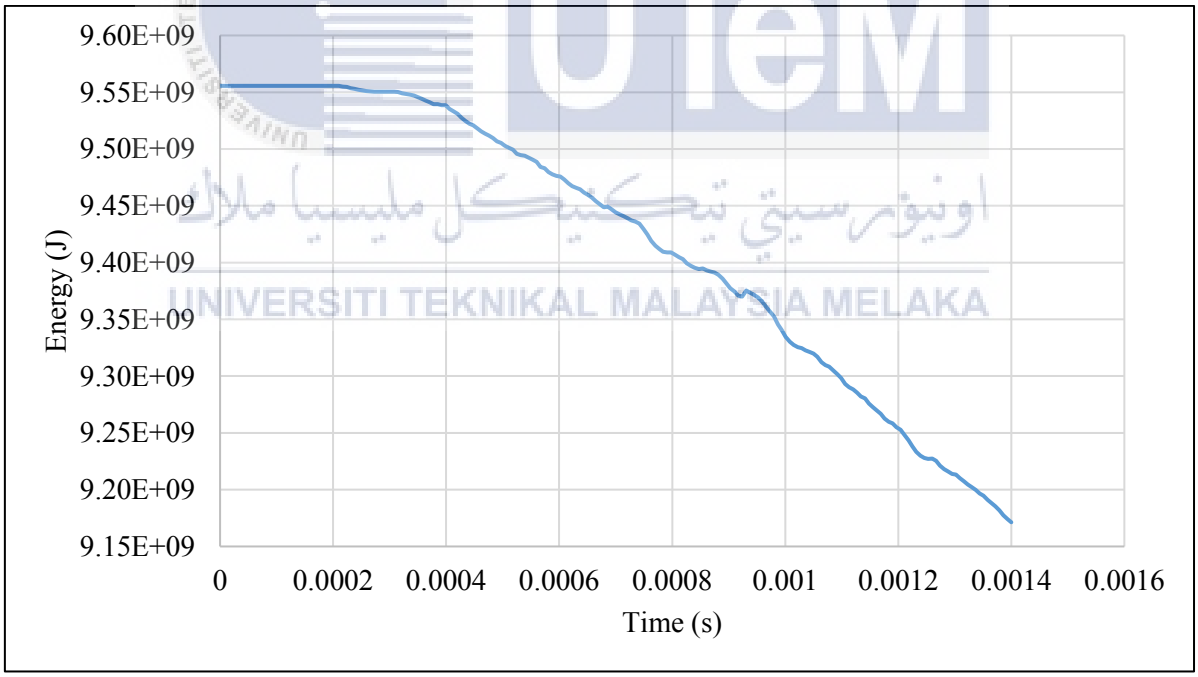

Figure 4.40: Kinetic energy graph for -45˚ impact.

4.5.3 Comparison between impact angles of 30˚, 45˚, -30˚, and -45˚.

The data for counter-clockwise and clockwise is compared to ensure it have the same characteristics.

4.5.3.1 30˚ and -30˚ impact angle.

This comparison is done to validate whether the 30˚ and 45˚ impact angle results are acceptable by comparing the data of 30 ˚and 45˚ impact angle with -30˚ and -45˚ impact angle and it should show that the data have similar pattern. However, it is impossible for the data to have same value because of the discrepancy in meshing element. Therefore, the validation is done by comparing the pattern of graph for both sets of data.

For the average force-displacement graph, the data in bold indicates at what point of displacement the force has noticeable increase in the graph. Given the value for 30˚ is 9.7745 mm and -30˚ is 10.9800 mm with difference only smaller than 1 mm as shown in the Table 4.6 making the results more convincing.

Table 4.6: Average displacement and force values in 30˚ and -30˚ impact.

Displacement (mm)	**30˚**	0.2335	0.4280	5.7067	**9.7745**	21.6241
	-30˚	0.0879	0.4206	5.7451	**10.9800**	20.7154
Force (N)	**30˚**	0	9.30E-13	1.40668	**214.77**	85506.4
	-30˚	0	6.41E-14	0.403981	**381.295**	57747.2

However, to further the validation both 30˚ and -30˚ impact data are plotted on a same graph. From Figure 4.41 to Figure 4.43 below, all the results involving average force-displacement, internal energy, and kinetic energy graphs show that both data have similar point where the force or energy increase/decrease is noticeable. The graphs also show that both data have similar point where the force or energy has sudden increase/decrease and similar gradient of increasing/decreasing force or energy after that.

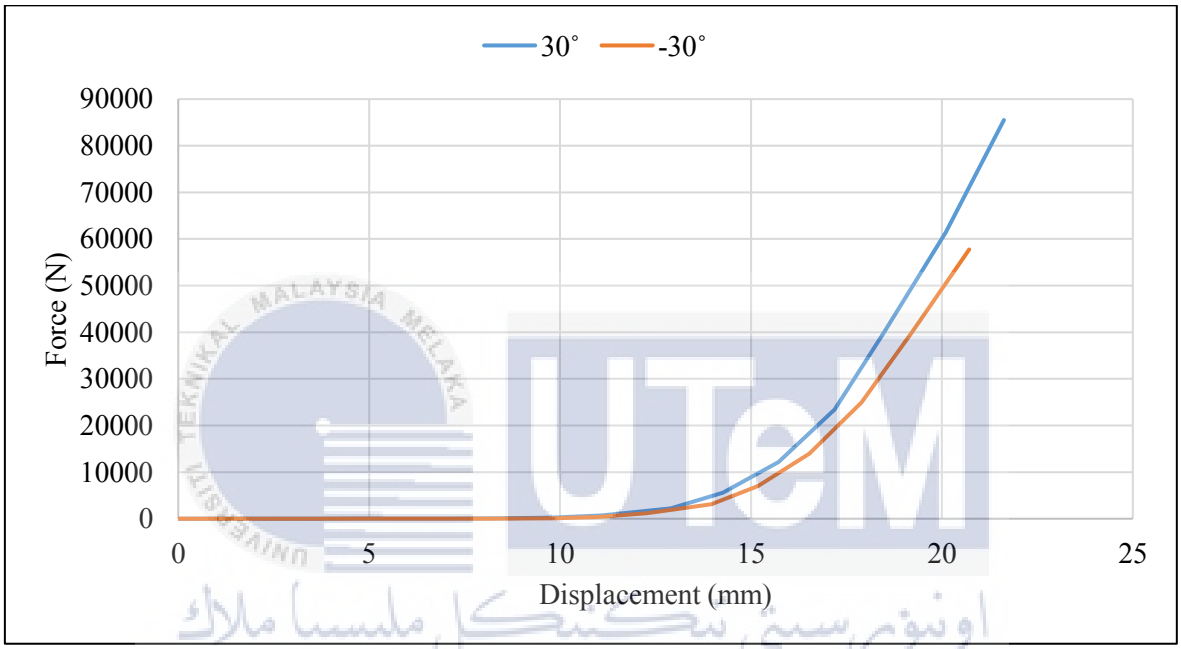

Figure 4.41: Average force-displacement graph for 30˚ and -30˚ impact.

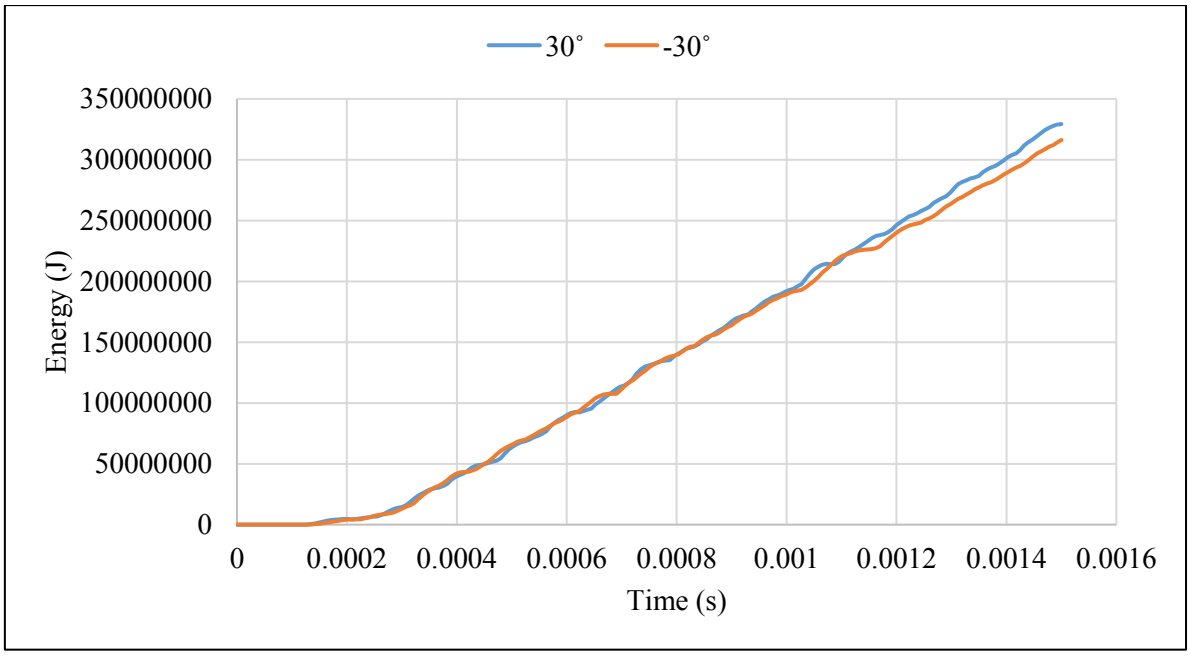

Figure 4.42: Internal energy graph for 30˚ and -30˚ impact.

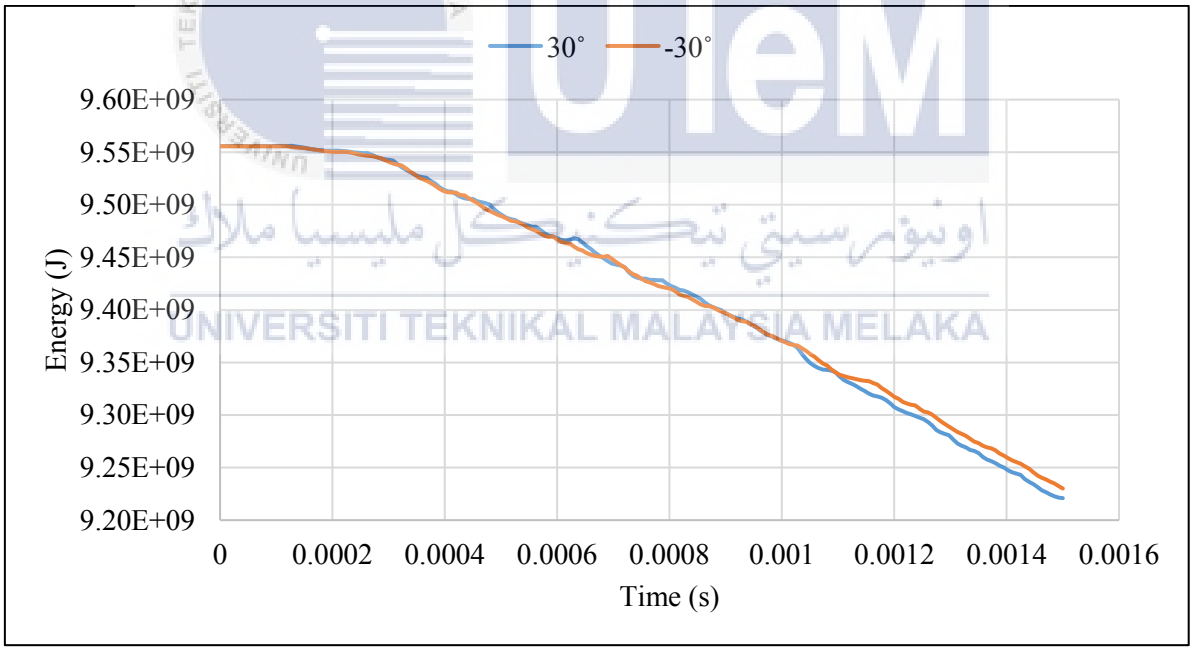

Figure 4.43: Kinetic energy graph for 30˚ and -30˚ impact.

These indicate that from both angle the data obtained are valid, along with the graphs that show similar pattern and shape.

4.5.3.2 45˚ and -45˚ impact angle.

For the average force-displacement graph, the data in bold indicates at what point of displacement the force has noticeable increase in the graph. Given the value for 45˚ is 10.98869 mm and -45˚ is 10.9374 mm with difference less than 1 mm as shown in the Table 4.7 making the results currently convincing.

Table 4.7: Average displacement and force values in 45˚ and -45˚ impact.

Displacement (mm)	**45˚**	0.03378	4.77258	**10.98869**	15.53183	22.25425
	-45˚	0.2460	5.2193	**10.9374**	15.3789	20.3726
Force (N)	**45˚**	2.00E-18	2.72282	**2448.47**	45588.1	385019
	-45˚	3.07E-11	3.75666	**1706.92**	32852.6	183893

However, to further the validation both 45˚ and -45˚ impact data are plotted on a same graph. From Figure 4.44 to Figure 4.46 below, all the results involving average force-displacement, internal energy, and kinetic energy graph show that both data have similar point where the force or energy increase/decrease is noticeable. For the point where the force or energy has sudden increase/decrease and gradient of increasing/decreasing force or energy after that, the graphs show some discrepancy.

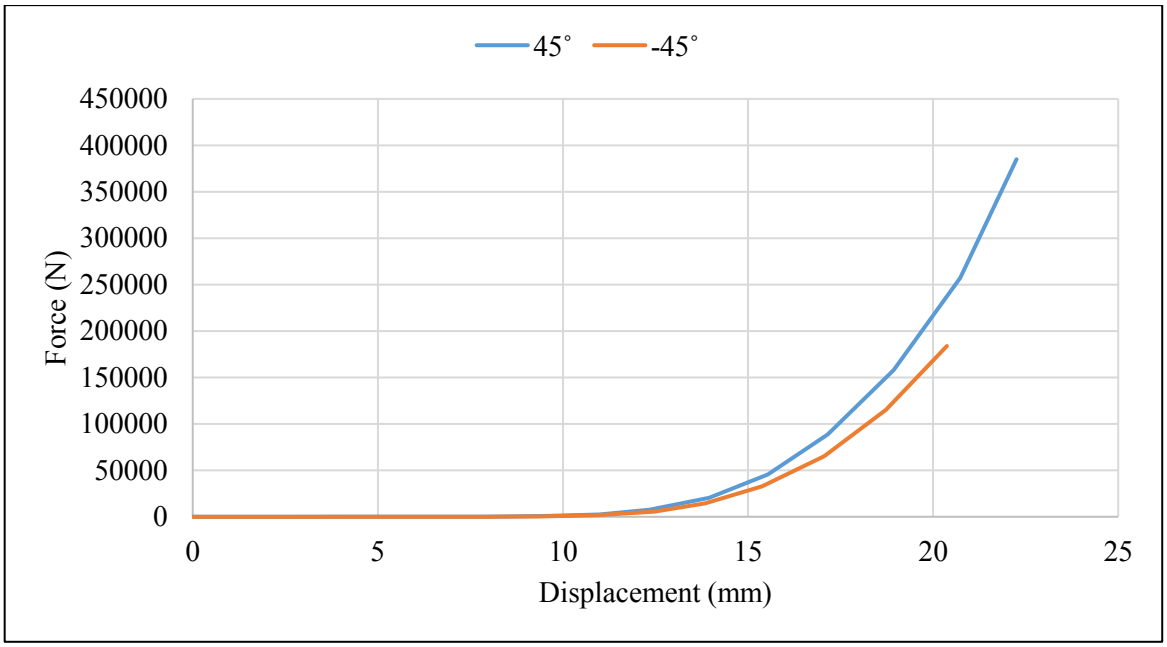

Figure 4.44: Average force-displacement graph for 45˚ and -45˚ impact.

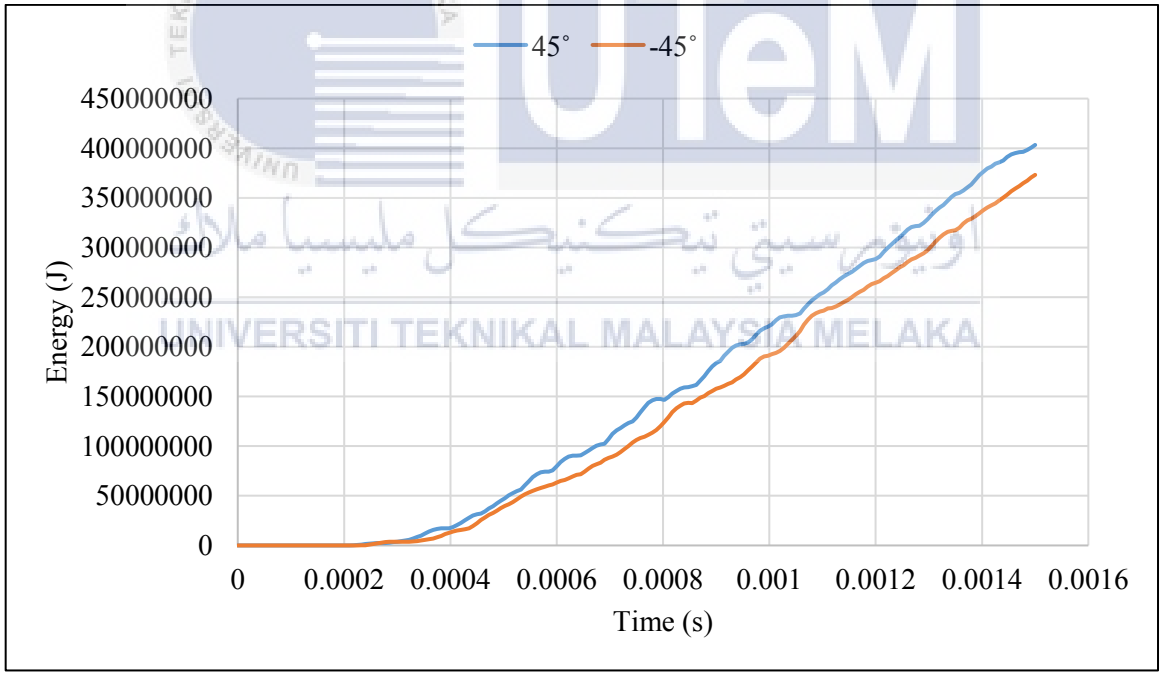

Figure 4.45: Internal energy graph for 45˚ and -45˚ impact.

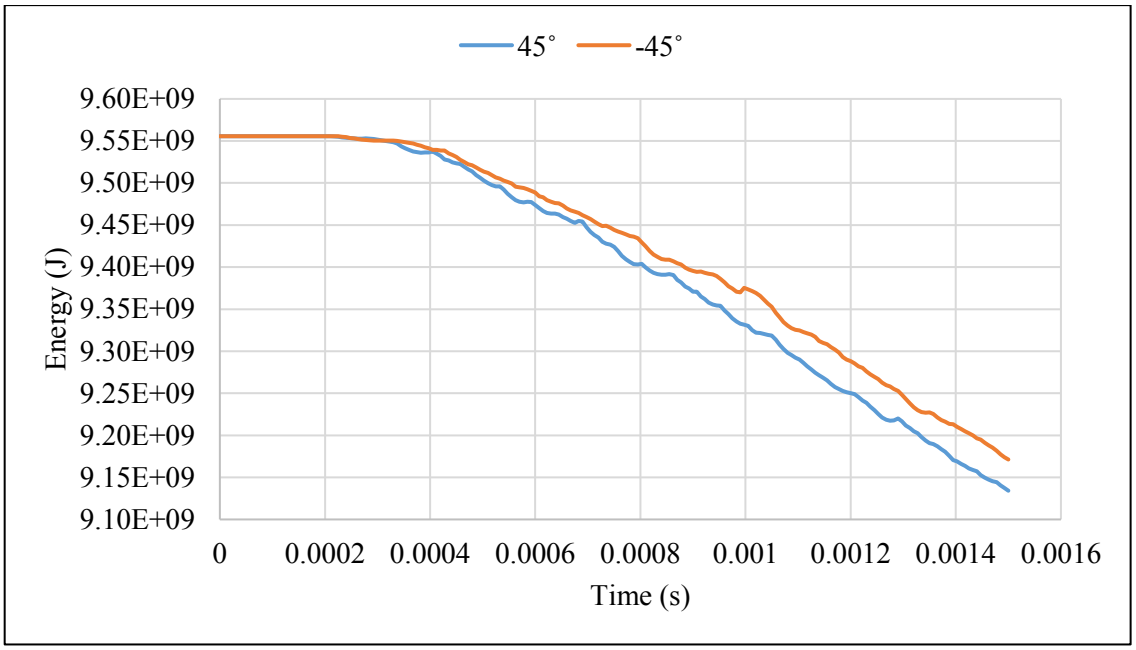

Figure 4.46: Kinetic energy graph for 45˚ and -45˚ impact.

These indicate that the simulation for -45˚ impact angle has poor meshing in that area of impact causing it has a little discrepancy from 45˚ impact angle result and this also forced the -45˚ impact angle simulation to run only 0.0014 second compared to other simulation that runs 0.0015 second. It can be concluded that the results obtained from both simulation are still valid as the pattern and shape of the graphs are similar.

4.6 Energy Absorption of Bumper on 0˚, 30˚ and 45˚ Impact Angles.

The finite element analysis is carried out for three different kind of impact angle of 0˚, 30˚, and 45˚ with all other parameters being constant under impact velocity of 80 km/hr or 22222.2 mm/s. Table 4.8 below shows the comparison between the results for forces and displacements obtained in the simulations for all three simulations.

It is observed that final displacement in all the simulations are different even though all other parameters are the same where the with increase of angle 0˚, 30˚, and 45˚ the displacement are 26.0182, 21.6241, and 22.25425 mm. However, the final force obtained increase with the angles where for angle 0˚, 30˚, and 45˚, the forces are 407.805, 85506.4, 385019 N. In the 30˚ final result for displacement, the value is lower than the 45˚ value because the 4 nodes that were taken in 30˚ simulation had large different in values causing the average to lower than it supposed to be.

Table 4.8: Average data comparison for 0˚, 30˚ and 45˚ impact angles.

						Final Results
Displacement (mm)	**0˚**	0.2018	1.3879	17.6279	**19.1626**	26.0182
	30˚	0.2335	0.4280	5.7067	**9.7745**	21.6241
	45˚	0.03378	4.77258	10.98869	**15.53183**	22.25425
Force (N)	**0˚**	0	5.14E-17	0.560333	**1.2244**	407.805
	30˚	0	9.30E-13	1.40668	**214.77**	85506.4
	45˚	2.00E-18	2.72282	2448.47	**45588.1**	385019

Graph in Figure 4.47 below shows that during the 0.005 m or 5 mm, force has high gradient line before dropped and did not have any other higher peak after that. Then for Figure 4.47 and Figure 4.48 below the graphs show that energy absorbed increases with the angle of attack or impact angle with the exception in Figure 4.49 where the pyramidal lattice that has high porosity and back plate that has lowest energy absorption in 60˚ compared to other angles because during that time the projectiles moves mostly in x-axis rather than y-axis (Ni et al., 2014).

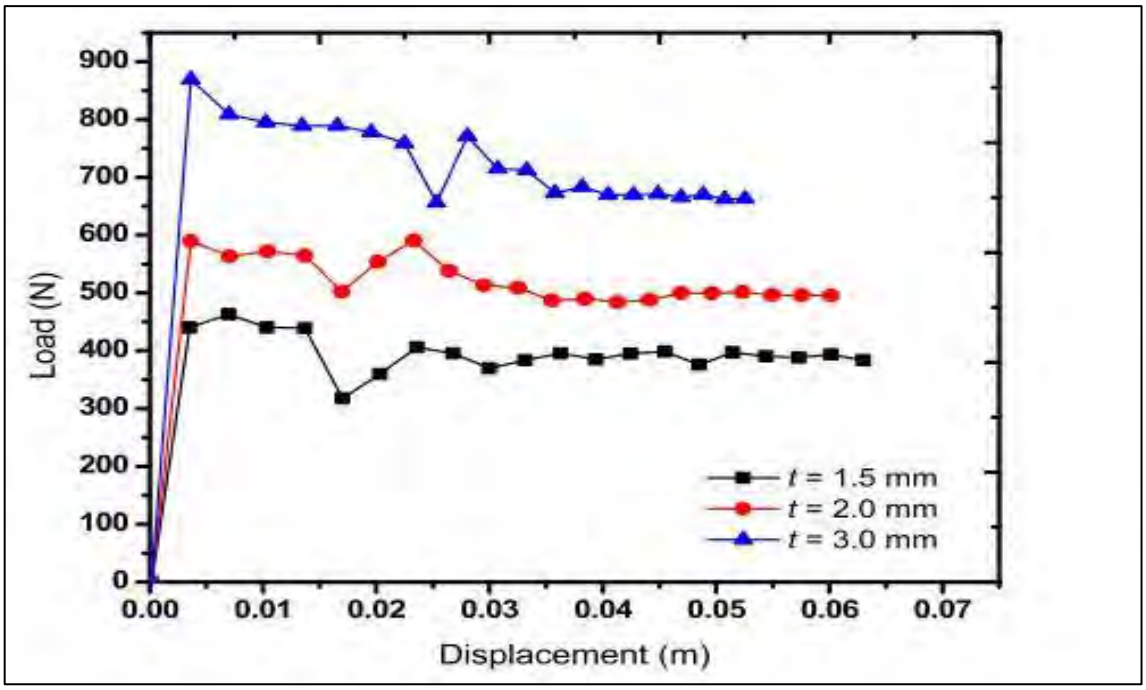

.Figure 4.47: Load-displacement rsponse for velocity of 50 km/hr for three difeferent thickness of twisted tube (Goel, Pandharkar, & Hora, 2017).

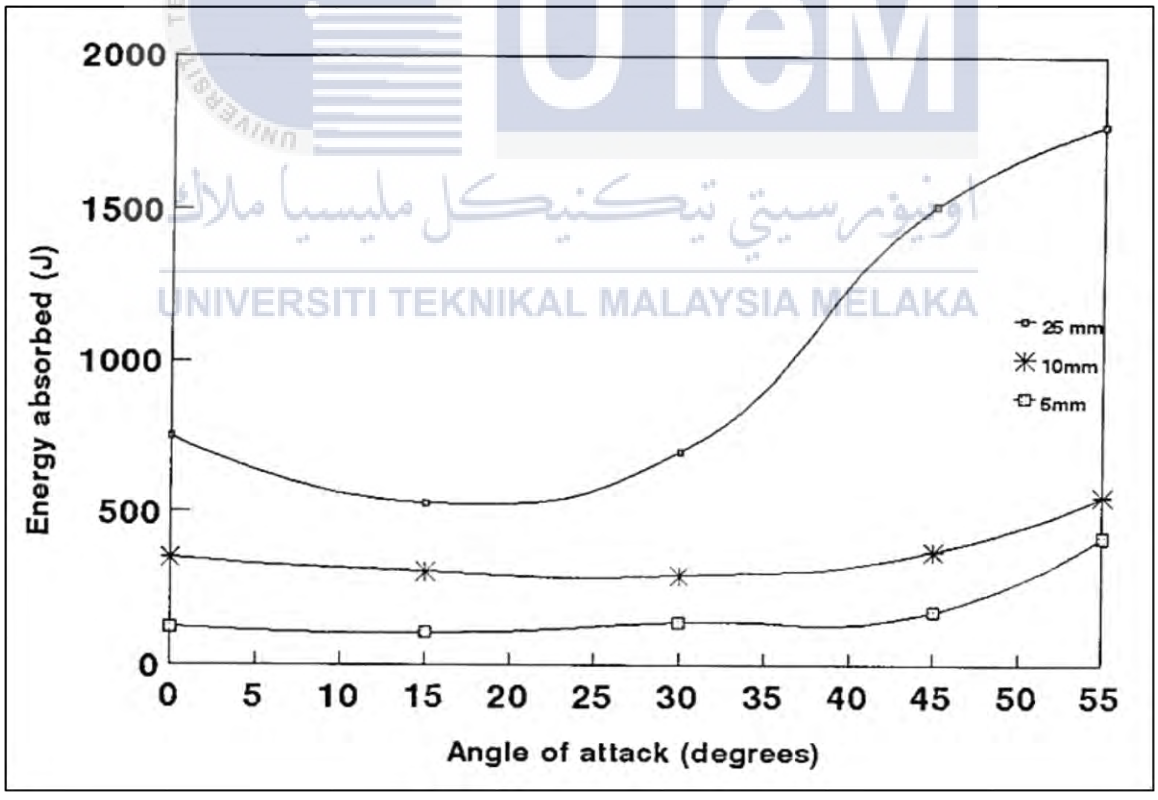

Figure 4.48: Effect of angle of attack on energy absorption by composite laminates of different thickness (Siva Kumar & Balakrishna Bhat, 1998).

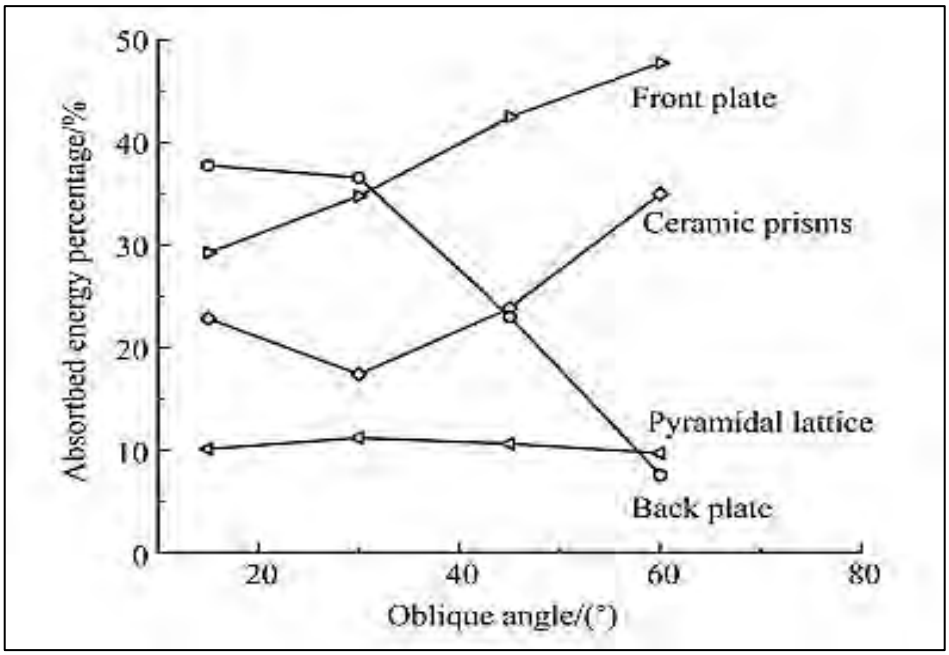

Figure 4.49: Energy absorption percentage of each sub-structure of hybrid-cored sandwich plate plotted as a function of oblique angle, with initial impact velocity fixed at 2.4 km/s (Ni et al., 2014).

From Figure 4.50 below, the graph for force-displacement shows that there is no noticeable force immediately after the impactor touches the bumper. This can be seen in bolded results in Table 4.8 where for 0˚, 30˚ and 45˚ impact angle, the displacements where the forces are noticeable are 19.1626, 9.7745, 15.53183 mm with the forces value are 1.2244, 214.77, 2448.47 N respectively. The delayed respond is because the shape of the bumper and the material of aluminium that is low in density that can absorb some amount of force before the reaction force starts.

Energy absorption can be obtained in force-displacement graph by calculating area under the curve for each angle using relation (1) where F is the applied force and U is the corresponding displacement.

$$E_A = \int F(U)dU \quad (1)$$

The values given for 0˚, 30˚ and 45˚ impact angle energy absorption are 3.525, 269.151, and 1316.26 J respectively. By isolating the delayed respond in graph of force-displacement in Figure 4.50 below, it shows similarity with graph in Figure 4.47 where the peak force starts at the beginning. It also shows the same results with the graphs in Figure 4.48 and Figure 4.49 where higher angle of impact has higher energy absorption.

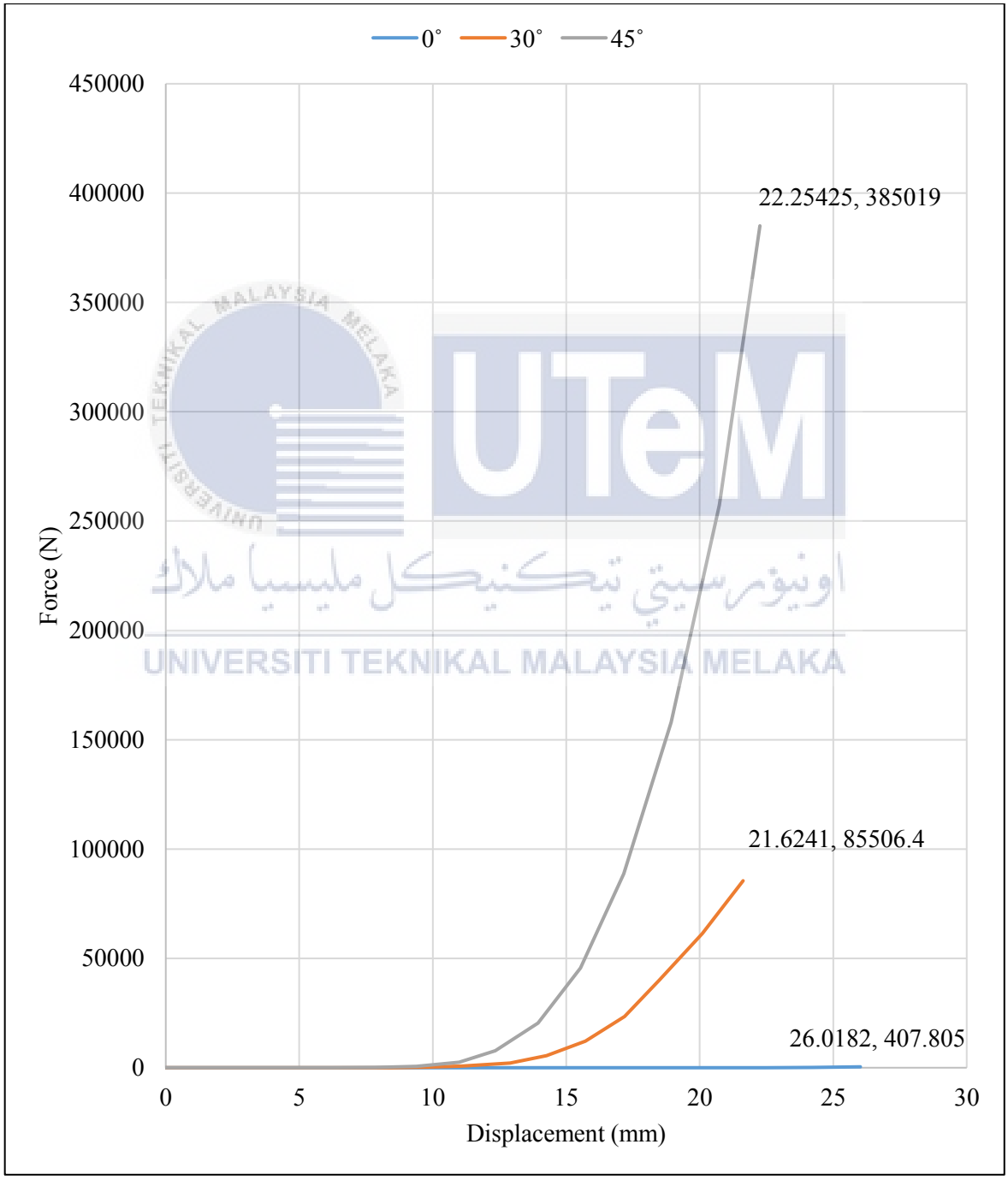

Figure 4.50: Average force-displacement graph for 0˚, 30˚ and 45˚ impact angle.

The graphs in Figure 4.51 and Figure 4.52 show that for the 45˚ impact angle, it has the highest internal energy and lowest kinetic energy during the 0.015 second. This indicates that in the 45˚ impact angle the energy is the quickest to transfer from kinetic energy to internal energy making the energy absorption higher compared to the other impact angle. The reason is as the impact angle increases to 45˚, the impactor moves in between the x-axis and y-axis thus when the impactor touches the bumper's surface the cross section of the bumper that received the impact increases as shown if Figure 4.53 below.

This increase the ability to withstand impact and greatly increase the amount of energy absorbed by the bumper. From Figure 4.50 also the value of force for 45˚ impact exponentially increased compared to the 0˚ is because the influence of the impactor's positioning. During the simulation for 45˚, the impactor is located at the bumper's area that almost has a semicircle geometry and this caused the better ability to withstand impact compared to 0˚ impact.

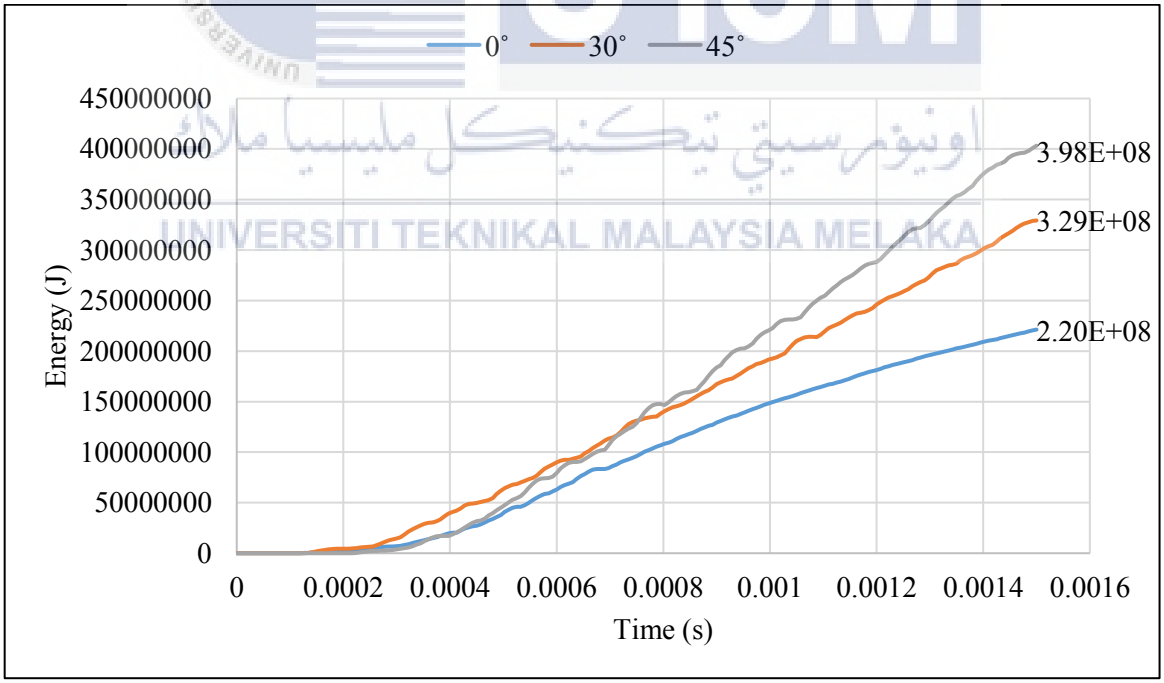

Figure 4.51: Internal energy graph for 0˚, 30˚ and 45˚ impact angle.

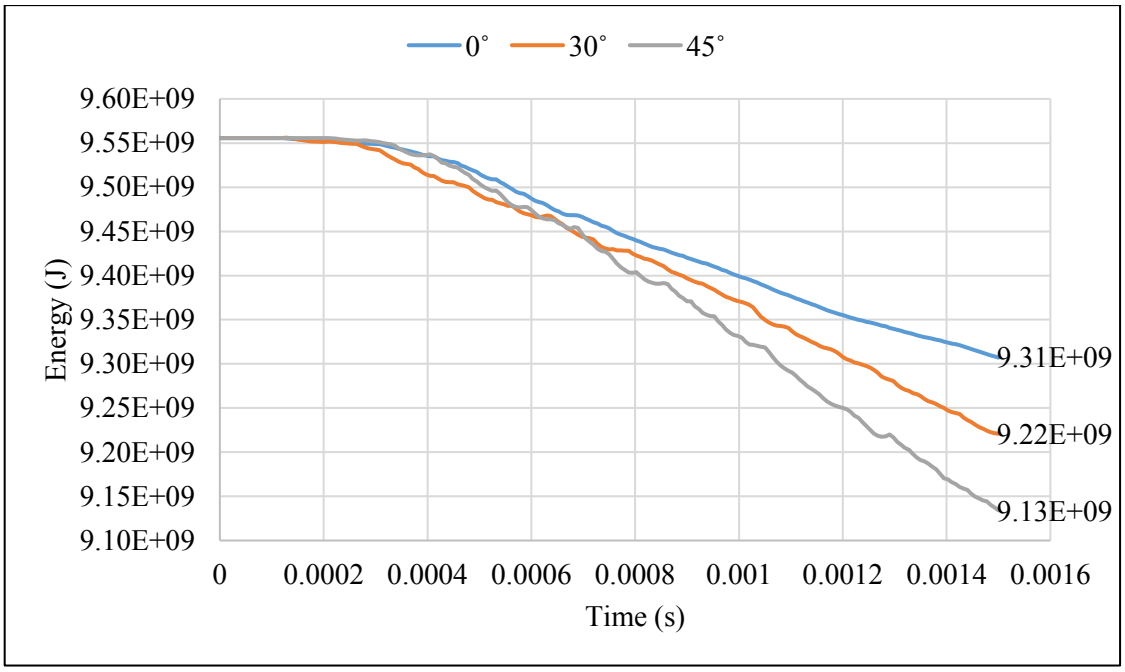

Figure 4.52: Kinetic energy graph for 0˚, 30˚ and 45˚ impact angle.

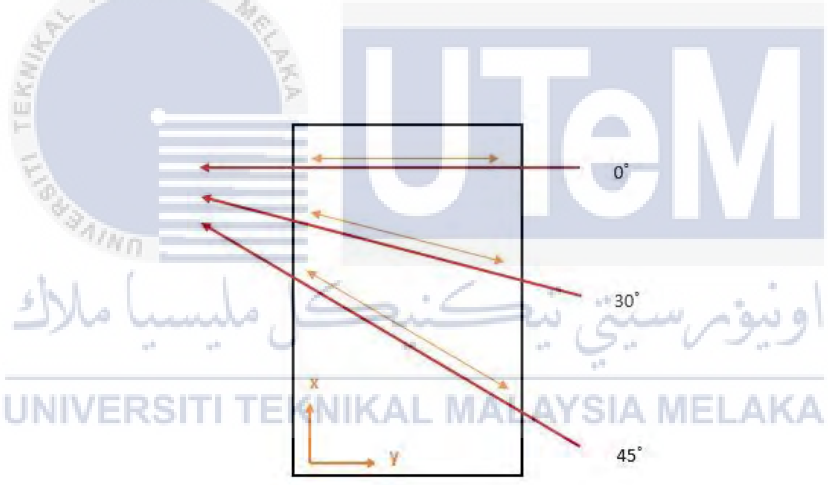

Figure 4.53: Cross section from front to back of bumper.

4.7 Chapter Summary

The outcome for the simulations have been discussed in this chapter. The simulations are carried out to investigate the energy absorption in front car bumper where aluminium material has been used. For each simulation, the impact angle is different starting from 0˚, 30˚ and 45˚. The simulations finding show that area under the curve for simulations increase and displacement decrease with the increase of the impact angle value. This also shows that with higher impact angle, energy absorption increases and deformation decreases.

Chapter 5

CONCLUSION AND RECOMMENDATION

5.1 Introduction

This chapter concludes the study of front car bumper structure and finding and included also in this chapter is the recommendation of future works. The aim of this study is to investigate the energy absorption of impact test simulation with different impact direction of 0˚, 30˚ and 45˚ using ABAQUS FEA software for a GEN2 front bumper car.

5.2 Conclusion

Figure 5.2 shows the graph force-displacement with all the data from the 0˚, 30˚ and 45˚ impact angle simulations. From this graph, the highest energy absorption can be identified in 45˚ impact angle graph that is 1316.26 J where the area under the curve is the highest then followed by the 30˚ and 0˚ impact angles with 269.151 J and 3.525 J respectively. The reasons are because the increasing impact angle significantly increases the ability of the impactor to move in x-axis as shown in Figure 5.1 and this caused the cross section at the point of impact increase as shown in Figure 5.2. Bigger cross section provides better ability to resist impact thus increasing the energy absorption.

Plus, the positioning of the pins also play an important role in ability of energy absorption. The simulations result also are compared with previous results where both show that when the angle of attack/impact angle is increased the energy absorption also increased.

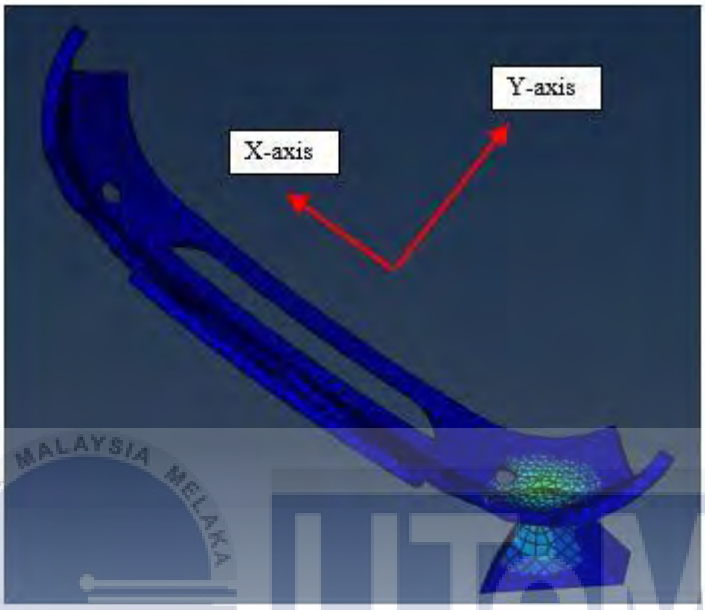

Figure 5.1: Y-axis and x-axis in all simulations.

Figure 5.2: Cross section from front to back of bumper.

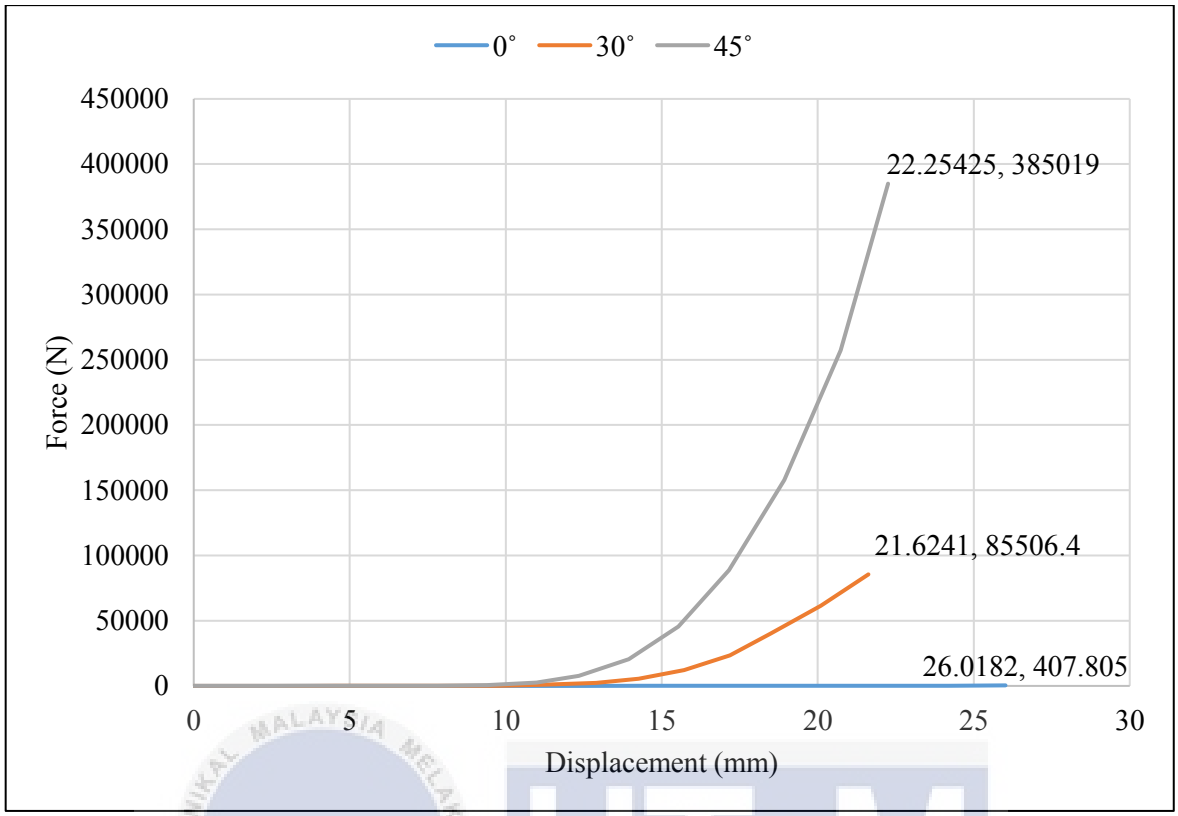

Figure 5.2: Force-displacement graph for 0˚, 30˚ and 45˚ impact angle.

5.3 Recommendation

In this study, the material for front car bumper was aluminium however modern car bumper mostly are made from polypropylene a type of tough and robust plastic that is also lighter than aluminium. The constant velocity for the impactor for all the simulation in this study is 80 km/hr which is a high-velocity impact. Due to the meshing limitation also, all the simulations are not capable of running till the bumper ruptures. In future ABAQUS simulation, the study can use polypropylene as the bumper car material, with various velocities and better meshing of bumper to further obtain the energy absorption results with different impact directions.

References

Belingardi, G., Beyene, A. T., & Koricho, E. G. (2013). Geometrical optimization of bumper beam profile made of pultruded composite by numerical simulation. *Composite Structures*, *102*, 217–225. https://doi.org/10.1016/j.compstruct.2013.02.013

Beyene, A. T., Koricho, E. G., Belingardi, G., & Martorana, B. (2014). Design and manufacturing issues in the development of lightweight solution for a vehicle frontal bumper. *Procedia Engineering*, *88*, 77–84. https://doi.org/10.1016/j.proeng.2014.11.129

Bohra, B. A., & Pawar, P. D. B. (2014). Comparative analysis of frontal car bumper during impact. *International Journal of Innovations in Engineering and Technology (IJIET) Comparative*, *3*(12), 89–93.

Calienciug, A. (2012). DESIGN AND FEA CRASH SIMULATION FOR A COMPOSITE CAR BUMPER. *Bulletin of the Transilvania University of Braşov Series I: Engineering Sciences • Vol. 5 (54) No. 1 - 2012 DESIGN*, *5*(1).

Cambridge University Engineering Department. (2003). *Materials Data Book*.

Cheon, S. S., Choi, J. H., & Lee, D. G. (1995). Development of the composite bumper beam for passenger cars. *Composite Structures*, *32*(1–4), 491–499. https://doi.org/10.1016/0263-8223(95)00078-X

Dange, M. V, Buktar, R. B., & Raykar, N. R. (2015). Design and Analysis of an Automotive Front Bumper Beam for Low-Speed Impact. *IOSR Journal of Mechanical and Civil Engineering Ver*, *12*(2), 2320–334. https://doi.org/10.9790/1684-12241727

Davoodi, M. M., Sapuan, S. M., Ahmad, D., Aidy, A., Khalina, A., & Jonoobi, M. (2011). Concept selection of car bumper beam with developed hybrid bio-composite material. *Materials and Design*, *32*(10), 4857–4865. https://doi.org/10.1016/j.matdes.2011.06.011

Davoodi, M. M., Sapuan, S. M., Aidy, A., Abu Osman, N. A., Oshkour, A. A., & Wan Abas, W. A. B. (2012). Development process of new bumper beam for passenger car: A review. *Materials and Design*, *40*, 304–313. https://doi.org/10.1016/j.matdes.2012.03.060

Davoodi, M. M., Sapuan, S. M., & Yunus, R. (2008). Conceptual design of a polymer composite automotive bumper energy absorber. *Materials and Design*, *29*(7), 1447–1452. https://doi.org/10.1016/j.matdes.2007.07.011

Donga, A. (2011). Application of Sandwich Beam in Automobile Front Bumper for, (December).

Fadhil, B. M. (2012). Finite Element Modeling of Cylindrical Projectile Impact on Aluminum Plate, *2*(9), 1631–1638.

Goel, M. D., Pandharkar, A., & Hora, M. S. (2017). Numerical Simulation of Crushing and Energy Absorption Behavior of Twisted Tubes under Impact Loading. *Procedia Engineering*, *173*, 1365–1373. https://doi.org/10.1016/j.proeng.2016.12.182

Hershman, L. L., & Hershman, L. L. (n.d.). THE U . S . NEW CAR ASSESSMENT PROGRAM (NCAP): PAST , PRESENT AND FUTURE United States, (390).

Hollowell, W. T., Gabler, H. C., Stuckl, S. L., Summers, S., & Hackney, J. R. (1999). UPDATED REVIEW OF POTENTIAL TEST PROCEDURES FOR FMVSS NO. 208.

Jamal, J. B. I. N. (2009). STRESS ANALYSIS ON FRONT CAR BUMPER, (November).

Kleisner, V., & Zemˇ, R. (2009). Analysis of composite car bumper reinforcement. *Computational Mechanics*, *3*, 287–296.

Marzbanrad, J., Alijanpour, M., & Kiasat, M. S. (2009). Design and analysis of an automotive bumper beam in low-speed frontal crashes. *Thin-Walled Structures*, *47*(8–9), 902–911. https://doi.org/10.1016/j.tws.2009.02.007

Moona, N., Yadav, A., Singh, A., & City, I. (2015). ANALYSIS ON BUMPER DURING COLLISION. *International Journal of Advances in Engineering & Technology*, *8*(3), 404–411.

National Highway Traffic Safety Administration (NHTSA), NHTSA, N. H. T. S. A., & National Highway Traffic Safety Administration (NHTSA). (2012). Laboratory Test Procedure For New Car Assessment Program Frontal Impact Testing, (September), 409. Retrieved from file:///C:/Users/NCAC/Downloads/Frontal_TP_NCAP.pdf

Ni, C., Jin, F., & Lu, T. (2014). Penetration of sandwich plates with hybrid-cores under oblique ballistic impact. *Theoretical and Applied Mechanics Letters*, *4*(2), 21001. https://doi.org/10.1063/2.1402101

Peraire, J., & Widnall, S. (2009). Linear Impulse and Momentum. Collisions. In *Dynamics Fall 2009, Version 2.0* (pp. 1–13).

Pernas-Sánchez, J., Artero-Guerrero, J. A., Varas, D., & López-Puente, J. (2014). Experimental analysis of normal and oblique high velocity impacts on carbon/epoxy tape laminates. *Composites Part A: Applied Science and Manufacturing*, *60*, 24–31. https://doi.org/10.1016/j.compositesa.2014.01.006

Roopesh, E. S., & Rao, L. B. (2015). Design and Analysis of an Automotive Frontal Bumper Beam for Low-Speed Crashes. *Journal of Multidisciplinary Engineering Science and Technology*, *2*(5), 3159–40.

Siva Kumar, K., & Balakrishna Bhat, T. (1998). Response of Composite Laminates on Impact of High Velocity Projectiles. *Key Engineering Materials*, *141–143*, 337–348. https://doi.org/10.4028/www.scientific.net/KEM.141-143.337

Steel Market Development Institute. (2013). *Steel Bumper for Passenger Vehicles and Light Trucks*.